# The effect of viral plasticity on the coexistence and eco-evolutionary dynamics of host-phage systems

## Mélinda Choua

This thesis is submitted in fulfilment of the requirements for the

degree of Doctor of Philosophy in the Faculty of Science

Department of Mathematics and Statistics

University of Strathclyde

Glasgow, UK

2019

# Copyright declaration

# Abstract

Viruses infect host cells to hijack the host machinery for viral reproduction, which can lead to host mortality for unicellular organisms. In marine environments, viruses are recognized as an important factor altering phytoplankton and bacterioplankton growth and dynamics. However, it is still unclear the exact role that viruses play in the regulation of their host populations. As a consequence, generalizing viral-mediated processes is still a big challenge in ecology as well as in other fields (e.g. medical or commercial, where viruses are suggested as an alternative to antibiotics for humans, plants, or animals).

Lab experiments reveal that viral performance (represented by infection time and offspring number) varies with physiological changes in their hosts, effectively the virus' environment. These variations are referred as viral phenotypic plasticity, as the viral traits vary when environmental conditions change. In the past, models studying viral plasticity focused on intracellular dynamics. However, these latter are too detailed to be included in models that study host-virus population-level interactions in the long term, which hinders our understanding of systems that range from pathogens infecting gut bacteria to marine phage shaping the ocean communities.

Here, we compiled experimental data to represent lytic viral plasticity through functional forms that are biologically meaningful, and which we included in a standard host-virus model to understand the effect of viral plasticity on (i) the evolutionary response of the viral traits as well as population dynamics, (ii) the persistence of the host-virus systems, and (iii) the coevolution between host and virus. We show that the plasticity of the viral offspring number mostly drives the phage ecological and evolutionary dynamics. Moreover, plasticity can invert predictions on the short-term population dynamics of the viral-host system made by classic models that neglect viral plasticity.

Considering viral plasticity leads to a dynamic viral control of the host population, and enables coexistence in region where classic (nonplastic) models predict the collapse of the population. Finally, the coevolution of host-phage populations shows beneficial mutualistic interactions where the presence of virus, instead of having a negative effect, increases the fitness of the host.

# Published Work

Choua, M. and Bonachela, J.A. 2019. "Ecological and Evolutionary Consequences of Viral Plasticity." *The American Naturalist* 193, no. 3: 346-358. http://dx.doi.org/10.1086/701668.

Choua, M., Heath, M.R. , Speirs, D.C. and Bonachela, J.A. "The Effect of Viral Plasticity on the Persistence of Host-Virus Systems". *Coming soon in Journal of Theoretical Biology*.

Choua, M., Heath, M.R. and Bonachela, J.A. "Coevolution Between a Plastic Virus and its Microbial Host" (*in preparation*).

# Acknowledgements

# Contents

# List of figures

# List of tables

# CHAPTER I

# Introduction

## 1. Why Do We Care About Viruses?

"There are more viruses on Earth than stars in the universe" (Zimmer 2012).

Viruses are microscopic particles that infect a host cell to replicate. They can infect any individual cells coming from unicellular organisms, whales, humans, etc. Here, we focus on viruses that infect bacteria, simple unicellular organisms. These viruses, known as phage or bacteriophages, can be lethal for bacteria through their lysis (i.e. lytic). They thus arouse a strong interest in diverse sectors such ecology but also in medical or commercial field where phages are suggested as an alternative to antibiotics for humans, plants, or food animals (Abedon, et al. 2011; Gutiérrez, et al. 2017). In this thesis, we focus on the effect of the phages on marine bacteria (autotrophs and heterotrophs). Predicting the fate of marine bacteria is essential as they play a role in shaping the carbon cycle through photosynthesis (autotrophs) and enhance nutrient cycling through the remineralisation of organic matter (heterotrophs) (Gaedke, Hochstädter, and Straile 2002).

Early studies unveiled that the predation of bacterioplankton by larger microorganisms is insufficient to explain their mortality rate (Fuhrman and McManus 1984; Servais, Billen, and Rego 1985; Sherr and Pedrós-Alió 1989). This mismatch can be fixed by considering the mortality induced by viruses (O'Malley 2016). Today, bacteriophages are well characterized and recognized as a key factor in the regulation of phytoplankton population, removing up to 40% of the standing stock of marine bacteria present in the ocean each day (Fuhrman, 1999).

This regulation leads to a new representation of the marine microbial food web that includes the so called viral loop, introduced by (Bratbak, Egge, and Heldal 1993)(see Fig.1.1). In the classic microbial loop, the nutrients are replenished in the water column by external sources (e.g. upwelling, remineralisation, etc.) to be later taken up by bacteria and other microorganisms for growth. Microbes can also consume Dissolved Organic Matter (DOM) resulting from either excretion or bacterial remineralization of Particulate Organic Matter (POM) (Buchan, et al. 2014). In the new description of the microbial loop, bacteria are also removed out of the system by "viral shunt". This lysis induces an alternative pathway in the microbial loop by releasing the organic (i.e. POM and DOM) and inorganic (i.e. nutrient) material contained in the cells, which also delays the transfer of carbon toward higher trophic levels (Fuhrman 1992). The released POM, DOM and nutrient can then be taken up by the other bacteria, closing thus the loop.
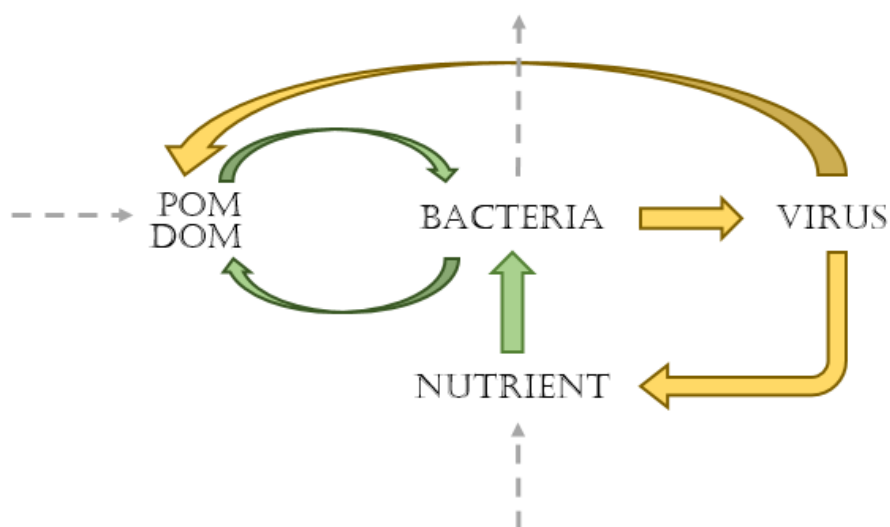


*Figure 1.1: Diagram showing the microbial loop (green arrows) with the added viral loop (yellow arrows) where the dashed arrows show interactions with the rest of the environment. Bacteria grow on the nutrient, the particular organic matter (POM) and the dissolved organic matter (DOM) then are removed by viral lysis or other external source (e.g. predation). Viral lysis releases the organic material and the nutrient contained in the cells.*

This bacteriophage regulation contributes to shaping the composition and diversity of the bacterial community (Koskella and Brockhurst 2014). Indeed, the presence of bacteriophages promotes the emergence of resistant bacteria by mutation and natural selection, which in return triggers the evolution of

phage infectivity (Miller, White, and Boots 2005). This evolutionary response is not exempt from substantial fitness costs: the resistance of bacteria to lytic phage may decrease their growth performance or increase their susceptibility to other phages (Koskella and Brockhurst 2014), while infectivity of phages becomes more host specific and thus reduces their host range. These trade-offs lead to multistrain coexistence and thus help to understand phenomena such as the paradox of the plankton. This paradox states that a wide range of plankton can coexist in spite of competing for the same resources (Hutchinson 1961).

## 2. *Caudovirales* Bacteriophages

The use of the electron microscopy in the early 1900s enabled the identification of differences in size, shape, and composition among viruses (see Fig. 1.3). A first classification was established based on the classical Linnaean hierarchical system (phylum, class, order, family, genus and species) (Lwoff and Tournier 1966). Nowadays, the International Committee on Taxonomy of Viruses suggests a universal virus taxonomy based on the type of nucleic acid and the morphology (Gelderblom 1996). Fig.1.2 shows the seven categories of viruses built on the different types of genomes: (i) double stranded DNA (dsDNA), (ii) single stranded DNA (ssDNA), (iii) double stranded RNA (dsRNA), (iv) single stranded RNA negative (ssRNA -), (v) single stranded RNA positive (ssRNA +), (vi) double stranded DNA retrovirus (dsDNA-RT) and (vii) single stranded RNA retrovirus (ssRNA-RT).

In this study, we focus on the most dominant virus that attack bacteria: dsDNA viruses with a tail (Calendar and Abedon 2005). This family, called *Caudovirales*, is divided into three sub-families according to the tail morphology (see phages marked with a star in Fig.1.3): *Myoviridae* (long contractile tail), *Siphoviridae* (long non-contractile tail) and *Podoviridae* (short non contractile-tail). Within the family, we center our research on the most studied phages, the phages T4 (*Myoviridae)* and T7 (*Podoviridae)* that attack the

*Escherichia Coli* bacterium. These phages are thus called coliphages. Although *E.coli* is an enteric bacterium, its coliphages T4 and T7 are the archetypes of the most abundant phages in the ocean (Roux, et al. 2016), so-called T4-like and T7-like phages that can infect cyanobacteria (Sullivan, et al. 2005; Sullivan, et al. 2010).

The *Caudovirales* bacteriophages are formed by only two components: protein and nucleic acid. The nucleic acid is encapsulated in the head of the virus. The head is a protein coat (capsid) that protects the nucleic acid from the environment.

The unique structure of this family shows a tail joined to the capsid (see Fig.1.2). The tail is entirely composed of proteins that make up a hollow tube (inner tube) covered by a protein sheath (tube tail). The inner tube serves as a channel for the nucleic acid to move from the capsid to the host. The tube tail ends with a baseplate to which are attached tails fibres, both entirely composed of proteins. The tail fibres are the first element to interact with the host before the baseplate securely attaches the bacteriophage to the host's surface to initiate an infection (further details in following sections).
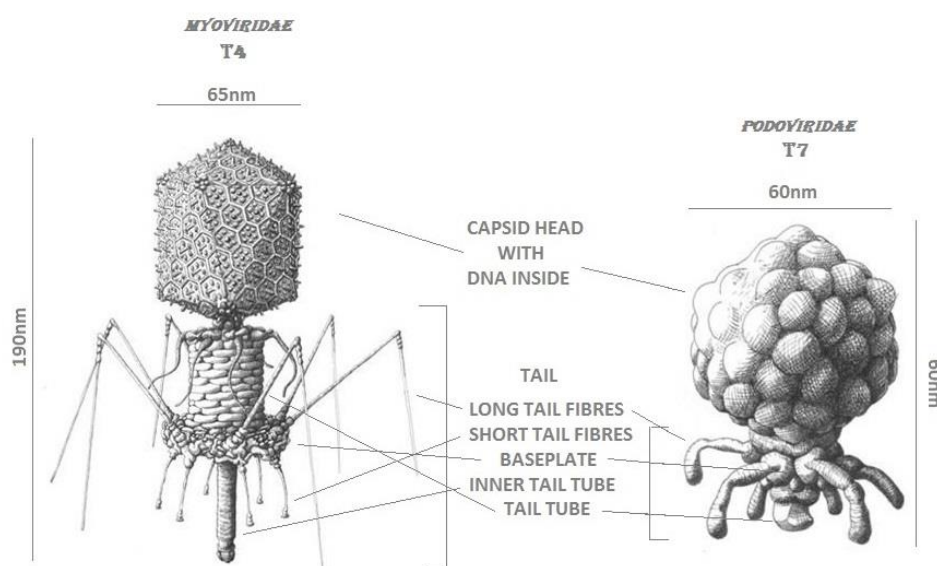
*Figure 1.2: Anatomy of Caudovirales bacteriophages. Left: Myoviridae T4 (long contractile tail). Right: Podoviridae T7 (short non contractile-tail). [Illustrations: Ben Darby - http://darbyarts.com/].*
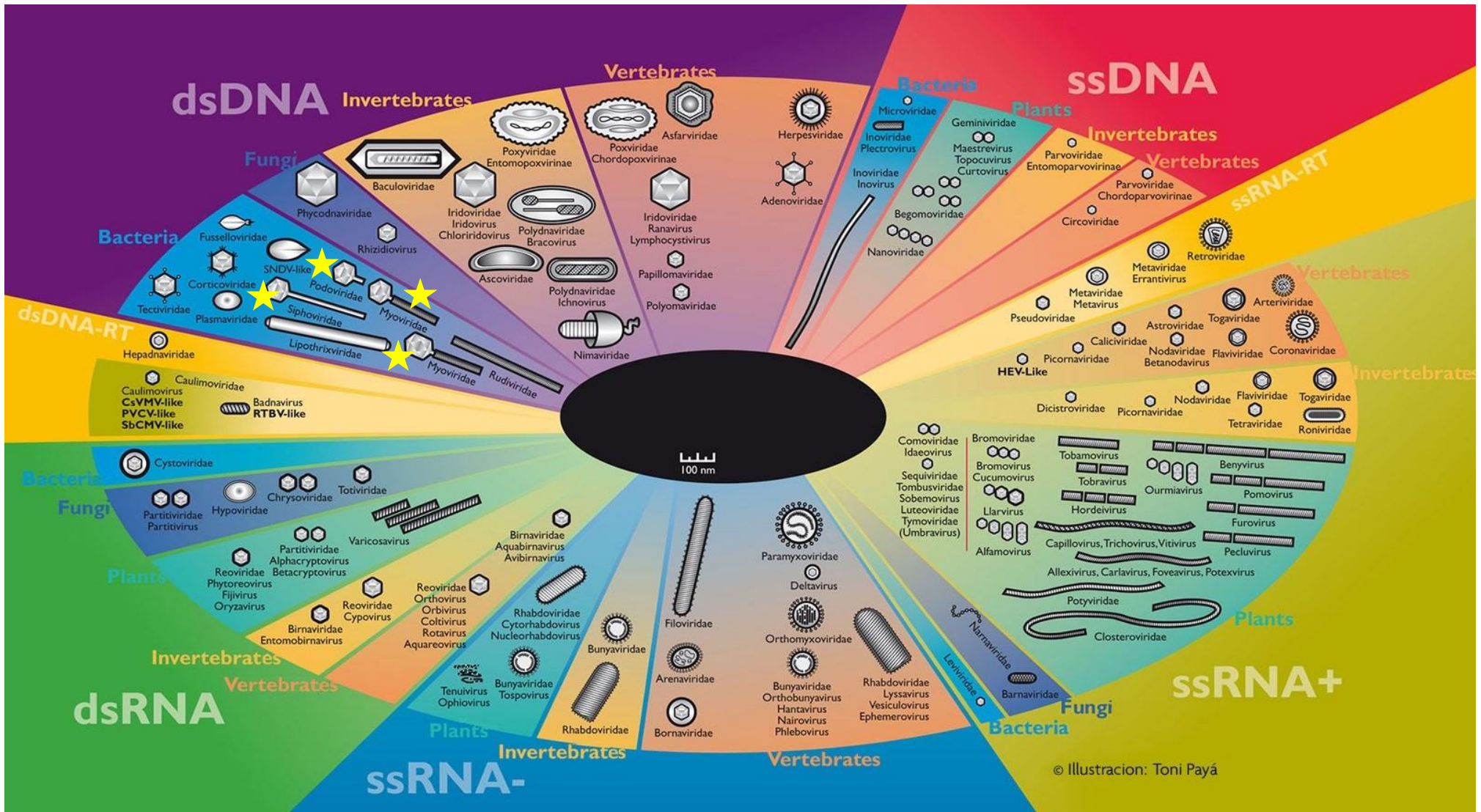
*Figure 1.3: The virosphere represents all the viral families grouped according to their type of genome. It gives a general visualisation of the complexity and diversity of replication strategies. The phages marked with a star conform the family Caudovirales. [Illustration: Toni Paya]*

# 3.    The Life Cycle Of Lytic Phage

Bacteriophages must initiate an infection in order to replicate, due to their lack of a metabolic machinery that can work on its own. They can present two kind of life cycles: lytic and lysogenic (Wilson and Mann 1997) although these terminologies have been debated (Hobbs and Abedon 2016). The lytic infection process can be described in four steps (Calendar and Abedon 2005): (i) viral **attachment**, (ii) **viral genome penetration and biosynthesis**, (iii) **assembly** and (iv) **lysis**, which entails the death of the host. Lysogenic cycle adds a dormant phase into the lytic cycle (Lwoff 1953). After the viral genome penetration, lysogenic viruses remain inactive by incorporating their DNA into the host genome. The host divides and passes the phage DNA to the daughter cells until the phage DNA is excised and the lytic cycle is triggered (from biosynthesis until lysis). In this thesis, we focus on the lytic cycle.

For a virus to start an infection, it must first encounter a host and irreversibly adsorb onto its surface (**attachment)** (Calendar and Abedon 2005). Once adsorbed, the virus perforates the cell's membrane and inserts its genome into the host cytoplasm (**viral genome penetration**). The viral genome has promoters (i.e. binding sites in the DNA that initiate the transcription) similar to those of the host (Calendar and Abedon 2005). These sites allow the host machinery to recognize the viral DNA as host DNA and trigger the **biosynthesis** of viral genome and proteins. The genome of bacteriophages shows a highly conserved organisation. Its transcription generates a cascade of phage-induced proteins divided in 3 classes. The class I proteins, first transcribed, are essential to prevent the host from interacting with the viral products and to stop the host replication. The class II proteins dismantle the host DNA and efficiently reuse the nucleotides to replicate the viral genome. The host machinery (ribosomes, ATP, etc.) is therefore monopolized to transcribe the proteins that will constitute the viral offspring (Calendar and Abedon 2005). The biosynthesis step ends with the synthesis of the class III

proteins, mostly structural (e.g. head-tail connector protein, tail fibre protein, etc.) and scaffolding proteins. The scaffolding proteins assemble the structural proteins that compose the new virions during the **assembly** period. This period lasts until the so-called holing gene is expressed to facilitate the host membrane **lysis** in order to release the virions into the environment (Abedon, Hyman, and Thomas 2003).

The timing and rates of these processes define the main phage's life-history traits (see Fig.1.4):

i) ***Adsorption rate***, or the number of successful viral attachment to the host per unit of time;

ii) ***Eclipse period***, or time between adsorption and the assembly of the first virion;

iii) ***Maturation rate***, or number of virions assembled per unit of time;

iv) ***Latent period***, or time between adsorption and the lysis of the cell and

v) ***Burst size***, or number of virions released to the environment.
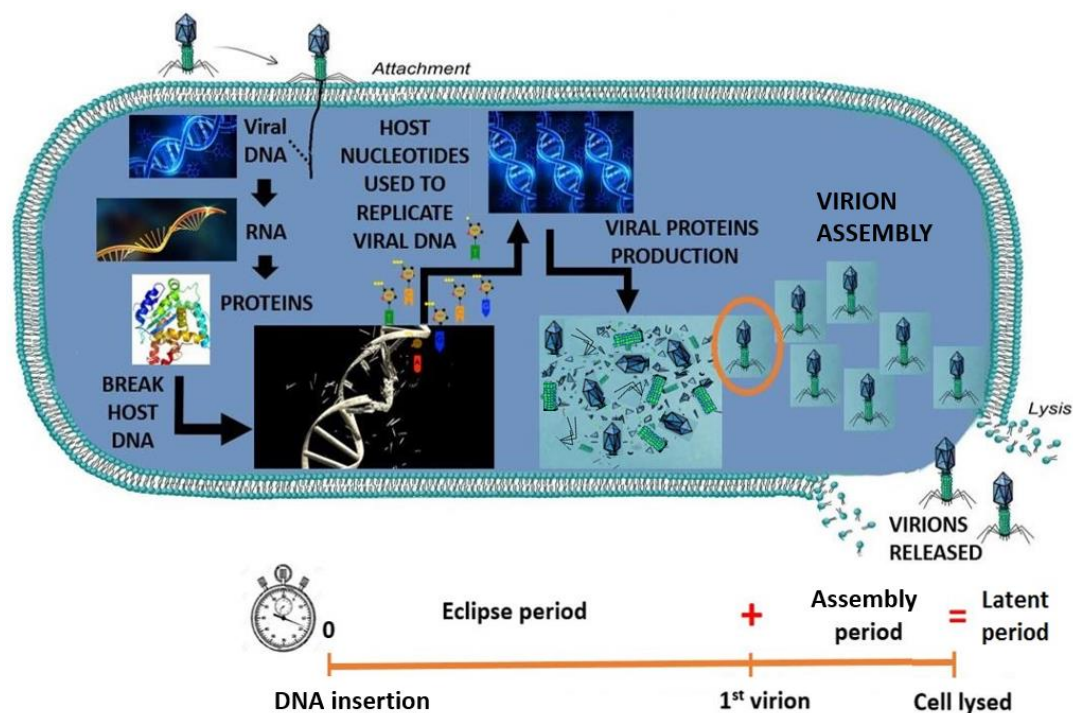


*Figure 1.4: Cartoon of the life cycle of a lytic phage as explain in the text; the phage attaches to its host, inserts is DNA that is transcribed in RNA then translated in viral proteins. First produced protein break the host DNA and reuse the nucleotides to replicate its own DNA. Structural proteins are then produce and assemble in virion. The first assembled virion marks the end of the eclipse period, and then other virions are assembled until the lysis.*

The binding of a virus to its host is the initial step of a viral infection. Each virus type uses a specific kind of host receptor. For example, the coliphage λ (*Siphoviridae)* hijacks the receptors LamB, which is a pore that the host usually uses for the transport of maltose; the coliphages T7 and T4 attack through the receptor lipopolysaccharide (LPS) which is ironically responsible of the immunogenic properties of the bacteria (Bertozzi Silva, Storms, and Sauvageau 2016).

This adsorption process and rate depend of a combination of multiple factors such as the physiology of the host (Delbrück 1940), the density of bacteria and phage, the stirring of the medium (Anderson 1949) or the probability that the virus, after colliding with the host, finds its specific receptor (Schwartz 1976).

Delbrück (1940) observed that larger host sizes increase the adsoption rate by viruses (Delbrück 1940; Hadas, et al. 1997). The same work points to host motility as another factor that influences the adsorption rate, point contested by subsequent work showing a negligible effect of cell motility on the adsorption rate (Berg and Purcell 1977).

Stirring is another factor influencing the adsorption rate (Anderson 1949). Experiments revealed that, while strong stirring increases the collision frequency between host and phage, the phage cannot adsorb on the cell surface. Adsorption is much more successful in an undisturbed media (Anderson 1949). Based on this, Anderson hypothesized that small elements located on the virus collide many times during the time the virus and host diffuse near each other. If one of these protuberances is well oriented during one of the collisions, it leads to "the steric fitting of the element and the formation of a weak bond between virus and host" (Anderson (1949). This weak bond would break under violent agitated environment while it would lead to irreversible attachment in calm media. Modern techniques have confirmed Anderson's hypothesis. Hu and al. (2013) showed by using cryo-electron tomography that the virus folds-back its tail fibres to the capsid during free diffusion, which enables a higher rate of diffusion. Once the virus

detects the presence of bacterial cells through the sensors near its capsid (Calendar and Abedon 2005), it extends these fibres one by one (Hu, et al. 2013). The extension of its tail fibres decreases its diffusion rate and allows the phage to have a first contact with the host surface. Once in contact with the host, the virus randomly walks with its tail fibres on the cell surface in search of its specific receptors (see Fig.1.5) (Rothenberg, et al. 2011). The virus is susceptible of dissociating from the host until all its six tail fibres interact with its receptors, which orients the phage tail perpendicular to the cell surface and triggers the conformational changes of phage baseplate leading to the irreversible attachment (Rakhuba, et al. 2010).
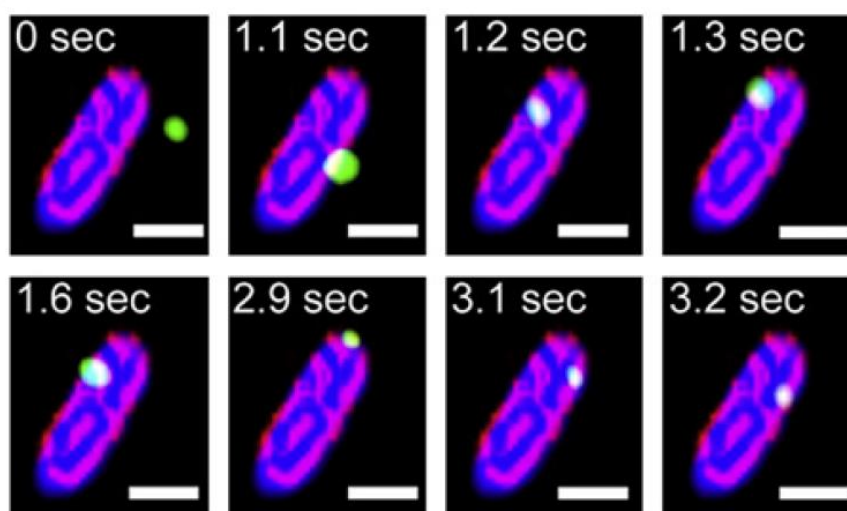


*Figure 1.5: High-resolution fluorescence microscopy images showing the colocalization of a free virus (green) that moves on a cell (blue) with highly labeled bio-LambB receptor bands (purple). The virus is observed to be predominantly moving on the LamB receptor bands (scale bar = 2µm) (Rothenberg, et al. 2011).*

The adsorption rate depends thus mainly on the host size that influences the probability of the first contact, and on the number of receptors to assure an irreversible attachement. Selecting the appropriate adsoption model is really phage and environment dependant (Rakhuba, et al. 2010).

*Our focal system*

Bacteriophages T4 and T7 attack E.coli, a gram-negative bacterium. Gram-negative bacteria are diderm: they have an outer membrane and an inner membrane separated by a thin peptidoglycan cell wall (see Fig.1.6). The phage adsorbs on the receptors located on the outer membrane such as lipopolysaccharides (LPS), porins, or membrane proteins.
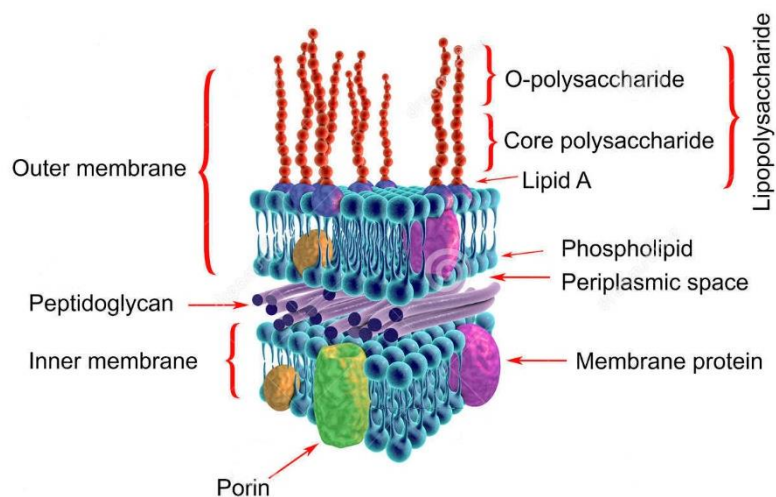


*Figure 1.6: Gram-negative cell wall structure [illustration: Kateryna Kon - https://fr.123rf.com/profile_drmicrobe]*

The coliphages T4 and T7 adsorb through uptake proteins, but this process requires energy (Yu and Mizushima 1982; Hantke and Braun 1975; Noinaj, et al. 2010), or through LPS (Stoddard, Martiny, and Marston 2007). Although these coliphages are the archetypes of the marinephages T7-like and T4-like, the number and identity of the host receptors used by these phages remain uncertain (Mann 2003; Stoddard, Martiny, and Marston 2007). However, there are biochemical evidences that LPS may be involved in cyanophages binding (Xu, Khudyakov, and Wolk 1997). We thus assume that LPS are the main receptors targeted by the phages in our study.

LPS are endotoxins produced by the bacteria to provide a protection against antimicrobial compounds. They render the membrane impermeable and cover a large part of the surface, up to 75% (Nikaido and Vaara 1985; Stoddard, Martiny, and Marston 2007). With such amount of receptors, we can assume that even if the virus does not collide directly with its receptors during the first

contact with the host, it meets its receptor with total certainty during its random walk on the surface. Consequently, we assume that each collision leads to an infection.

## 3.1 Eclipse period, E

The eclipse period (*E*) starts with the viral genome insertion. After the viral tail fibres attach to the host receptors, a signal is transmitted into the phage capsid then the phage disaggregates liberating proteins that are part of its internal core (Calendar and Abedon 2005). These proteins are injected into the outer membrane of the cell and carve a pathway across bacterial cell wall. Once the phage channel is in contact with the host inner membrane, a signal is sent in order to translocate the viral genome from the capsid into the host along the inner tube. (Calendar and Abedon 2005).

The complete internalization of the genome into the host differs across phages: the phage λ injects its DNA within 1 min while the phage T7 takes about 10 min (García and Molineux 1996). It has been reported that the slow entry of T7 DNA is a way to control genes expression (McAllister, et al. 1981) as their DNA is read as it is injected. Phages such as λ or T4 do not show clearly separated sections in their DNA and thus have to proceed to the full internalization of their genome into the host before the transcription starts (Calendar and Abedon 2005). In both cases, the time course of protein synthesis reveals the three classes of viral gene products: early, middle and late transcribed proteins (or class I, II and III proteins, see above).

Early genes have specific sequences (promoters) that are recognized by the host RNA polymerase (enzyme that binds to a specific sequence of DNA (i.e. gene) and transcribes it in messenger RNA). The host RNA polymerase (RNAp) thus initiates the transcription of the early viral genes in their related proteins. These proteins inhibit the host transcription, suppress host innate defences and enable the transcription of the middle genes by producing T7 RNAp in the case of T7, or by producing proteins required for the recognition

of the middle promoters by the host RNAp in the case of T4 (Calendar and Abedon 2005). This recognition of middle promoters explains how the viral DNA orchestrates the production timing of its components while the full genome is inserted in the host (e.g. in T4 case). This problem is not met in the T7 case as the DNA is read as it is internalized.

The middle genes mainly produce nucleases and proteins to replicate the viral DNA (Calendar and Abedon 2005). They also produce several transfer RNA (tRNA) that are supplements to the host tRNA during translation. In the T4 case, the middle genes produce also adapter proteins in order to allow the transcription of the late genes. Late genes code for virion components (e.g. tail proteins, capsid proteins, etc.), scaffolding proteins, and a soluble lysozyme that attack the cell wall (see further details in the section Latent Period, L). The first assembled virion marks the end of the eclipse period.

All these transcription-translation processes that interpret viral DNA in viral proteins require the host machinery (see Fig.1.7). The host RNA polymerase (replaced by T7 RNAp in the T7 case) opens and unwinds the DNA double helix and covalently links incoming nucleotides (coming from the host pool) that match with the DNA template to produce the messenger RNA (mRNA). Then, the host ribosomes bind on this mRNA and link incoming tRNA (those coming from the host pool and those synthetized by the viral proteins) that matches with the mRNA and produce the proteins. These interactions require energy also provided by the host in the form of ATP.

The number of ribosomes and their rate of elongation determine the rate of protein synthesis. The elongation rate is limited by the pool size of tRNA, or, when tRNA is provided in sufficient quantity, the elongation rate reaches saturation due to structural rearrangement within the ribosome (Bremer and Dennis 2008). The concentration of ribosome and tRNA increase with the growth rate (Schaechter, MaalØe, and Kjeldgaard 1958) which can increase the rate of protein synthesis. Webb et al. (1982) suggested that viral development can be limited either by RNAp activity or by ribosome activity.

Thus, viral development depends not only on their genome-encoded functions but also on the intracellular resources of their hosts.
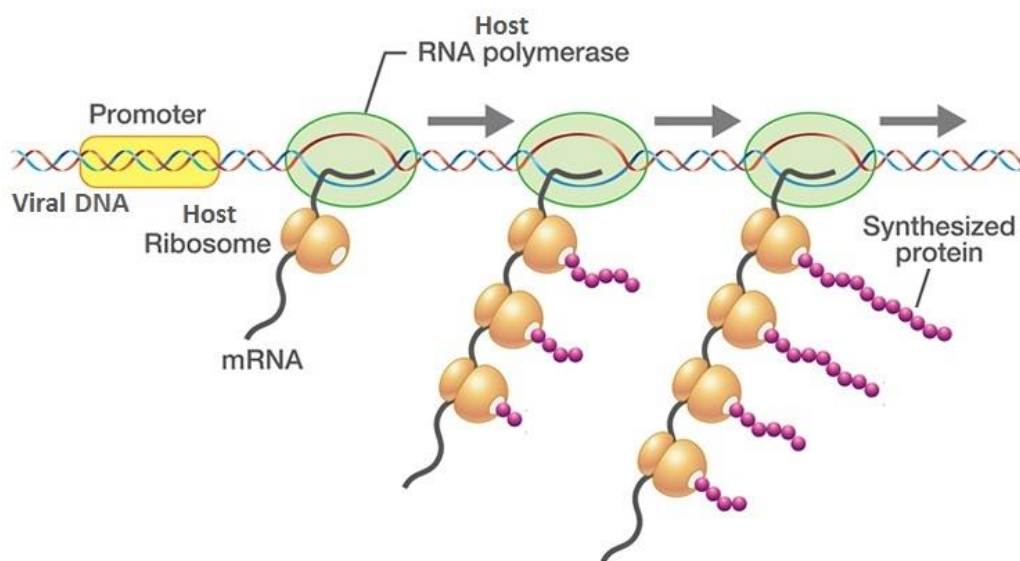


*Figure 1.7: Transcription of the DNA in messenger RNA (mRNA) through the RNA polymerases followed by translation of the mRNA in proteins by the ribosomes.*

## 3.2    Maturation rate, M

Once the viral components have been produced at the end of the eclipse period, the assembly process can start: the maturation rate (*M*) is the number of virions that are assembled intracellularly per unit of time. The assembly stage follows a strict order of steps that is not controlled by the order of gene expression but just by proteins interactions such as conformational switching (when the protein structure changes upon attachment to a complex), chaperons (proteins that assist the assembly of other proteins in functional structure), and others (Aksyuk and Rossmann 2011). Consequently, if one of the components is missing during the assembly, the assembled part is pending and remains free until the missing component is produced (Aksyuk and Rossmann 2011).

Despite their phenotypic and genetic diversity, phages show similarities in their component proteins and structure of assembly (Aksyuk and Rossmann 2011). The assembly of heads and tails occurs independently and simultaneously. The capsid of the head is produced empty first then is subsequently filled with the viral genome. The translocation of the genome inside the head requires energy provided by the host via ATP molecules. Once the heads and the tails are completed, they are sequentially attached to each other forming the new virions.

## 3.3    Latent period, L

The latent period refers to the total infection time, and therefore starts when the virus inserts its genome into the host and ends when the host is lysed. Host lysis is necessary in order to release the assembled virions to the environment. The rupture of the host membrane requires the virus to produce two specific genes: one that encodes the endolysin enzyme and another one that encodes the holing protein (Young 1992). The interaction between the two product results in the rupture of the host membrane.

The endolysins are enzymes that utilize water to break chemical bonds in the peptidoglycan (located between the *inner* and the *outer* membrane of the host, see Fig. 1.6). During their synthesis, no signal peptide is produced (Woznica, Bigos, and Lobocka 2015). This signal is a sequence produced as part of the growing protein and act as a flag that can be recognized by particles located freely in the cytoplasm and that transport the protein to its specified location (Woznica, Bigos, and Lobocka 2015). However, in the case of endolysins, these flags are not produced and endolysins are thus accumulating fully folded and active in the cytoplasm (Young and Bläsi 1995). If these endolysins were equipped with a signal peptide (i.e. flag), they would be able to lyse the host membrane within seconds. They are thus voluntarily trapped in the cytoplasm until a specific time "programmed" into the holin gene of the virus (Wang, Smith, and Young 2000).

The holins are proteins that are "hole- formers". They accumulate in the membrane under a harmlessly form until suddenly aggregating to form a hole in the *inner* membrane (White, et al. 2011). This hole allows the release of the endolysins from the cytoplasm into the periplasm that rapidly degrades the peptidoglycan followed by the macroscopic lysis of the host (Young and Bläsi 1995).

Evidence points to the holin gene as the sole responsible of the timing of the lysis following infection by a single phage (Ramanculov and Young 2001; Young and Bläsi 1995). How the hole-formation is scheduled in time remains unknown (White, et al. 2011; Wang, Smith, and Young 2000). The latent period is the physiological barrier limiting the virions production. Abedon (1989) stated: "…this cessation of replication is the result rather than the cause of lysis". He justified his statement by the fact that any delay in the lysis, either caused by superinfection (i.e. when a second homologous phage adsorbs to a cell already infected) or genetic mutation, leads to an increase in the amount of virions released. All else being equal, a longer latent period allows the release of a bigger amount of virions (Wang 2006).

The question about what determines the latent period still remains open. Early models analysed how natural selection influences latent period in different environments. For example, in (Levin and Lenski 1983) results revealed that if lysis happens too early, a small amount of virions are made but multiple infections can rapidly occur. Oppositely, if the lysis is too long, more virions are produced but opportunities for them to attack new hosts are lost during the long latent period. This argument establishes the evolutionary costs and benefits associated with the two opposite strategies, with an emphasis on the role of host density in the evolution of the latent period.

Abedon (1989) confirmed that the host cell density plays a role in the selection of the latent period by simulating phage growth under different fixed host densities, for a variety of latent periods. High host cell density favours the

survival of phages with a short latent period, while low host cells density favors longer latent periods.

### 3.4    Burst size, B

The burst size ($B$) is the number of assembled virions per infected cell released into the environment at the end of the latent period. The number of virus particles liberated at lysis depends on the number of particles that have been assembled up to that moment.

One-step growth experiments (Ellis and Delbrück 1939) reveal great variation in the magnitude of the bursts size, from below 20 to over 1000 per infection (Maat, et al. 2016). In situ data have also revealed a substantial seasonality in the magnitude of individual bursts for marine hosts (Ashelford, et al. 2000).

A correlation between the burst size and the size of individual host has been observed (Delbrück 1945) although the burst size distribution was much wider than the host size distribtution. The latent period plays an important role in the final value of the burst size, as a longer latent period leads to a larger burst size (Abedon 1989). However, the wide variation of burst sizes has been contrasted with a very small variation of the latent period (Delbrück 1945). Delbrück (1945) concluded that the large fluctuation in the burst size must then be due to intracellular mechanisms involved in the viral growth.

# 4.    Viral Phenotypic Plasticity

Phenotypic plasticity refers to the short-term changes in traits of an organism that are triggered by changes in the environment but do not involve genetic change. Plasticity can be active or passive, instantaneous or delayed, continuous or discrete, permanent or reversible (Forsman 2015).

Until recently, viral traits ($E$, $M$, $L$, $B$) were considered constant values obtained with experiments under optimal conditions. For example, Molineux

estimated the eclipse period at 8 to 15 minutes for the phage T7 at 30°C in rich media (Calendar and Abedon 2005). However, as explained in section 3, the viral development depends on the intracellular resources of their host such as the RNAp and ribosome activity (Webb, Leduc, and Spiegelman 1982). The activity of these latter are host growth rate dependant (Schaechter, MaalØe, and Kjeldgaard 1958).

One-step growth experiments revealed how the variation in the host growth rate affects the main life-history traits involved in viral growth (You, Suthers, and Yin 2002; Hadas, et al. 1997; Golec, et al. 2014; Birch, Ruggero, and Covert 2012). In such experiments, the host cultures are infected by phages during a short period of time then diluted to cease infection in order to guarantee a single infection (Ellis and Delbrück 1939). Samples of infected cells are withdrawn then treated periodically with chloroform to artificially lyse the hosts and count the number of virion produced (through the number of plaque forming unit – PFU). The data show that the eclipse and latent period decrease when the host growth rate increases while the maturation rate and burst size increase. These changes in the viral traits due to changes in the host, effectively the phage's environment, are referred to as viral phenotypic plasticity (Abedon, Herschler, and Stopar 2001).

## 4.1 Plasticity in *E* and *M*

In addition to the experiments, models simulated the dependence of the eclipse period (*E*) and maturation rate (*M*) on host growth rate (You, Suthers, and Yin 2002; Birch, Ruggero, and Covert 2012; Endy, Kong D Fau - Yin, and Yin). These simulations at molecular level decouple the effect of individual host parameters on phage growth and analyse the sensitivity of *E* and *M* to each host parameter independently. (You, Suthers, and Yin 2002) results revealed that the viral growth is mainly limited (i.e. bottleneck effect) by the number of ribosome allocated to the protein synthesis rather than by the host transcription rate (i.e. number of host RNAp) (see Fig.1.8, left). Indeed, when

the number of host RNAp is high, this excess of host RNAP will bind to promoter of early genes producing thus an excess of mRNA of the early genes (see Fig.1.8, right). These mRNA will then compete with the mRNA of the late genes for the ribosomes, decreasing the ribosome number attributed to the late genes.
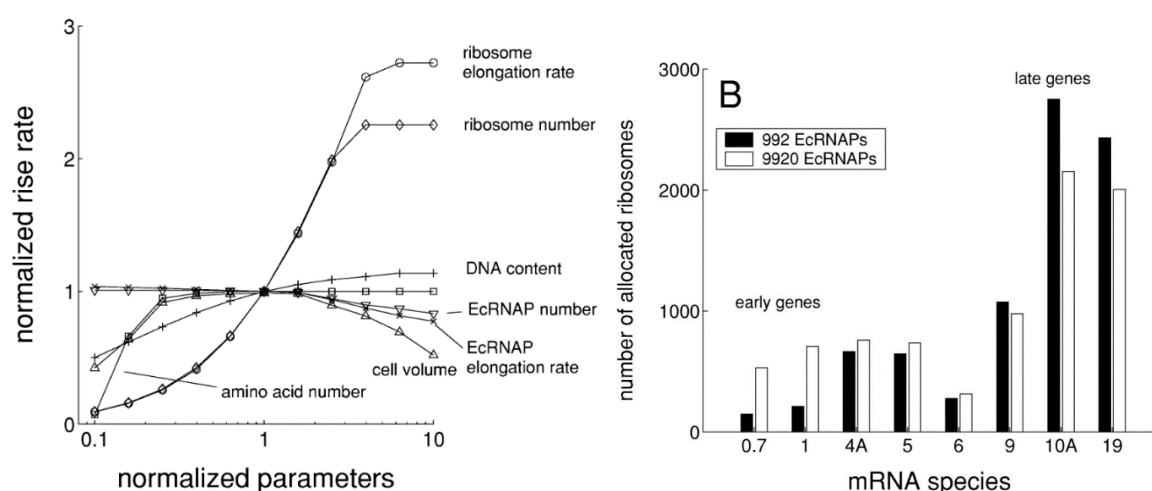


*Figure 1.8: The bottleneck effect for the phage T7 and the host E.coli with respect to host parameters. LEFT: Sensitivity of the intracellular maturation rate (also called rise rate) to host physiological parameters. The parameters were normalized by their defaults setting for the host growth rate of 1.5 doublings per h. The maturation rate was normalized to the value calculated for this default case. RIGHT: The allocation of ribosomes to mRNAs of different genes (early, middle and late genes) when the host RNA polymerase (EcRNAP) is in low amount (black bands) or in excess (white bands) (You, Suthers, and Yin 2002).*

The number of ribosomes increases with the host growth rate, which accelerate the protein synthesis affecting thus the traits E and M (see Fig.1.8, left), until reaching a physiological saturation at high growth rate.

## 4.2    Plasticity in *L*

Wang et al. (1996) first explored the effect of host quality (i.e. host growth rate) on the evolution of phage lysis timing. They assessed the optimal latent period (e.g. the latent period that maximizes the phage population growth) for different scenarios where host quantity and host quality were considered independent from each other and fixed at different values. The relative importance of each factor revealed that the host quantity is more determinant in the lysis selection at low host density, whereas when host density is high,

the host quality is more important. Later, Abedon et al (2001) argued that the effect of host quality on phage latent period evolution is small. However, the fact that they assumed that both host density and host growth rate are independent from each other is not realistic (Wang, Dykhuizen, and Slobodkin 1996).

## 4.3    Plasticity in *B*

The burst size, *B*, is the resulting number of phages that has been assembled during the infection time. The plasticity in this trait is thus an emergent result of the combination of the changes in the other traits (*E*, *M* and *L*).

# 5.    Outline Of The Project

Although viral and host interaction and their coevolution have been studied in the past, no studies considered the viral dependence on host physiology (viral plasticity). This thesis focuses on the effect of the viral plasticity on the interaction between host and phage in the short and in the long term.

In the following chapter, we first represent viral plasticity with mathematical functions. To this end, we compiled independent data sets that measured the dependence of phage traits on the host growth rate, and then we deduced expressions for the E and M. We justify and discuss the generic mechanism behind these expressions before using them as functional forms in the next steps of the project.

In chapter III, we include these functional forms in an eco-evolutionary model where only the virus evolves in order to understand mechanistically how plasticity affects the emergent evolutionary strategies of the virus. With such emergent strategy, we then analyse the dynamic behaviour of the host-phage system under a diversity of environmental conditions (e.g. nutrient pulses and host starvation). We compare this behaviour with a host-phage system where

the phage is non-plastic (i.e. its viral traits are independent of the host growth rate and thus stay fixed).

In chapter IV, we study the effect of viral plasticity on the stability of the ecological interactions. More specifically, whether plasticity plays a role in the oscillations typically observed for antagonistic systems like ours, and in the maintenance of the host-phage coexistence. We discuss on the stability regions drawing a comparison with a nonplastic version of the model.

In chapter V, we study the coevolution of the host-phage system. We analyse if the presence of phages alters competition among bacteria and maintains diversity for both the plastic and nonplastic version of the model.

Finally, the thesis concludes with a summary that brings together all our results.

# CHAPTER II

# Modelling hosts and plastic viruses

Ecological descriptions that include viruses have been added in biogeochemical models that consider several trophic levels (Mateus 2017). These models, however, neglect the viral dependence on its host and thus their realism is limited. In a recent review, Mateus (2017) states: "The specificity host-virus relationships and their complexity means that the simple inclusion of viruses as a collective pool in models may be considered too simplistic or even unrealistic." adding that both viruses and hosts need to be explicitly modelled. In this chapter, we introduce a simple way to model host-virus interaction that considers the dependence between the bacteriophage and its host ("viral plasticity", see previous chapter).

## 1. Interactions Host-Virus

Host-virus models are typically like prey-predator models, as Lotka-Volterra (1926), where the host (prey) grows at a constant rate and dies infected by viruses (the predator) while the viral population grows infecting the prey and dies at a constant rate. They do not consider the latent period but instead assume a continuous release of virions (Beretta and Kuang 1998). These latter are referred as a "lytic-rate model". Host-virus interactions with an explicit delay between infection and the lysis of host were first modelled by Campbell (1961). Nonetheless, this model did not take into account host resource dynamics, resource uptake, or growth. Later, Levin et al. (1977) added the

interaction with the environment and thus developed a "delay model" with three trophic levels: main resource, host, and virus. This model was validated using experimental data of E.coli and its coliphage T2. The lytic-rate model, frequently used (Mateus 2017), shows similar qualitative ecological results than the delay model. However, it fails to describe the long-term (i.e. evolutionary) behaviour of host-bacteriophage interaction (Bonachela and Levin 2014). As here we will study both the short-term and the long-term ecological and evolutionary behaviour of the system, we represent the ecological dynamics of host-phage systems by the well-known model of (Levin, Stewart, and Chao 1977). This model keeps track of the dynamics of the free host cells (C), infected host (I), free viruses (V) and nutrient concentration (N).

In this version of the model, environmental conditions are set up using a chemostat where host and phage encounter each other randomly. We also assume that multiple infections do not occur and the host machinery is entirely used for the viral replication (i.e. the growth of the host stops once infected). The latter implies that the latent period is not limited by host's generation time. These hypothesis lead to the following delayed differential equations:

$$\frac{dN(t)}{dt} = w(N_0 - N) - \mu\, C/Y \tag{2.1}$$

$$\frac{dC(t)}{dt} = \mu\, C - k\, C\, V - w\, C + w\, C_0 \tag{2.2}$$

$$\frac{dI(t)}{dt} = k\, C\, V - (k\, C_{t-L}\, V_{t-L})e^{-wL} - w\, I \tag{2.3}$$

$$\frac{dV(t)}{dt} = (B\, k\, C_{t-L}\, V_{t-L})e^{-wL} - k\, C\, V - m\, V - w\, V \tag{2.4}$$

(see symbols and units in Table 2.1). The first equation represents the dynamics of the nutrient concentration, given by the chemostat's inflow and outflow of nutrient (first term) and the uptake of nutrient by the host (second

term). The second equation describes the dynamics of the free host population as a result of bacterial reproduction (first term) and an inflow of fresh hosts (last term), reduced by infection events (second term), and the chemostat dilution process (third term). The infected host population increases through the adsorption of virus (first term in Eq.(2.3)) and decreases through dilution (last term) or the lysis of the cell infected a latent period in the past (second term, where $e^{-wL}$ is the probability for infected cells to not be washed of the system during the lytic cycle). The lysis of such cells contributes to the inflow of free phages (first term of the last equation), which decline by adsorption (second term), natural mortality (third term) and dilution (last term).

*Table 2.1: Symbols for variables used in the model.*

| Symbol | Description | Units |
|--------|-------------|-------|
| $N$ | Dissolved Inorganic Nutrient Concentration | mol l$^{-1}$ |
| $C$ | Non-infected Host Concentration | cell l$^{-1}$ |
| $I$ | Infected Host Concentration | cell l$^{-1}$ |
| $V$ | Free Virus Concentration | virus l$^{-1}$ |
| $\mu$ | Non-infected Host population Growth Rate | d$^{-1}$ |
| $Y$ | Yield Parameter | cell mol$^{-1}$ |
| $k$ | Adsorption Rate | l virus$^{-1}$ d$^{-1}$ |
| $L$ | Latent Period | d |
| $B$ | Burst Size | Virions cell$^{-1}$ |
| $m$ | Virus Mortality Rate | d$^{-1}$ |
| $w$ | Chemostat Dilution Rate | d$^{-1}$ |
| $N_0$ | Dissolved Inorganic Nutrient Supply Concentration | mol l$^{-1}$ |
| $C_0$ | Non-infected Host supply Concentration | cell l$^{-1}$ |
| Conversion constants | | |
| $Conv_1$ | Constant to convert from (ml) to ($\mu m^3$) | $10^{-12}$ $\mu m^3$ml$^{-1}$ |
| $Conv_2$ | Constant to convert from (hour$^{-1}$) to (d$^{-1}$) | 24 hour d$^{-1}$ |

## 1.1 Host representation

We assume that the host grows following the simple Monod model:

$$\mu = \mu_{max}\,[N]/([N] + K_n) \tag{2.5}$$

where $\mu_{max}$ (the maximum growth rate) and $K_n$ (the half saturation constant for growth) characterize the affinity of the uptake/growth machinery for the bacteria and are both size dependents (Chien, Hill, and Levin 2012). They can be coupled through the following convex function (Wirtz 2002) that ecologically represents a trade-off constraining the uptake mechanism:

$$K_n(\mu_{max}) = K_{ref}\,e^{\mu_{max}/(\mu_{ref}-\,\mu_{max})}$$

$$\tag{2.6}$$

where $\mu_{ref}$ represents the asymptotic $\mu_{max}$ for infinitely high $K_n$, and $K_{ref}$ represents half-saturation constant at $\mu_{max} = 0$. The exact shape of this positive relationship does not affect qualitatively our results (Choua, et al. 2020).

For chapter IV onwards, we embraced the fact that these traits are tightly related to the host size. Thus, as explained in those chapters, we can use allometries to parametrize the model. Although the metabolic theory of ecology states that the growth rate of microbes decreases with increasing body size, recent experimental data showed that maximal growth rate tend to increase with body size for organisms smaller than 6 microns (Ward, et al. 2017; Gallet, et al. 2017). These data revealed a key trade-off between rates of resource acquisition and the rate of internal metabolism (i.e. $\mu_{max}$), which emphases different limiting factors between small and large organisms. For small cells, molecular transit time inside the cell rather than uptake rate (Gallet, et al. 2017), or the rate at which the internal quota is replenished by nutrient uptake rather than the nutrient conversion in biomass (Ward, et al. 2017), can be the limiting factor. Specifically, for the bacteria E.coli, experimental work provides the following allometric expression (Gallet, et al. 2017; Shestopaloff 2016):

$$\mu_{max}(r) = \text{Conv}_2 \ 10^{f \ log_{10}\left(4\pi \text{Conv}_1 \ r^3/3 \right)+p} \tag{2.7}$$

where the parameters $f$ and $p$ determine how steeply $\mu_{max}$ increases with the volume. When parametrizing our model, we used the (Gallet, et al. 2017) values as it allows reasonable (i.e. observed experimentally) values for $K_n$ when calculated through the Eq. (2.6).

## 1.2    Adsorption

Adsorption rates, $k$, were first estimated by applying the theory of coagulation of von Smoluchowski (1917) (see (Delbrück 1940) and references therein). Then, Delbrück (1940) defined the adsorption rate as the portion of particles crossing the surface of a sphere of radius r (representing the bacterium) suspended in a medium that contains particles (phages) initially uniformly distributed. In this theory, a particle is adsorbed each time it collides with the sphere surface, and thus there is a 100% success rate of adsorption. With this setup, the maximum adsorption constant, $k_{max}$, is given by the collision equation:

$$k_{max} = 4\pi r \text{D} \tag{2.8}$$

where $r$ is host radius and D is the diffusion constant of the virus. This expression agrees with the observation that larger host sizes increase the adsoption rate (Delbrück 1940; Hadas, et al. 1997). It however assumes a kinetic model where each collision is leading to irreversible binding providing the one-step mechanism of Krueger (1931):

$$V + C \xrightarrow{k} I \tag{2.9}$$

where $V$ is the free virus, $C$ the free cell, $I$ the infected cell and $k$ the adsorption rate. Eq. (2.9) is widely  used (Delbrück 1940; Hadas, et al. 1997; Guerrero-

Ferreira, et al. 2011; Zarybnicky, Reich, and Wolf 1980; Puck Tt Fau - Garen, Garen A Fau - Cline, and Cline ; Storms and Sauvageau 2015). However, assuming that the frequency of collision equals to the adsorption rate overestimates the values measured for the adsorption rate (Schwartz 1976). The frequency of collision is actually higher than the actual adsorption rate, which supports indirectly Anderson's hypothesis (i.e. that unsuccessful attempts limit the adsorption rate, see chap I section 3.1).

In reality, after a collision, the phage may detach from the host which leads to a two-step process that considers a reversible binding before the irreversible attachment. Such a process can be expressed as:

$$V + C \overset{k_1}{\leftrightarrow} VC \overset{k}{\rightarrow} I \qquad (2.10)$$

where $VC$ represents the reversibly attached phage and $k_1$ the collision rate. Fig.2.1 represents the dynamics of the different adsorption process (Eq.(2.9) and (2.10)) which can show significant difference along the time. The appropriate adsorption model is really phage and environment specific (Rakhuba, et al. 2010). Eq.(2.10) enables an expression for the adsorption rate $k$ that considers aspect such as the probability for the phage tail to be well oriented and to react with a host receptor within the average collision time (Schwartz 1983):

$$k = k_{max}(1 - e^{-\frac{k_1 \tau_e R}{l}}) \qquad (2.11)$$

where $k_{max}$ is given by Eq.(2.8), $k_1$ is the collision frequency, $\tau_e$ the fraction of time that the phage tail is well oriented within the average collision time, $R$ the receptor surface density, and $l$ a constant related to the size of the receptors and the phage tail. This expression, however, is hard to parametrize as there

is only information about the specific example used in Schwart's experiment (phage λ).

A more general approach for nutrient-uptake receptors provides further insight about mathematical ways to estimate the adsorption rate. Berg and Purcell (1977) applied an expression that considers the number of receptors covering the surface of the host to bacteriophage adsorption. They assumed an electrostatic problem where an insulating sphere (bacteria) shows conducting disk at the surface (receptors) rendering the sphere permeable to an electric field (in this case phage adsorption):

$$k = k_{max} \frac{R \, r_s}{R \, r_s + \pi \, r} \tag{2.12}$$

where $r_s$ is the radius of the receptors. This expression confirmed the observed positive correlation between adsorption rate and receptor density (Schwartz 1976). In the extreme case where the number of receptors entirely covers the surface, the cell becomes a perfect sink and the adsorption rate equals the collision rate and becomes maximal (i.e. equal to $k_{max}$). Schwart's observations indeed revealed that $k_{max}$ is quickly reached, and the increase in the $k$ with R is observed only when the number of receptors is sufficiently small (in agreement with Berg and Purcell's expression).

In our case, the amount of the viral receptors on the cell's surface facilitates the choice of the adsorption rate expression (see chap I section 3.1). As the receptors cover a large percentage of the surface, we assume that each collision leads to an infection and thus $k$ is represented by Eq.(2.8) and kinetic model in Eq.(2.9). Specifically, we will use this expression in chapter IV and onwards, as in those cases we pay special attention to host size.
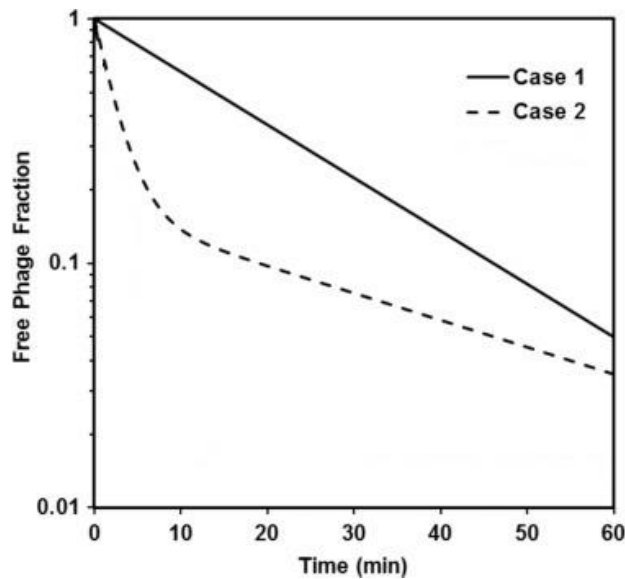
*Figure 2.1: Representative adsorption curves normalized by the initial phage titer, Case 1 represents the one-step model and case 2 the two-step process (Storms and Sauvageau 2015)*

# 2.  Viral Plasticity

The determination of values for the viral traits L and B, appearing in Eqs.(2.3)-(2.4), demands some background steps. In classic models, those traits are determined by fixed values extracted from experiments conducted under ideal conditions where the host grows at its maximum rate. In nature, those conditions are more the exception than the rule, which potentially biases the prediction that classic models cast on the marine microbial community structure, population density, and dynamics. We refer to this kind of models as "nonplastic case".  Indeed, the parasitic life style of the virus entails a dependence of its performance on the host physiological state (Wang, Dykhuizen, and Slobodkin 1996) that needs to be acknowledges.

One-step growth experiments (Ellis and Delbrück 1939) have been used to measure the response of viral traits to changes in the host growth rates (You, Suthers, and Yin 2002; Hadas, et al. 1997; Rabinovitch, et al. 1999; Birch, Ruggero, and Covert 2012; Golec, et al. 2014). In these experiments, the host is cultured in chemostats maintained at a certain temperature, and the growth rate is controlled by using either different dilution rate or different carbon sources. Each of these cultures was monitored during one infection cycle by a

phage. Samples of infected cells are withdrawn, and some of them are used to estimate the number of infected centres (IC) while others are treated periodically with chloroform to artificially lyse the hosts and extract the intracellular virions assembled during the interval of time since the phage addition. To quantify the amount of these virions, a gel layer is added to the solution that renders the medium semi-solid and restricts each virion to the infection of the cells in its neighbourhood. After an incubation period, regions of cells destruction (called Plaque Forming Unit – PFU) can be counted to quantify the number of virions that have triggered the first infection process. This counting process is repeated several times to obtain statistically-significant data of eclipse period (E), maturation rate (M), latent period (L) and burst size (B) for different host growth rates.

Previous studies attempted to find a mathematical expression for the eclipse period (*E*), maturation rate (*M*) and latent period (*L*). However, they used a small experimental data set, focused on one single system, failed to capture bottleneck effects (see chapter I section 3.2 and 3.3), and considered *L* independent from *E*, which is not statistically and physiologically meaningful (i.e. Rabinovitch, et al. (2002) fitted Hadas et al's data (1997)). Others represented viral plasticity by modelling the interaction at a molecular level (You, Suthers, and Yin 2002) rending the long-term study impracticable and difficult to parametrize (Birch, Ruggero, and Covert 2012). Others dynamical models have also attempted to include viral plasticity using a viral predation that depend on the host density (Weitz and Dushoff 2008), different fixed trait values for different fixed host growth rates (Middelboe 2000), or case-specific expressions (Rabinovitch, et al. 2002) which hampers the understanding and predictability of any specific host-virus system.

In our study, we compiled the data of several independent one-step growth experiments found in the literature for different host-virus systems. From these data sets, we focused on the effect of plasticity on the eclipse period (E) and the maturation rate (M) because they are both well understood at the

physiological level (see chap I section 3.2 and 3.3). The main aim is to use the data to deduce expressions capturing the effect of host growth rates on these viral traits. On the other hand, the lack of information about the mechanism underlying lysis prevents us from making an informed decision on the functional form for L (and, therefore B) just based on available data (see below).

## 2.1   Data compilation

Table 2.2 summarizes the main characteristics of all the data sets we could compile for the infection of *Escherichia coli* by T-phages (the most studied infection). In all data sets, *E* and *M* were either directly reported or the original data provided, which facilitated our extraction of the traits values. Original data (OrD) provided the number of virions per infected cells, i.e the ratio between the number of plaque-forming unit (PFU) and the number of infected centers (IC) at each interval of time. In order to extract the values of *E* and *M* from this data, we used the definition of eclipse period and maturation rate. The eclipse period is the time after infection at which the first intracellular virion is assembled (i.e the time where the ratio PFU/IC equals 1). The maturation rate is defined as the increase rate of intracellular virions from the eclipse period until the lysis, approximating the increase as a linear function of time (You, Suthers, and Yin 2002; Rabinovitch, et al. 1999). *M* is thus provided as the slope of the PFU/IC over the time between *E* and *L*.

*Table 2.2: Compilation of data from literature.*

| Source | Host | Phage | Temperature (°C) | Factor to control the host growth | Data for fits |
|--------|------|-------|------------------|-----------------------------------|---------------|
| You et al., 2002 | *E. Coli* | T7 | 30 | dilution rate | Extracted from OrD |
| Birch et al., 2012 | *E. Coli* | T7 | 37 | carbon sources | Extracted from OrD |
| Hadas et al., 1997 | *E. Coli* | T4 | 37 | carbon sources | From reported data |
| Golec et al., 2014 | *E. Coli* | T4 | 37 | dilution rate | Extracted from OrD |

Based on the only publication that provides the original data and also reports $E$ and $M$ (You, Suthers, and Yin 2002), Fig.(2.2) shows that our extracted points qualitatively agree with the reported points.

In the case of (Hadas, et al. 1997), we used an updated version of the dataset provided by (Rabinovitch, et al. 1999) that used moving averages, as the original dataset showed a high level of noise (Choua and Bonachela 2019). The older dataset did not change qualitatively our results. Moreover, we pooled the updated dataset with data extracted from Golec et al. (2014), as both experiment used the same temperature and phage. This combination of dataset allows a more complete picture of plasticity as Golec et al. (2014) focused on low-growth rates only.
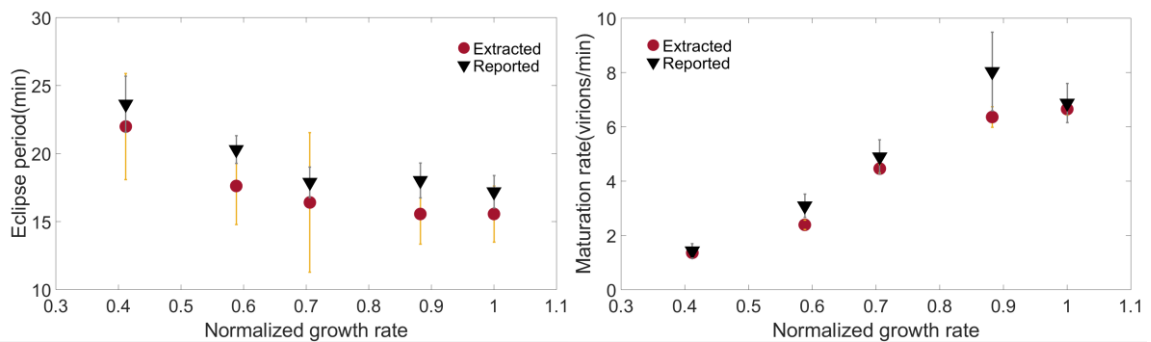


*Figure 2.2: Data exctracted from the original one-step growth experiment data in You et al. (2002) (red circles) and values provided in the publication (black reverse triangle). Left: Eclipse period, E; Right: Maturation rate, M. The maximum growth rate used for normalization is $\mu_{max} = 1.7\ h^{-1}$.*

## 2.2    Data Analysis

To enable comparison across experiments, we normalized the host growth rate $\mu$ dividing it by the maximum growth rate ($\mu_{max}$) reported in each experiment. These $\mu_{max}$ are compatible with previous published data that provide the growth rate of E. coli in optimal conditions at the respective temperature (Herendeen, VanBogelen, and Neidhardt 1979). Such normalization does not influence qualitatively the results. In all experiments, the plots of the extracted values for each growth rate show a decreasing eclipse period with an apparent plateau that occurs for high growth rates (see Fig.2.3 left column). On the other hand, the curve of the maturation rate shows a slow

start for low growth rates that accelerates for intermediate growth rates, followed by a slowdown for high host growth rate (see Fig.2.3 right column). The combination of the data from (Hadas, et al. 1997; Rabinovitch, et al. 1999) with those from (Golec, et al. 2014) connect reasonably well, suggesting a negligible effect of the factor used to control the host growth on viral traits (see Table 2.2 and Fig.(2.3) middle row).

In order to capture the dependence of $E$ and $M$ on the normalized host growth rate, $\mu_n$, we explored different custom fittings to the data with parameters that can be biologically meaningful. Thus, we used a parametric fit on the data using the Matlab Curve Fitting Toolbox with the Nonlinear Least Square method and the Trust-region algorithm to adjust the coefficient (algorithm by default in Matlab that is an improvement over the Levenberg-Marquardt algorithm which is the other option available in Matlab R2018a). Based on graphical results and two goodness of indicators, the Adjusted R-square ($Adj.R^2$) and the normalized root-mean-square deviation (NRMSD), we selected the best equations that match all sources separately (see Fig.(2.3)).
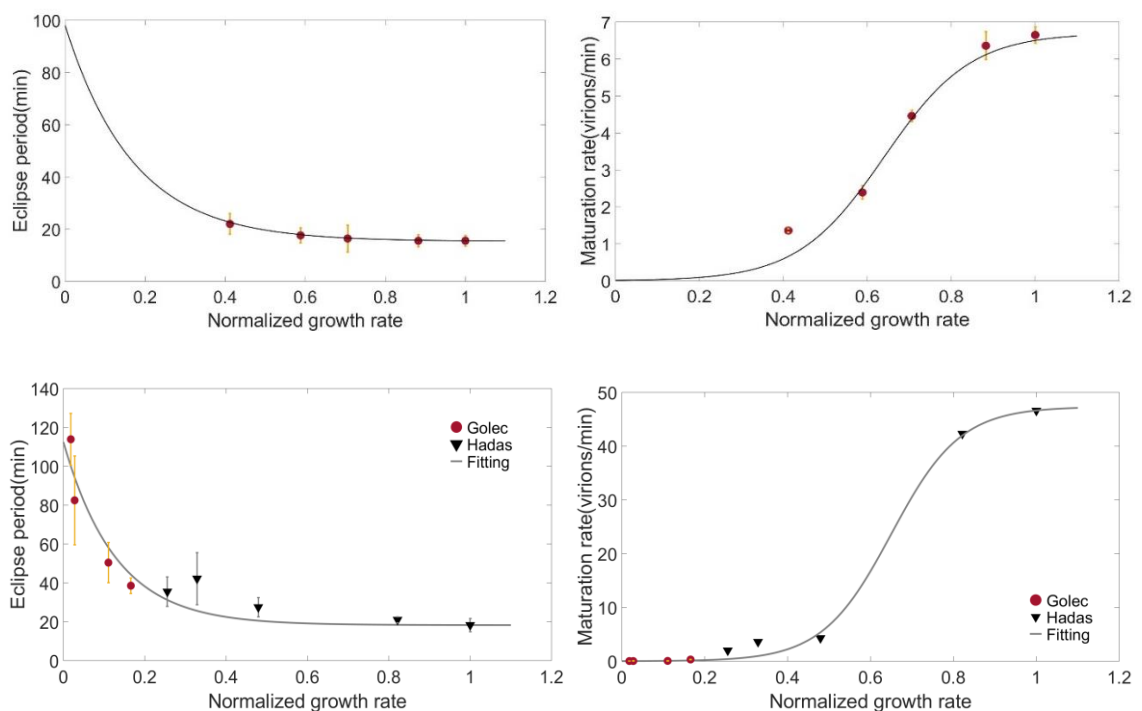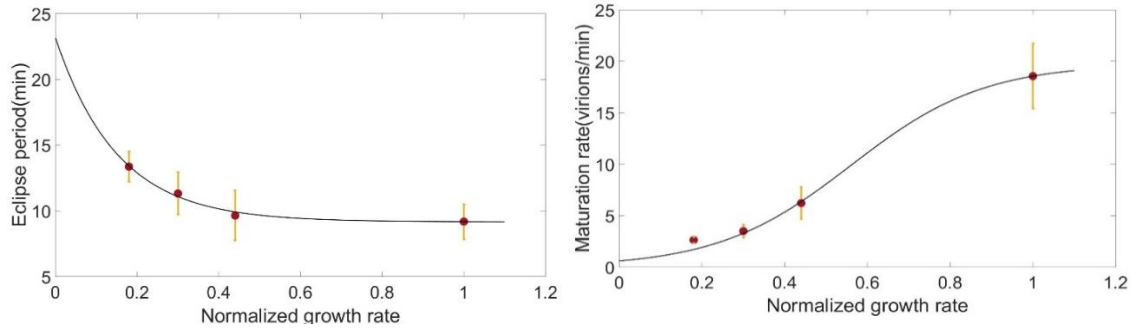
*Figure 2.3: Data extracted (red circle) or reported (black reverse triangle) from the one-step growth experiment in You et al. (2002) (top lane), Golec et al. (2014) and Rabinovitch et al. (1999) (middle lane) and Birch et al. (2012) (bottom lane). The curve correspond to our fit (Table 2). Left: Eclipse period, E, Right: Maturation rate, M. The maximum growth rate used for normalization is respectively from top to bottom; $\mu_{max} = 1.7\ h^{-1}$, $\mu_{max} = 1.8\ h^{-1}$ and $\mu_{max} = 1.5\ h^{-1}$.*

As shown in Fig.(2.3) (left panels), Equ.(2.13) captures the eclipse period behaviour showing high values for very low growth rates given by $E_\infty$ and $E_0$ that decrease at the rate $\alpha_E$ until the non-zero minimum-value plateau (see values of parameters and indicators in Table 2.3).

$$E(\mu_n) = E_\infty + E_0 e^{\frac{-\alpha_E}{\mu_n}} \qquad (2.13)$$

The indicators of closeness show particularly-high goodness of fit at the expense of high error bars for some of the obtained parameters due to the few points per dataset and the three parameters contribution (see Table 2.3). In some cases, we forced the fitted curve to pass through the $E(\mu = \mu_{max})$ value of the database, effectively defining $E_\infty$ and thus reducing the number of parameters. Other functions with a reduced number of parameters have also been tested, e.g:

$$E(\mu_n) = E_\infty e^{\frac{-\alpha_E}{\mu_n}} \qquad (2.14)$$

This function assumes that the virus requires infinite time to produce its proteins when the host growth rate is null, effectively preventing viral

production. Although initially a plausible assumption, experimental data show that viral reproduction is still possible for very low growth rates (Golec, et al. 2014); moreover, low growth rates may instead lead to lysogenic infections (Erez, et al. 2017). Finally, such function does not capture the minimum-value plateau apparent in the data. For these reasons, we opted for Eq.(2.13) to represent the eclipse period.

The behaviour of the maturation rate (Fig.(2.3), right panels) is qualitatively well described by a sigmoid function:

$$M(\mu_n) = \frac{M_\infty}{(1 + e^{\alpha_M(\mu_n - M_0)})} \tag{2.15}$$

where $M_\infty$ represents the saturation plateau at high growth rate, $\alpha_M$ how fast such plateau is reached, and $M_0$ the position of the inflexion point of the function.

*Table 2.3: Parameters obtained with the chosen functional forms for E and M, Eq. (2.13) and (2.15).*

| Equations | Parameters | You | Birch | Hadas+Golec |
|---|---|---|---|---|
| $E(\mu_n) = E_\infty + E_0 e^{\frac{-\alpha_E}{\mu_n}}$ | $E_\infty(min)$ | 15.33 (2.38) | 9.16 (1.42) | 18.26 (3.58) |
| | $E_0(min)$ | 82.71 (34.29) | 14.00 (12.6) | 94.18 (25.12) |
| | $\alpha_E$ | 5.9 (1.0) | 6.62 (4.30) | 7.76 (4.15) |
| | Adj. $R^2$ | 0.99 | 0.98 | 0.89 |
| | NRMSD | 0.017 | 0.063 | 0.109 |
| $M(\mu_n) = \frac{M_\infty}{(1 + e^{\alpha_M(\mu_n - M_0)})}$ | $M_\infty(vir.\,min^{-1})$ | 6.7 (0.7) | 23.14 (13.75) | 47.32 (6.82) |
| | $M_0$ | 0.64 (0.09) | 0.68 (0.31) | 0.65 (0.04) |
| | $\alpha_M$ | 9.70 (8.45) | 4.33 (2.49) | 12.03 (2.83) |
| | Adj. $R^2$ | 0.98 | 0.99 | 0.99 |

| | NRMSD | 0.076 | 0.017 | 0.027 |
|---|---|---|---|---|

Although other qualitatively similar functions may also fit the data, the selected fittings are robust across experiments and their related coefficients are biologically meaningful.

## 2.3    Biological justification

The biological interpretation of the selected functional forms $E(\mu_n)$ and $M(\mu_n)$, stems from how the changes in host growth affect viral protein synthesis machinery and rates. An increase in the host growth rate leads to an increase in the rate of protein synthesis due to an increase of ribosome and tRNA concentration (Bremer and Dennis 2008). Consequently, it takes less time to the host machinery to produce all the viral proteins, inducing a decline in $E(\mu_n)$ until reaching a lower plateau that may correspond to physiological limits for synthesis (see chapter I section 4.1). For similar reasons, $M(\mu_n)$ increases reaching a saturation plateau that can be limited to ribosome efficiency or late protein expression (see chapter I section 4.1).

This biological interpretation is consistent with how these curves change for across phage strains and temperatures (see Fig. (2.4)). For a same host growth rate, an increase in temperature reduces the time of viral protein synthesis and increases the maturation rate. According to (Farewell and Neidhardt 1998), for a constant temperature regardless of growth rate, the elongation rate of ribosomes is fairly constant only the number of ribosomes changes; however, when the temperature increases, not only the number of ribosome but also the elongation rate increases. This renders a cell with a same host growth rate more efficient as temperature increases, which could explain the differences between the curves at 30C and 37C for the phage T7:  reduction in the difference between synthesis time for low and high growth rate, decrease in the minimum plateau for $E$ and increase in the assembly rate, $M$. Comparing

phage T7 and T4 at the same temperature shows an increase in the synthesis time but a better performance for the maturation rate. The fact that T7 produces its own RNA polymerase, more efficient, may contribute to a decrease in the synthesis of proteins (Calendar 2006) but may entail an excess of RNAp in the cell, which limits the maturation rate (more details in chap I section 4.1). The closeness of the eclipse period curve for T7 at 30C and T4 at 37C may indicate a compensating effect of temperature over host RNAp performance for T4.
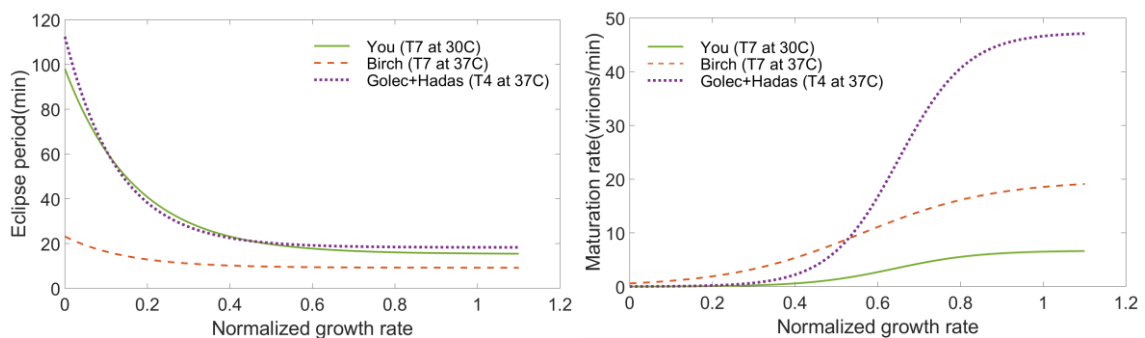


*Figure 2.4: Compilation of the three data-informed curves obtained for E (left) and M (right) which, with table 2, helps to understand the role of the temperature and viral species on viral plasticity.*

## 2.4   The trade-off latent period — burst size

Eqs.(2.13) and (2.15) represent the E and M as a function of the host growth rate but… what about L and B?

In spite of the experimental and theoretical work done (see chap I section 3.4 and 4.2), the mechanism behind the timing of lysis remains largely unknown. Evolution seems to be key in the timing of lysis (see chap. I section 3.4) and experiments revealed that L is not only a long term response obtained by natural selection but also presents a short term response that depends on the host quality ((You, Suthers, and Yin 2002) ; Webb *et al.*, 1982; Hadas *et al.*, 1997; Golec *et al.*, 2014). The latent period decreases with increasing host growth rate. We thus use here a trait-based approach that merges evolution and ecology where different L (and their associated B) characterize different virus populations (see further details in section 3). When those populations compete

against each other, a phenotype emerges as a result of ecological interactions rather than being prescribed. This emerging phenotype (see our results in the next chapter) sheds light on the mechanism underlying the timing of lysis and shows how plasticity affects such timing.

This timing is important as it also determines the burst size, which sets an obvious life-history trade-off: "immediate release but smaller offspring" or "delayed release but larger offspring". Mathematical expressions can capture this trade-off. For example, assuming that the number of intracellular phage is limited and declines with time because the host resources (concentration in nucleotides, ATP, t-ARN, etc.) decreases as they are used but not replenished (Wang et al. (1996)):

$$B = \frac{M}{\gamma}[1 - e^{-\gamma(L-E)}] \qquad (2.16)$$

where $\gamma$ is the specific rate of decline of host-synthesizing machinery, and $M$ and $E$ are considered constant. Although this simple expression captures phenomenological complicated molecular dynamics, the value of $\gamma$ is difficult to parametrize. Moreover, evidences show that the time needed to deplete host resources is much larger than the latent period, thus simplifying Eq.(2.16) to (Rabinovitch, et al. 1999; Wang 2006):

$$B = M(L - E) \qquad (2.17)$$

Considering the viral plasticity, the burst size can be rewritten as:

$$B(\mu) = M(\mu)(L - E(\mu)) \qquad (2.18)$$

# 3. Ecological and Evolutionary Analyses

To obtain an initial understanding about the effect of viral plasticity on the long-term behaviour of the system above, we analyse the ecological and evolutionary stationary states. The ecological stationary state is obtained by calculating the solutions to the equations $dN/dt = dC/dt = dI/dt = dV/dt = 0$, while the evolutionary stationary state is obtained by studying the stability of such equilibrium when a mutant challenges it (more details below).

According to Charles Darwin (1859), the basic principle of evolution is the survival of the population that presents the highest *capacity to survive and reproduce* (i.e. *fitness*). By natural selection, mutations that improve the fitness in a specific environment see their frequency grow generation after generation.

Evolutionary models are useful to gain insight on the role of natural selection in shaping life history characteristics. In 1973, John Maynard-Smith applied Game Theory (i.e. in which the gain of a player results in the losses of the other players that share the same environment) to study natural selection. He introduced the concept of Evolutionary Stable Strategy (ESS), the strategy which, once adopted by a population in a specific environment, cannot be displaced through natural selection by any other alternative strategy (Maynard-Smith 1982).

ESSs can be calculated through Evolutionary Invasion Analysis, which is a technique that uses differential equations to study the stability of the stationary state of a resident population when perturbed by an invader (i.e mutant) (Dercole and Rinaldi 2008). This analysis is based on a few assumptions: (i) populations reproduce asexually (i.e cloning), (ii) the magnitude of mutations is small and (iii) mutations rarely happen, which means that mutant populations either die, replace the resident population, or coexist with the resident before a new mutant arises (Dercole and Rinaldi 2008). The latter assumption is equivalent to assuming that evolutionary changes are substantially slower than ecological changes, which implies that the ecological steady state is reached before a mutant population enters the

medium. This facilitates an analytical approach to calculate the ESS (see further details in chap III). However, for microbial systems, where evolutionary change occurs in timescales comparable to ecological timescales, this assumption might fail to capture potential feedback loops between ecology and evolution, for example overlooking the influence of plasticity on the long-term behaviours of the system. This eco-evolutionary feedback loop refers to the fact that, for rapidly evolving organisms, ecological interactions alter evolutionary processes, which in return affect ecological processes (see Fig.2.5).
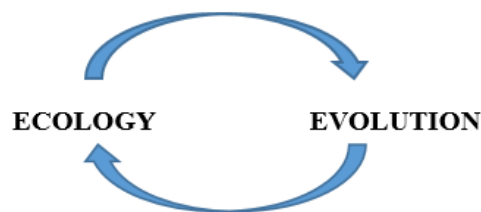


*Figure 2.5: feedback loop between ecology and evolution*

In order to capture a potential feedback loop between ecology and evolution in our system, we included our ecological model (Eqs.(2.1)-(2.4)) in an unconstrained evolutionary framework successfully employed by Bonachela and Levin (2014). In this computational framework, both ecology and evolution can occur at the same timescale, which thus allows the potential interaction of phenotypic plasticity and evolution but precludes the analytical calculation of a closed expression for the ESS. Thus, starting with an initial viral and host populations, Eqs. (2.1)-(2.4) are integrated providing the ecological dynamics of the system. At a random time, not necessarily coinciding with the ecological steady state, mutants originate from the parental phenotype through a genetic algorithm. This algorithm selects randomly the parental population that mutates with a probability proportional to the its population size (Menge and Weitz 2009); the phenotype with the highest probability to be selected for mutation is the one with the highest relative abundance in the system. At any given time, multiple resident and mutant phenotype populations compete against each other until,

eventually, a phenotype arises by natural selection that cannot be invaded by any other mutant. Such a strategy is the ESS.

Although bacteria can also show plasticity, here we focus on viral plasticity only. On the other hand, evolution is considered for the virus only (chapter III), then for both virus and host (see chapter V).

# CHAPTER III

# An emergent latent period

In spite of the experimental and theoretical work available, the effect of the host physiology on the ecological and evolutionary dynamics of the phage-host system remains largely unknown. Here, we aim to fill this knowledge gap by addressing the following questions: How does viral plasticity affect the evolutionary response of the latent period and burst size? How do these trait changes affect the ecological interactions between host, phage, and environment in the short-term?

To answer to these questions, we include the functional forms representing viral plasticity in the standard host-phage model described in chapter II. We first study the long-term ecological and evolutionary behaviour of the system for different host growth rate, μ, to deduce the expression of the latent period, $L(\mu)$, and burst size, B(μ). Then, we use these expressions, which allow us to include a fully plastic virus (i.e. all fours traits respond to change in the host), in diverse short-term scenarios to compare the outcome of plastic and nonplastic descriptions.

Note that the following study has been recently published (Choua and Bonachela 2019).

# 1. Methodology

## 1.1 Environment

We focus here on the evolution of the virus only. When host and virus coexist for long enough, however, the bacteria is expected to also adapt to the environment and/or to the phage (Weitz, Hartman, and Levin 2005). Host adaptation resulting from coexistence between bacteria and virus can be avoided in the lab by frequently diluting cells and re-establishing the culture with fresh ones (Bull, et al. 2006). One of such setups is two-stage chemostats (see Fig.3.1), in which a first chemostat contains a culture of the host supplied (and nutrients supporting growth), and such culture "feeds" the second chemostat where the interaction with the phage happens (Husimi Y Fau - Nishigaki, et al. 1982). Such a setup thus reduces the evolutionary pressure on the host, allowing us to focus on the evolution of the phage only.
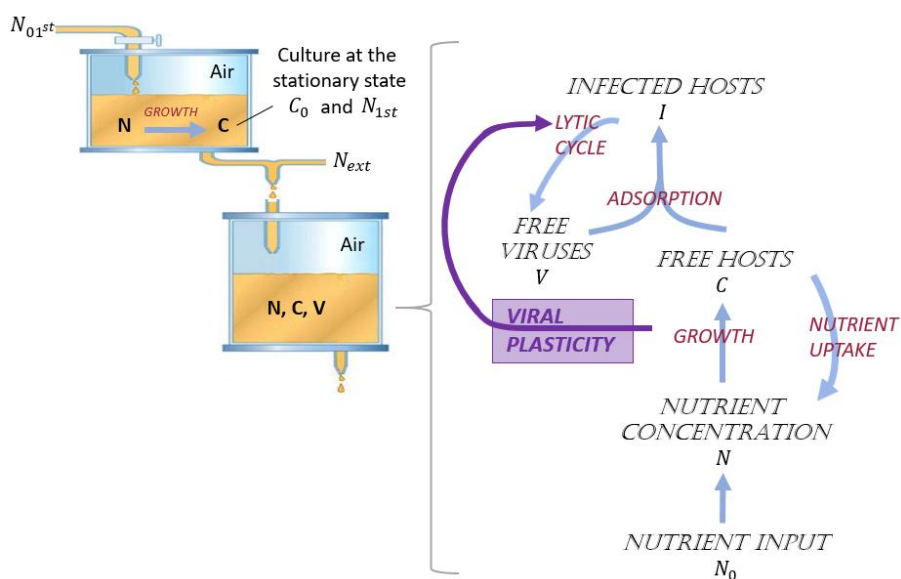


*Figure 3.1: two-stage chemostat setup with the flow diagram showing the interactions for host, phage, and environment as described by Eqs. (2.1) to (2.4) (blue arrows) and the role of plasticity (purple arrow). Black type represents the state variables whereas red type represents processes.*

Note that the inflow and outflow rates (i.e. $w$) are equal across the system in order to keep a volume of the culture constant. Because the first chemostat can be described by the equations:

$$\frac{dN_1(t)}{dt} = w(N_{01^{st}} - N_1) - \mu\, C/Y \tag{3.1}$$

$$\frac{dC(t)}{dt} = (\mu - w)\, C \tag{3.2}$$

the stationary state of nutrient and bacterial concentrations in the first chemostat are given by:

$$N_{1st} = \frac{w\, K_n}{\mu_{max} - w} \tag{3.3}$$

$$C_0 = Y\, (N_{01^{st}} - N_{1st}) \tag{3.4}$$

(see symbols and units in table 3.1). Eq. 3.4 reveals that we can control the concentration of fresh hosts entering in the second chemostat ($C_0$) independently from $N_{1st}$ by changing $N_{01^{st}}$. In order to also be able to control independently the inflow of nutrient in the second chemostat (i.e. $N_0$), we add an external source of nutrient $N_{ext}$ to the output of the first chemostat to compose the total input: $N_0 = N_{1st} + N_{ext}$ (see Fig. 3.1). This $N_0$ is one of the ways we will use to alter the host growth rate in the second chemostat. Following the experiments compiled here, see table 2.2, we will alternatively control the host growth rate via the dilution rate, $w$, or using different sources of carbon, which we emulate by using a variety of growth affinities (i.e. $K_n$).

## 1.2 The second chemostat

The equations describing the dynamics occurring in the second chemostat are provided by Eqs. (2.1)-(2.4). As the host does not evolve, we consider a single-host phenotype (i.e. a fixed host size). This entails constant host trait values, which we parametrize based on the literature. Regarding the virus, eclipse period, $E$, and maturation rate, $M$, are determined by the host growth rate following Eqs. (2.13) and (2.15). For these expressions, we used the parameters obtained when fitting the You et al. (2002) database (i.e. T7 phage infecting E.Coli at 30C), the most complete dataset (see chapter II). The two remaining traits, $L$ and $B$, emerge from our evolutionary framework (see more details below).

*Table 3.1: Symbols for variables used in the model and parameter values.*

| Symbol | Description | Units | Value | References |
|---|---|---|---|---|
| N | Dissolved Inorganic Nutrient Concentration | mol l$^{-1}$ | Ecological variable | Eqs. (2.1) – (2.4) |
| C | Non-infected Host Concentration | cell l$^{-1}$ | Ecological variable | |
| I | Infected Host Concentration | cell l$^{-1}$ | Ecological variable | |
| V | Free Virus Concentration | cell l$^{-1}$ | Ecological variable | |
| $\mu$ | Non-infected Host population Growth Rate | d$^{-1}$ | Ecological variable | (Monod 1949) |
| $\mu_{max}$ | Maximum Host Population Growth Rate | d$^{-1}$ | 40.8 | (You, Suthers, and Yin 2002) |
| $K_n$ | Half-Saturation Constant the Nutrient | mol | $10^{-6}$ to $2 \times 10^{-4}$ | Range fixed by sensitivity analysis and supported by (Füchslin, Schneider, and Egli 2012; Schulze and Lipe 1964) |
| Y | Yield Parameter | cell mol$^{-1}$ | $9 \times 10^{13}$ | Sensitivity analysis |
| k | Adsorption Rate | l virus$^{-1}$ d$^{-1}$ | $9 \times 10^{-10}$ | (Delbrück 1940) |
| E($\mu$) | Eclipse Period | d | Eq. (2.8) | This thesis |
| M($\mu$) | Maturation Rate | virion d$^{-1}$ | Eq. (2.9) | This thesis |
| L | Latent Period | d | Evolutionary variable | This thesis |
| B | Burst Size | virions cell$^{-1}$ | B = M (L-E) | (Wang 2006) |
| w | Chemostat Dilution Rate | d$^{-1}$ | 0.24 to 21.84 | range fixed by sensitivity analysis |
| $C_0$ | Non-infected Host Supply Concentration | cell l$^{-1}$ | $10^7$ to $10^8$ | fixed by sensitivity analysis |
| $N_0$ | Dissolved Inorganic Nutrient Supply Concentration in the second chemostat | mol l$^{-1}$ | 45 to $2000 \times 10^{-6}$ | range fixed by sensitivity analysis |
| $N_{1st}$ | Dissolved Inorganic Nutrient in First chemostat | mol l$^{-1}$ | calculated Eq. 3.1 | — |
| $N_{ext}$ | External Source for Dissolved Inorganic Nutrient | mol l$^{-1}$ | $N_0 = N_{1st} + N_{ext}$ | — |

| $N_{01^{st}}$ | Dissolved Inorganic Nutrient Supply in the first chemostat | mol l⁻¹ | calculated Eq. 3.2 | – |
|---|---|---|---|---|

## 1.3 Long-term behaviour

*Ecological long-term behaviour*

The ecological steady state in the second chemostat results from solving the equations $dN/dt = dC/dt = dI/dt = dV/dt = 0$. The trivial solution is $V_{st} = I_{st} = 0$, $C_{st} = w\ C_0/(w - \mu)$, and $N_{st} = (w\ N_0 - \mu_{st}\ C_{st}/Y)/w)$ with $w > \mu > 0$, while the solution that ensures coexistence between host and virus is:

$$C_{st} = \frac{(w + m)}{k\ (Be^{-wL} - 1)} \tag{3.3}$$

$$I_{st} = k\ C_{st}\ V_{st}(1 - e^{-wL})/w \tag{3.4}$$

$$V_{st} = \frac{(\mu_{st} - w)}{k} + \frac{w\ C_0}{k\ C_{st}} \tag{3.5}$$

For the nonplastic case, the stationary value of the nutrient concentration, $N_{st}$, is:

$$N_{st} = (-G \pm \sqrt{G^2 + 4FH})/2F, \tag{3.6}$$

with:

$$F = w > 0 \tag{3.7}$$

$$G = K_n\ w + \mu_{max}\ C_{st}/Y - w\ N_0 \tag{3.8}$$

$$H = K_n w\ N_0 > 0; \tag{3.9}$$

Because this non-trivial state of the system requires $N_{st} > 0$, the sign of $G$ determines the sign in front the square root in Eq. 3.6. For the plastic case, the fact that $\mu(N_{st})$, and L and B in turn depend on $\mu$, does not allow for a closed form for $N_{st}$.

We can also analyse the evolutionary stationary state by studying the stability

of the system when a mutant threatens this equilibrium.

*Evolutionary long-term behaviour*

As described in chapter II section 3, we conduct invasion analyses to estimate the evolutionary long-term behaviour (i.e. Evolutionary Stable Strategy, ESS) for the virus. As we do not know what determines $L$ and therefore $B$, we consider them evolutionary variables and let them emerge from our framework. In doing so, we assume that evolution affects only the *holin* gene on the viral DNA, which controls the latent period, $L$ (see chap I section 3.4). Thus, the viral genotype is characterized by the *holin* gene (and the viral phenotype by the latent period).

Therefore, in an invasion analysis a mutant virus characterized by a fixed $L = L_M$ (and its associated $B = B_M$) enters in a small amount in the medium that has reached its ecological steady state with the resident viral population ($L_R$) and host. Thus, we study the stability of the system after being perturbed by this mutant. If the system is unstable, the mutant displaces the resident, and vice versa. Covering any combination of mutant and resident, the ESS is the $L_R$ for which no mutant can invade. Thus, for a stationary state of the resident virus and the host (i.e. $C = C_{R_{st}} = C_{st}$, $I = I_{R_{st}}$ and $V = V_{R_{st}}$), we study the stability of the system of equations:

$$\frac{dI_M(t)}{dt} = kC_{st}V_M - (kC_{st}V_{M\,t-L_M})e^{-wL_M} - w\,I_M \tag{3.10}$$

$$\frac{dV_M(t)}{dt} = \left(B_M kC_{st}V_{t-L_M}\right)e^{-wL_M} - kC_{st}V_M - mV_M - wV_M \tag{3.11}$$

where $C_{R_{st}}$ is obtained from Eq. (3.9) with $L = L_R$. The system dynamics now revolve around these two equations only because the mutant is initially rare, and therefore $C_R$ and $V_R$ stay at their stationary values, $N$ stays around $N_{st}$, and

thus the host growth rate remains constant as well.

The stability of the system is given by the sign of the eigenvalues $\lambda$ obtained by solving the characteristic equation $\left| J + J_D e^{-\lambda L} - \lambda \mathbb{I} \right| = 0$ (Beretta 2001), with $J$ the jacobian matrix associated with the instantaneous term of Eqs. (3.12)-(3.13), $J_D$ the jacobian of the delayed terms, and $\mathbb{I}$ the identity matrix. The $L$ that leads to negative eigenvalues (i.e. a stable system) for any invader provides the $L_{ESS}$.

Repeating this analysis for several environmental conditions, which leads to several host growth rates, provides a first approximation for the $L_{ESS}(\mu)$ curve that aims at understanding the factors that influence plasticity in the latent period (and similarly for the burst size).

## 1.4    Unconstrained framework to calculate the ESS

The analytical approach above requires important assumptions such as ecological stationarity before any mutant enters the system. This explicit separation of the ecological and evolutionary timescales risks overlooking the dynamic influence of plasticity on the ESS.

Under realistic conditions, plasticity and evolution may interact (i.e. eco-evolutionary feedback loop, see chap II section 3). We thus need a numerical framework in which both ecological interactions and mutations can occur at the same time. To that end, we integrate Eqs. (2.1)-(2.4), considering that a pair of Eqs.(2.3) and (2.4) are added for each mutant that joins the system. New mutants are introduced in the system following a genetic algorithm (see chap. II section 3). Then, the multiple viral populations compete for the only host until, eventually, a viral phenotype arises that cannot be invaded by any other mutant (i.e. the ESS). This ESS is, thus, the latent period that maximizes fitness (i.e. $L_{ESS}$ is the most competitive phenotype) and will dominate the system in the long term even in presence of all possible phenotypic variability for the virus. Because ecology and evolution occur at the same timescales, this

numerical approach therefore does account for the dynamic impact of plasticity on the ESS. Thus, we compile the $L_{ESS}$ for different host growth rates, which facilitates an expression for $L_{ESS}(\mu)$ and $B_{ESS}(\mu)$.

## 1.5 Dynamic scenarios

Once we obtain $L_{ESS}(\mu)$, and therefore $B_{ESS}(\mu)$, we use a fully-plastic representation of the virus (i.e. all four traits depending on μ) to gauge how phage plasticity alters ecological prediction in the short-term. We explore three consecutive dynamic scenarios characterizes by sudden changes in nutrient availability ($N_0$): a big pulse of nutrient that brings the host to its maximum growth rate, a smaller pulse that takes the host to 70% of its maximum growth rate, and a scarcity period that reduces the host growth rate to below 50% of its maximum growth rate. Each of these events lasts 20 days and are separated by acclimation period of 20 days that sets the host growth rate to approximately half of its maximum. With this setup, we compare the predictions of three different versions of the model: (i) one that ignores phages, (ii) a nonplastic description of the phage; and (iii) our plastic description. We also repeat this same process for a parametrization that allows oscillations in the system in order to analyse the effect of plasticity on the antagonist oscillations.

# 2. Results

## 2.1 $L_{ESS}(\mu)$ estimated with invasion analyses

When the invading mutant perturbs the stable state of the resident population, the sign of the eigenvalues λ provides the condition for the strategy L to resist any invasion. The eigenvalues λ associated with the characteristic equation

$|J + J_D e^{-\lambda L_M} - \lambda \mathbb{I}| = 0$ are given by:

$$\begin{vmatrix} kC_{R_{st}}(B_M e^{-(w+\lambda)L_M} - 1) - w - m - \lambda & 0 \\ -kC_{R_{st}}(e^{-(w+\lambda)L_M} - 1) & -w - \lambda \end{vmatrix} = (F(\lambda) - \lambda)(G - \lambda) = 0$$

(3.12)

Because the trivial solution $\lambda_1 = G = -w$ is always negative, the stability of the system is determined by the sign of $\lambda_2 = F(\lambda) = kC_{R_{st}}(B_M e^{-(w+\lambda_2)L_M} - 1) - w - m$. Thus, we can focus on the condition $\lambda_2 = 0$, which leads to:

$$F(0) = kC_{R_{st}}(B_M e^{-(w+0)L_M} - 1) - w - m = 0 \leftrightarrow kC_{R_{st}}(B_M e^{-wL_M} - 1)$$
$$= m + w ;$$

$$C_{R_{st}} = \frac{m+w}{k(B_M e^{-wL_M} - 1)} \xleftarrow{using\ Eq.(3.3)} C_{R_{st}} = C_{M_{st}}$$

(3.13)

If $C_{R_{st}} < C_{M_{st}}$, then $\lambda_2 < 0$. Consequently, for the resident to resist any invasion it has to require a smaller host concentration than the mutant. Therefore, like in classic resource competition theory where the species, with the lowest resource requirement depletes the available resource to levels that no can survive with other species (Tilman 1982), the ESS is given by the virus that presents a $L$ minimizing the host concentration, which maximizes its fitness. Mathematically, the ESS is thus the solution to the equation $dC_{st}/dL = 0$, which leads to $dB/dL = w\,B$. Either way, using Eq.(2.18) we finally reach the expression for the ESS:

$$L_{ESS} = \frac{1}{w} + E(\mu_n)$$

(3.14)

This expression, together with Eq. (2.18), provides the burst size:

$$B_{ESS} = \frac{M(\mu_n)}{w}$$

(3.15)

where $w$ is contributed by the exponential term in Eq. (3.13) that represents the removal rate of intra-cellular virions (i.e. infected hosts). As shown in

(Bonachela and Levin 2014), this evolutionary solution is convergence-stable (i.e. uninvadable strategy even by phenotypes in the neighbourhood of the ESS).

The plastic potential of the viral latent period is thus encoded in the eclipse period, $E$, whereas it is expressed through the maturation rate in the burst size. Note that these expressions are valid regardless of the specific details of $E(\mu)$ and $M(\mu)$ functions. Due to the assumption of the ecological stationarity for the host, those expressions are similar to those obtained in the nonplastic case. We can thus obtain $L_{non}$ and $B_{non}$ from Eqs. (3.14) and (3.15) by fixing the host growth rate to its maximum value (i.e. corresponding to the optimal condition of the host).

$$L_{non} = L_{ESS}(\mu_n = 1) = \frac{1}{w} + E(1) \, , \ \ B_{non} = B_{ESS}(\mu_n = 1) = \frac{M(1)}{w} \qquad (3.16)$$

## 2.2  $L_{ESS}(\mu)$ estimated with the unconstrained framework

Using our eco-evolutionary framework, the ecological interactions including plasticity, together with evolution, give rise to trait dynamics such as those shown in Fig. 3.2. This figure shows the value of the latent period for the most dominant phenotype in the system, although many different phenotypes compete for the same host at any given time, which ensures a wide trait distribution for the population (see whiskers in the figure). These trait dynamics allow the system to explore the phenotypic space until the ESS is eventually found. Because this exploration is intrinsically stochastic, the evolutionary stationary state value ($L_{ESS}$) for each example, results from the mean value of the dominant phenotype at the end of 300 replicate simulations.
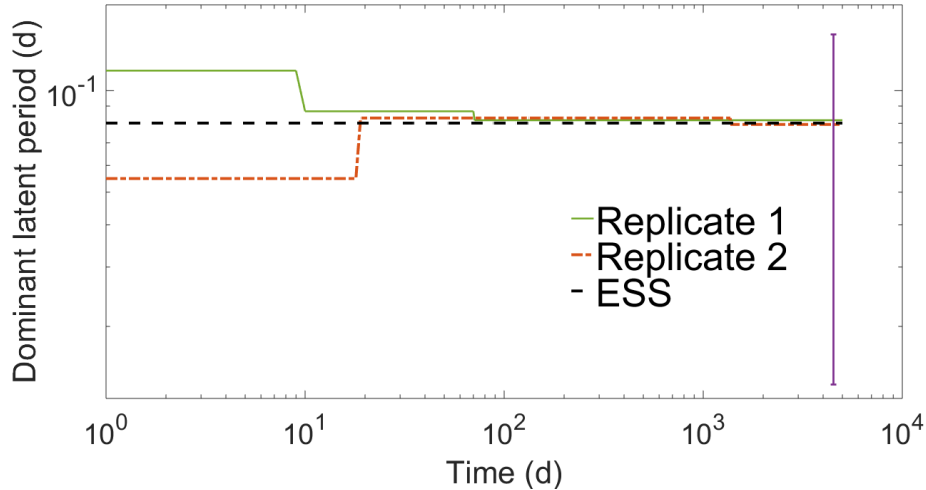
*Figure 3.2: Evolutionary path in two different replicates for $N_0 = 10^{-4}\ mol\ L^{-1}$ and $w = 15\ d^{-1}$, showing the convergence to the ESS by alternation in the dominant (i.e., most abundant) phenotype; B shows a similar road to reach $B_{ESS} \sim 146\ virion\ host^{-1}$. The whiskers represent the range of diversity of latent period sampled by the system for t > 4000 d in replicate 1.*

Compiling the ESS for several µ allows us to construct $L_{ESS}(\mu)$. First we vary µ by tuning the input concentration from $N_0 = 7.10^{-5}\ mol\ l^{-1}$ to $N_0 = 2.10^{-3}\ mol\ l^{-1}$, fixing $K_n = 9.10^{-5}\ mol\ l^{-1}$ and the dilution rate to $w = 15\ d^{-1}$. This variation gives respectively host growth rates ranged from $\sim 15.5\ d^{-1}$ to $\sim 39.0\ d^{-1}$, revealing a positive correlation between $\mu(N_{st})$ and $N_0$ that cannot be inferred easily from the stationary state equations (see Eq. 3.6). Fig.3.3 shows the $L_{ESS}$ and $B_{ESS}$ obtained in such environments, and the analytical expression calculated for such range of host growth rate which we also added as a reference.
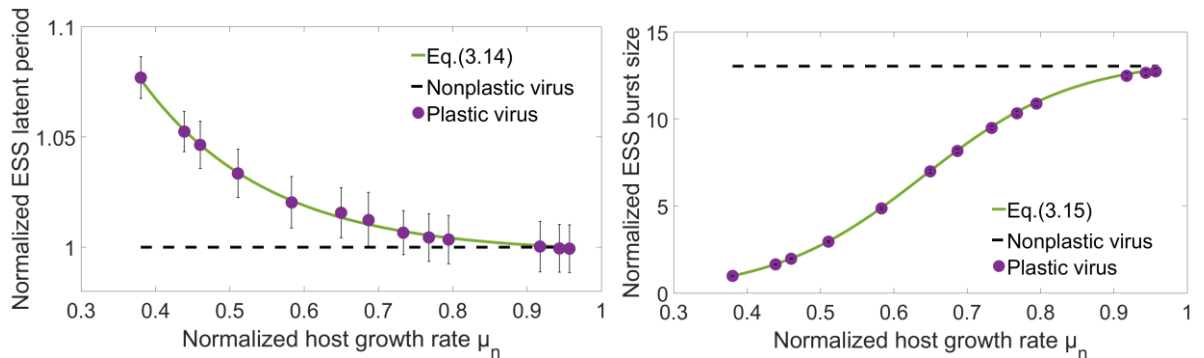


*Figure 3.3: Evolutionary results from theory (solid line) and averaging over simulations (points) obtained when altering the host growth rate using $N_0 = 7 \times 10^{-5} mol\ L^{-1} - N_0 = 2 \times 10^{-3} mol\ L^{-1}$, with $w = 15\ d^{-1}$ and $K_n = 9 \times 10^{-5} mol\ L^{-1}$. The whisker in all simulation results represent the standard deviation across replicates, and the dashed line represents the value that typical models ignoring plasticity would use. Both plastic curves and data have been normalized using the minimum value obtained in the simulations, while the nonplastic description shows the $\mu_{max}$ value for the traits. Left, latent period, L. Right, burst size, B. ESS= evolutionary stable strategy.*

Fig.3.3 shows that, within the range of host growth rates, there is ~ 8% decrease in $L_{ESS}$, while there is ~ 13 –fold increase for $B_{ESS}$. Thus, an increase in host growth rate leads to a higher burst size and a smaller latent period, which is opposite to the usual positive correlation between L and B. Thus, plasticity breaks the classic trade-off between those traits (see Fig.3.4).
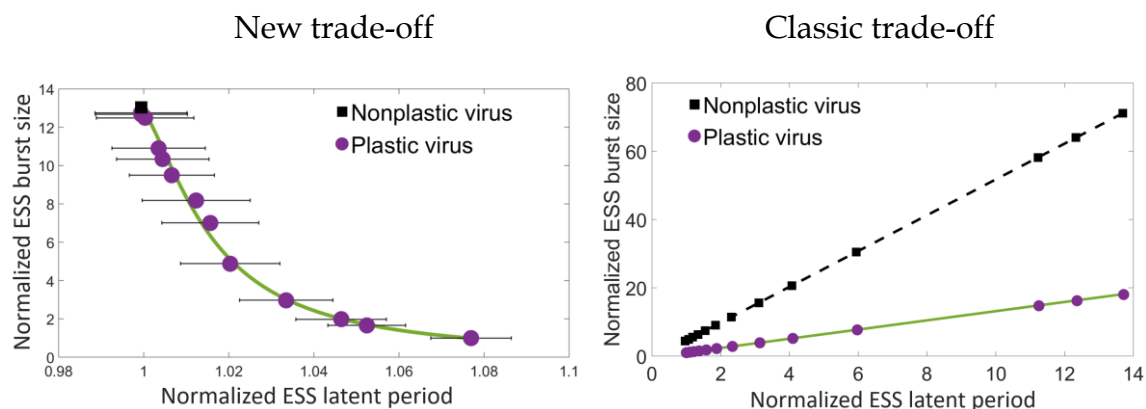


*Figure 3.4: Burst size as a function of the latent period for the evolutionary stable strategy (ESS) in the case where $N_0$ is used to control µ (left), breaking the classic trade-off observed when w is used to control µ (right).*

With this new trade-off, the virus improves its performance with host growth rate, which leads to an increase of viral individuals and a significant decrease in the concentration of hosts (see Fig. 3.5 left). In consequence, $L_{ESS}$ increases with the stationary concentration of free hosts while the nonplastic description for the system shows a number of free hosts that barely depends on the host growth rate (see black dots in Fig. 3.5).
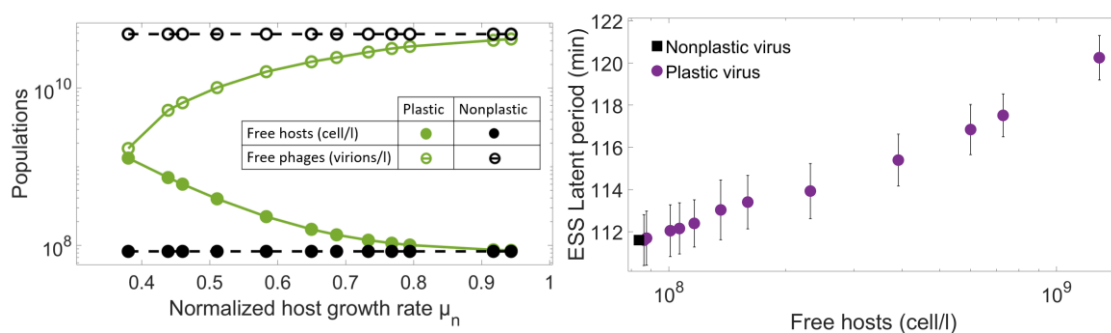


*Figure 3.5: Left, host and viral concentration as a function of the normalized growth rate. The dashed lines represent the predictionof a nonplastic description. Right, emergent $L_{ESS}$ as a function of the availability of hosts, $C_{st}$, when $N_0$ is varied to control the host growth rate as in the previous figure.*

Similar results are observed when varying the host growth rate using different $K_n$ values. $K_n$ directly affects $N_{st}$ and $\mu(N_{st})$ (see (see Eqs. 3.6-3.9 and Eq. (2.5)) leading to a negative correlation between $K_n$ and μ . When using the dilution rate to alter the host growth rate, $N_{st}$ shows an approximately constant value for any $w$ which translates into a very limited range of variation for μ. The analytical approach (Eqs. 3.6 and 3.8) shows that the associated variation in $C_{st}$ leads to a negligible contribution of $G$ to the overall nutrient concentration, and therefore $N_{st} \approx \sqrt{H/F}$ , which in turn leads to an approximately constant growth rate. Fig. 3.6 (left and right) shows the negligible role of plasticity on the qualitative form of the ESS due to these small changes in μ. Indeed, varying $w$ mostly affects the denominator in Eqs. (3.14) – (3.15), which dominates over the plastic term. This negligible effect of plasticity leads to the classic trade-off (positive correlation) between $L_{ESS}$ and $B_{ESS}$ (see Fig. 3.4 right), and a $L_{ESS}$ that decreases as the free host population increases (oppositely to Fig. 3.5 right). See table 3.2 for a conceptual summary. In Fig. 3.6, we observe that, in spite of the approximately constant host growth rate, varying $w$ provides an emerging picture that is quantitatively different between these cases especially for the burst size due to the significant difference between $M(\mu_n)$ in the plastic case and $M(1)$ in the nonplastic case (see Fig. 3.6).
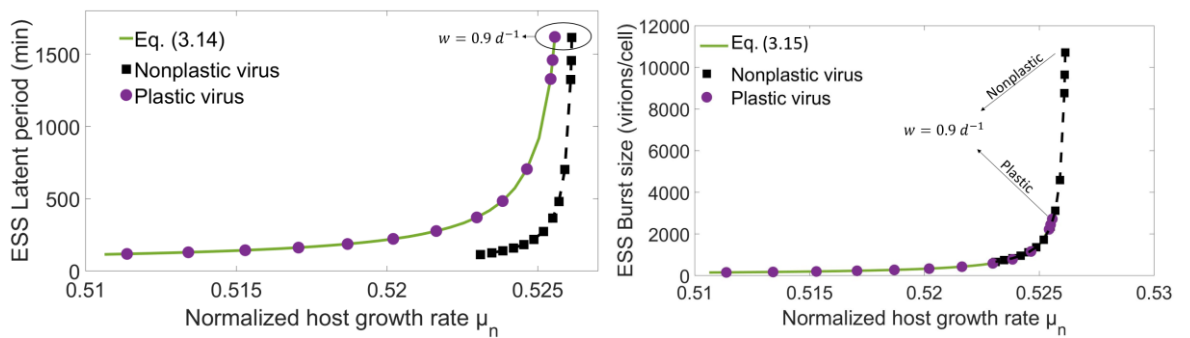


*Figure 3.6: : Evolutionarily stable strategy (ESS) obtained modifying the growth rate through $w = 0.9\ d^{-1}$ to $w = 15.1\ d^{-1}$, with $N_0 = 10^{-4}\ mol\ L^{-1}$ and $K_n = 9\ x\ 10^{-5}\ mol\ L^{-1}$. Left: emerging latent period as a function of host growth rate. Right emerging burst size as a function of the host growth rate.*

*Table 3.2: summary of the ecological and evolutionary expectations when varying the parameter $N_0$, $K_n$ and $w$. ⬆ means "increases" and ⬇ means "decrease".*

| Variation | $\mu_{st}$ | $C_{st}$ | $V_{st}$ | $L_{ESS}$ | $B_{ESS}$ |
|---|---|---|---|---|---|
| $N_0$ ⬆ | ⬆ | ⬇ | ⬆ | ⬇ | ⬆ |
| $K_n$ ⬇ | ⬆ | ⬇ | ⬆ | ⬇ | ⬆ |
| $w$ ⬇ | ⬆ | ⬇ | ⬆ | ⬆ | ⬆ |

## 2.3    Dynamic scenarios

With these expressions for $L_{ESS}(\mu)$ and $B_{ESS}(\mu)$, we can now focus on understanding how a fully-plastic description of the virus alters our expectations regarding the short-term population dynamics of the host-phage system, to this end, we compare the predictions of three different versions of the model (without virus, with nonplastic virus and with plastic virus) under dynamic environmental conditions. Specifically, we study a sequence of nutrient-related events (big pulse of nutrient, smaller pulse and scarcity period). We check this dynamic for different parametrizations: one that leads to a stable equilibrium and another one to a cycle limit in order to analyse the effect of plasticity on the oscillations.

### *Stable equilibrium*

The absence of virus allows the bacterial population to follow the qualitative behaviour of the nutrient input (i.e. higher nutrient leads to increases in population density and vice-versa, see Fig. 3.7). On the other hand, the nonplastic virus responds to free host variations and maintains the host population around a baseline level throughout the whole experiment. Different (fixed) phage parametrizations can alter quantitatively this baseline. Finally, with our plastic description, the free host population shows a counterintuitive behaviour as it decreases when the nutrient availability increases and vice versa. The qualitative behaviour of the host population thus radically differs across descriptions. Plastic and nonplastic descriptions and associated behaviour match quantitatively and qualitatively only when $\mu = \mu_{max}$ during the big pulse event.
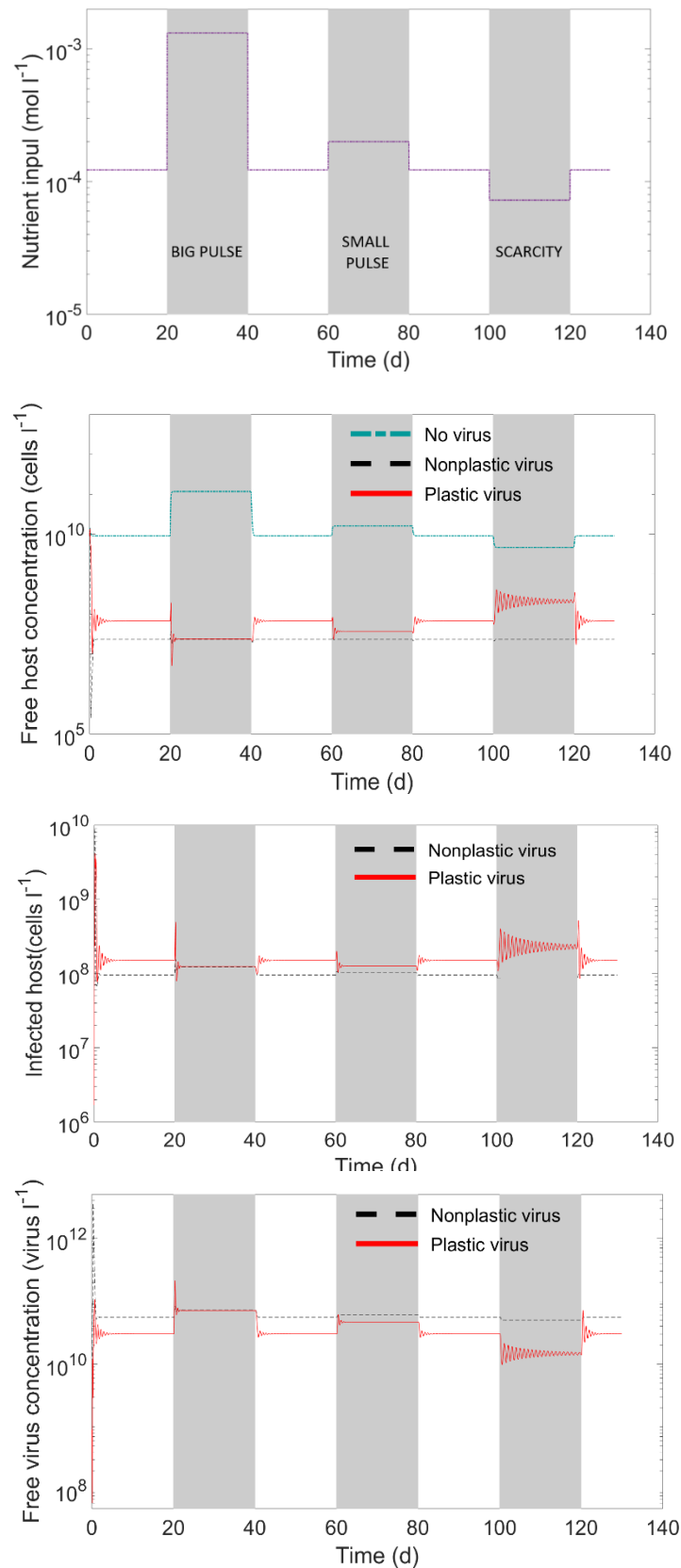
*Figure 3.7: Dynamic of one replicate of the two-chemostats setup for three different events (shaded areas) in which the nutrient inflow brings the host growth rate, respectively to $\mu \cong \mu_{max}$, $\mu \cong 0.7 * \mu_{max}$, $\mu = 0.55 * \mu_{max}$ , comparing a version of the model with no viruses to another one with nonplastic viruses and our plastic description. Top: nutrient profile. Second: available hosts concentration. Third: free phages concentration. Bottom: infected hosts concentration.*

*Limit cycle*

Reducing the supply of non-infected hosts enhances the possibility of emergent population oscillations. To analyse this oscillatory behaviour, we thus repeat the same simulation with $C_0 = 10^7$ for a high and low dilution rates ($w = 17d^{-1}$ and $w = 8.16d^{-1}$). We also alter the pulses to ensure the survival of both host and virus in all of the three nutrient-related events (see Fig. 3.8).
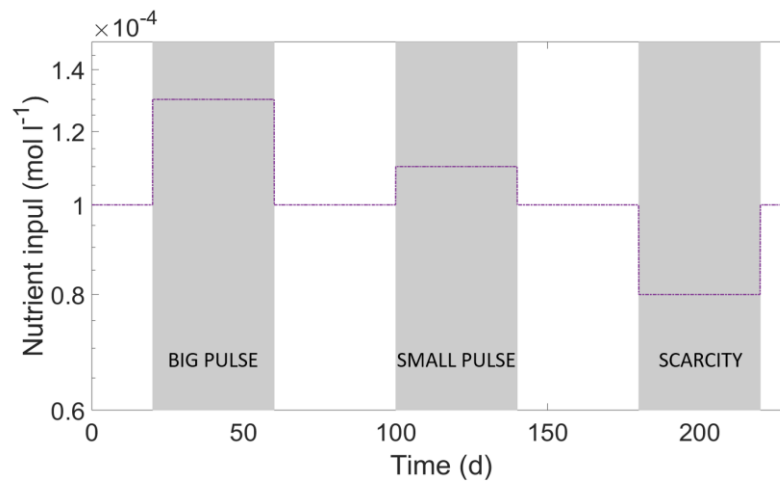


*Figure 3.8: Nutrient profile used in the second chemostat with $C_0 = 10^{-7}cells\ l^{-1}$ for three different events (shaded areas)*

$$w = 17d^{-1}$$                    $$w = 8.16d^{-1}$$
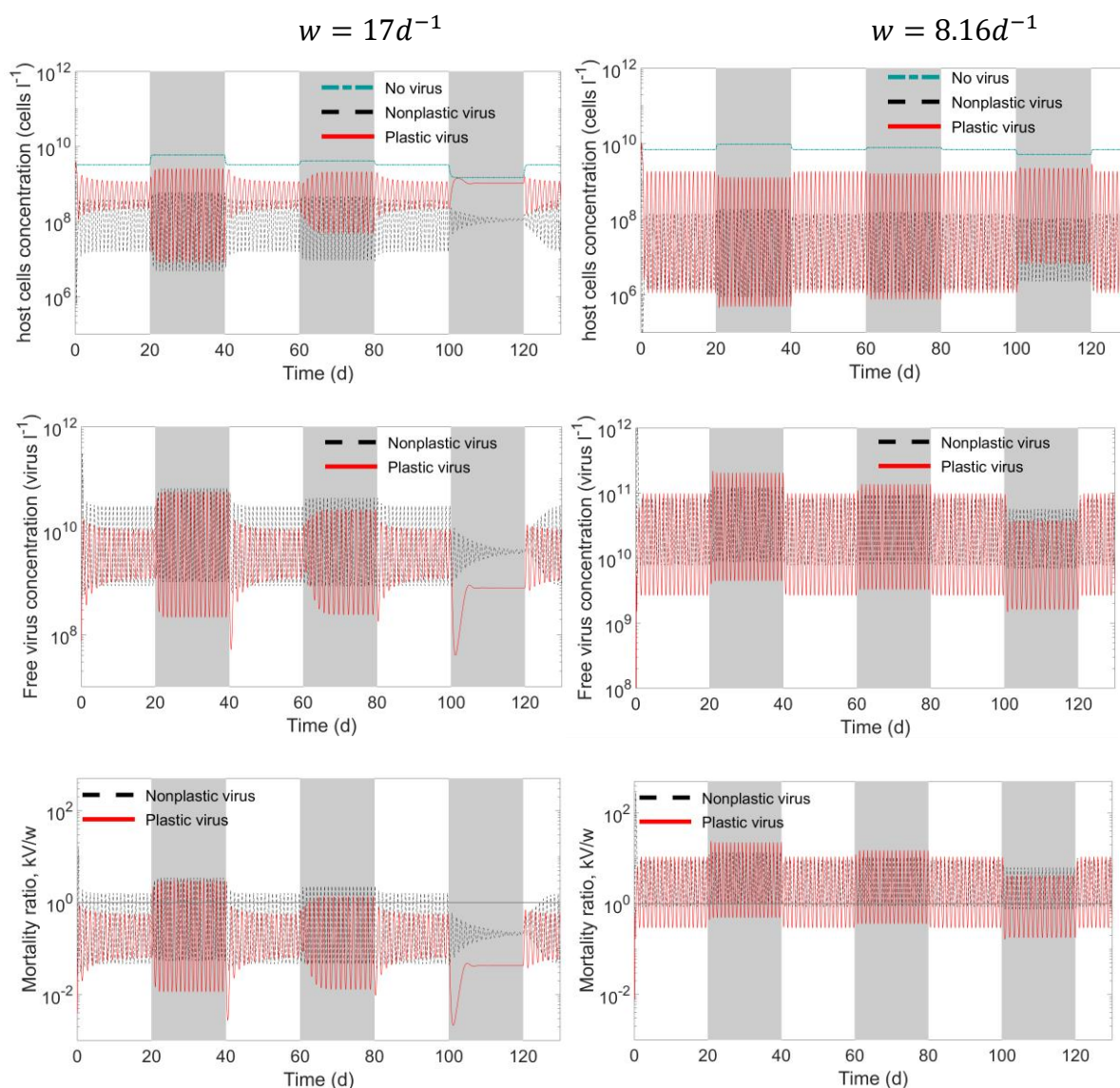


*Figure 3.9: Dynamics of one replicate of the two-chemostats setup for three different events (shaded areas), comparing a version of the model with no viruses to another one with nonplastic viruses and our plastic description. Top: available host concentration. Middle: Free virus concentration Bottom: ratio of bacterial mortality sources (i.e. viral mortality/dilution) with a grey line showing when the ratio equals 1.*

Without viral pressure, the hosts do not show oscillations and the bacteria follow the qualitative behaviour of the nutrient input (see Fig.3.9). The comparison of the relative amplitude of the host oscillations between the plastic and the nonplastic case are, however, unexpected. The ratio shows that the amplitude for the plastic case is smaller than that of the nonplastic case for most of the events at high dilution rate. On the other hand, low dilution rates lead to bigger oscillations. The bottom of the bacterial oscillations is the part most affected by the nutrient pulses while the top part of the oscillations concentrates the main difference between plastic and

nonplastic cases. The ratio of the source of bacterial mortality (i.e. viral mortality divided by mortality by dilution) shows the dominance of the viral-induced mortality for low dilution rates, and vice-versa.

# 3. Discussion

We used experimental data available to describe how T-phage $E$ and $M$ change with the host growth rate. We then embedded these functional forms $E(\mu)$ and $M(\mu)$ in an eco-evolutionary model to study analytically and computationally the effect of such plasticity on the remaining traits $L$ and $B$. We thus obtained the $L(\mu)$ curve from the optimal lysis timing emerging under various growth conditions that, with the eclipse period and maturation rate, determines $B(\mu)$. These results show how plasticity affects all four traits and its effects on the host and phage populations.

Our results agree with most of experimental work on viral plasticity a decreasing latent period and increasing burst size as growth rate increases (You, Suthers, and Yin 2002; Hadas, et al. 1997; Birch, Ruggero, and Covert 2012). They also agree on the degree of plasticity for $B$ significantly higher than for $L$, for example,(Abedon, Herschler, and Stopar 2001)) reported a mild influence of plasticity on $L$ while (Webb, Leduc, and Spiegelman 1982)) reported a 18-fold variation in $B$ as $\mu$ increases. Importantly, our results for $L(\mu)$ and $B(\mu)$ curves do not depend on the shape of the $E(\mu)$ and $M(\mu)$ see Eqs. (3.14) and (3.15).

## 3.1 Mechanism underlying the observed latent periods

Previous studies have stated that host density plays a role in the selection of the viral lysis timing (Abedon 1989; Wang, Dykhuizen, and Slobodkin 1996; Weitz and Dushoff 2008); low host cell density favours the survival of phages with a longer latent period to optimize the utilisation of host cell resources

while there is no other host to infect. We do observe such negative correlation between $L$ and host density but only when plasticity is negligible (i.e. when we tune $w$). On the contrary, an opposite trend occurs when plasticity is significant. Our results reveal that, in these cases, $L$ results from the timing for infected-cell removal ($w^{-1}$ term in Eq. 3.14) and from the plasticity in synthesis time (encoded in $E(\mu)$). A lower infected-cell removal, which increases the survival probability of latent offspring and decreases the abundance of available hosts, favours the survival of phages with a longer latent period. This small infected-cell removal rate (i.e. a small $w$) dominates over the plastic term, which thus leads in a small effect of plasticity on $L$. A higher $w$, however, results in a more noticeable plasticity for $L$, especially at lower $\mu$, which matches with high host density. This result is in line with past theories about the increasing role of plasticity in determining the length of latent period when host density is high (Wang, Dykhuizen, and Slobodkin 1996).

The classical expectation is that a longer latent period provides a bigger burst size (i.e. classic trade-off). We observe such classic positive correlation between $L_{ESS}$ and $B_{ESS}$ when controlling the host growth rate by tuning $w$ (i.e. when plasticity is negligible). However, a noticeable plasticity breaks this trade-off and reveals that an increase in host performance allows the phage to produce more virions with a shorter lytic cycle. This effect is due to the high sensitivity of the maturation rate to the host performance, which lead us to the hypothesis that the importance of viral plasticity does not reside in the generation time but rather in the burst size, in line with (Abedon, Herschler, and Stopar 2001).

This viral plasticity is limited, as the physiological range of the host lead to saturation of $M$ and $E$ at high $\mu$. Such limitations have been overlooked in the few existing attempts that include plasticity in dynamic models (Weitz and Dushoff 2008; Middelboe 2000; Rabinovitch, et al. 2002).

## 3.2 Plasticity inverts expectations for population dynamics

The wide variation in the burst size due to the difference in host performance can alter the ecological predictions of the host and phage populations. Plasticity adds non-trivial interactions between free hosts and phages affecting the feedback between host, virus, and environment (Fig. 3.1).

During a pulse of nutrient, the density as well as the physiological state of the host firstly increases. A nonplastic virus responds only to the variation in host density, increasing viral population, which leads to a constant density of available hosts (e.g., baseline C in Fig. 3.7). The plastic virus responds to both host density and the rise in host performance, which intensifies phage-induced mortality, enabling a higher phage reproduction in less time. For this reason, the density of hosts decreases when the host growth rate increases. On the other hand, during the starvation period the host growth is lower, which leads to a poorer viral performance and a consequent relief of viral pressure, leading to an increase of host density.

## 3.3 Plasticity reinforces the dynamic feedback between host, virus and environment

The feedbacks between host, virus, and environment emerging from viral plasticity can be most clearly observed in the sustained oscillatory behaviours.

The growth of the host population increases the competition for nutrient as well as the probability of viral infections. The consequent decrease in the host growth rate leads to a smaller burst size and longer infection time for the virus, which maintains these low-performing hosts at higher levels than the nonplastic virus (i.e. low part of the oscillations of the bacterial population is higher in the plastic case). However, in some cases (e.g. at low dilution rates), the lower viral production can be compensated by the higher host availability and leads to a viral population that reaches higher maximal values than the nonplastic virus. This extra population of virus drives later the bacterial population to lower values than in the nonplastic cases, resulting in bigger amplitude of oscillations. If the lower virulence of the plastic virus is not

compensated by the increase in host availability (e.g. at high dilution rates, or during the starvation period at low dilution rates), the plastic virus cannot draw the bacterial densities below the expectation from nonplastic models, resulting in smaller oscillation amplitudes. In any case, due to the lower virulence for low host growth rates, the recovery time for [C], [I], and [V] is significantly increased in the plastic description, which increases the delay among the three curves and consequently increases the oscillation period.

## 3.4 Applicability and limitations

Considering viral plasticity can improve the predictions regarding primary production of standard biogeochemical models. Our plastic expressions could be potentially adapted for such models, as the two-stage chemostat, inflow, and outflow of hosts and nutrient roughly represent a volume of oceanic water. In a more general approach, such flows could also represent those in the human gut, and therefore our expression could be extended to viruses affecting the human microbiome.

Note that our numerical framework is suitable for stationarity, but stationarity is hardly ever reached in nature. Moreover, although experimental work supports our plastic relationship between $L$ and $B$, and thus the underlying mechanisms, additional experimental information is required to improve and generalize our theory across systems, thus contributing to advancing our understanding of host-phage interactions.

Finally, accounting for a more accurate description of the phage (e.g., including the possibility of a lysogenic switch), or the host, may alter our expressions for the most dominant viral phenotype. In chapter V, we study how our results change when including the evolution of the host size, which affects its physiological state as well as the viral adsorption rate. First chapter IV delves in how viral plasticity affects the stability of the host-virus system.

# 4. Conclusion

Our results reveal plastic expressions that help to represent the dynamic phenotypic diversity of viruses without invoking genetic changes. Because these host-induced trait changes are an unavoidable feature of bacteriophages, our expressions render the model more realistic while keeping it simple, as it captures the influence of environmental variations without having to rely on parametrisation changes. This latter shows the variable effect on the host population that may help to unravel the complexity of host-phage interactions.

# CHAPTER IV

# The effect of viral plasticity on the persistence of host-virus systems

Viral plasticity revealed dramatic differences with respect to standard predictions that neglect such plasticity (Edwards and Steward 2018; Choua and Bonachela 2019). We saw in the previous chapter that it can affects the strength and timing of the interactions between host, virus and environment, including the emergent oscillations between host and phage (Choua and Bonachela 2019), which raises the question of the effect of viral plasticity on system stability and persistence. Many theoretical models have highlighted the importance of microbial phenotypic plasticity in their ecological interactions (Mougi and Kishida 2009; Ramos-Jiliberto, Duarte, and Frodden 2008; Hoverman 2010; Yamamichi, Yoshida, and Sasaki 2011; Bonachela, Raghib, and Levin 2011; Lomas, et al. 2014), for host-virus systems, however, it remains less well studied.

Few models have studied plasticity in host-virus system, for example, analysing how the host responded plastically to viral infection through a decrease in the receptor density at the host surface (Thyrhaug, et al. 2003) or how the viral plasticity affects the interactions (Edwards and Steward 2018; Choua and Bonachela 2019). Host-virus models with host plasticity show that the inducible defence of the host to changing infection levels resulted in an increase of the probability of coexistence between host and phage. Models that include plasticity in viral traits revealed dramatic differences with respect to standard predictions that neglect viral plasticity. Indeed, viral plasticity

affects, for example, the strength and timing of the interactions between host, virus and environment, including the emergent oscillations between host and phage (Choua and Bonachela 2019). None of these models, however, focused explicitly on studying the effect that viral plasticity can have on system stability and coexistence.

Here, we aim to understand whether viral plasticity makes coexistence between host and virus more or less likely. Specifically, we focus on understanding whether the existence of viral plasticity affects the region of the trait and environmental parameter space where coexistence is expected. To this end, we contrast the predictions from a classic host-bacteriophage model that neglects viral plasticity, with a version that includes viral plasticity using existing data-informed relationships between viral traits and the host growth rate for the most common host-phage model systems (T-phage infecting *Escherichia coli*). We compare the stability of the plastic and nonplastic version of these systems under a diversity of host and viral traits combinations, as well as under different environmental conditions. We analyse under which conditions viral plasticity translates into an increase of coexistence between host and virus, and how it alters the oscillations typically observed for antagonistic interactions.

# 1. Methodology

## 1.1 Model description

Similarly to the previous chapter, we represent the ecological dynamics of the host-phage system using the Eqs.(2.1)-(2.4). However, here we assume only one chemostat (i.e. $C_0 = 0$) and additionally, we introduce the effective influence of crowding on population growth. As bacteria grow in a limited volume, boundary effects can limit the space around cells as the population increases, triggering competition for space, light, or other resources not explicitly modelled here. We assume the crowding effect to originate mostly

from resource competition, which only affects free hosts as uptake and growth stop at infection (see models assumption in Chapter II). This density-dependent term is often characterized by a quadratic loss term, which has the advantage of preventing or damping oscillations, thus increasing the possibility to reach stability for the system with and without plasticity (Gibert and Delong 2015). These new assumptions lead to modifications in the Eq. (2.2), which becomes:

$$\frac{dC(t)}{dt} = \mu(N,r)\, C - k(r)\, C\, V - w\, C - \alpha\, C^2 \qquad (4.1)$$

This equation describes the growth of the free host population as a result of bacterial reproduction (first term), reduced by infection events (second term), dilution (third term) and crowding (fourth term), in which α represents the crowding strength.

*Host trait set*

In this chapter, the host size, $r$, is the main trait characterizing hosts. Cell size is a "master" trait for most microorganisms including bacteria, i.e. the rest of the host traits depends on size (Litchman, et al. 2007). Although our approach can be generalized to any bacterium, we parameterize the host according to *E.coli*, which allows us to use allometries and trade-offs linking host metabolic rate to its size (Eqs. (2.6) and (2.7)). The size of the host, additionally, affects the viral adsorption rate (see details in Chapter II section 1.2), which we represent by Eq. (2.8).

*Phage trait set and plasticity*

Regarding the viral traits, because the factors that determine the latent period, $L$, are unknown, we use here the latent period as a free parameter characterizing the virus. The burst size, $B$, is represented by the linear function linking, $L$, $M$ and $E$ (see Eq. 2.17), where $E$ and $M$ are represented by the functional forms in Eqs. (2.13) and (2.15).

The parametrisation of the functional forms we use here is based on experiments described in the chapter II, where the host *E.Coli* can reach a maximal growth rate of $40.8\ d^{-1}$ ($\mu_{\mathrm{max}\,experiment}$). At this growth rate, the performance of the host machinery is very high, which is reflected on the viral traits ($E$ and $M$). Here, however, we model different sizes for the host cell and because their $\mu_{max}$ is limited by size through the allometry in Eq.(2.7), the host growth rate cannot reach $\mu_{\mathrm{max}\,experiment}$. For this reason, in order to stay consistent with the experiments, the normalized growth rate ($\mu_n$) that appears in Eqs. (2.13) and (2.15) is here based on $\mu_{\mathrm{max}\,experiment}$, leading to the expressions:

$$E(\mu) = E_\infty + E_0 e^{-\alpha_E\ \mu/\mu_{\mathrm{max}\,experiment}} \tag{4.2}$$

$$M(\mu) = \frac{M_\infty}{1 + e^{\alpha_M\left(\mu/\mu_{\mathrm{max}\,experiment} - M_0\right)}} \tag{4.3}$$

As with classical models, the non-plastic version of the model uses viral traits ($E_{non}$ and $M_{non}$) obtained for a host grown under optimal conditions (i.e. $\mu = \mu_{max}$) (see Chapter III). These values are thus host-specific and, therefore, as $\mu_{max}$ changes with host size ($\mu_{max}(r)$), $E_{non}$ and $M_{non}$ change accordingly as well:

$$E_{non}(r) = E_\infty + E_0 e^{-\alpha_E\ \mu_{\mathrm{max}}(r)/\mu_{\mathrm{max}\,experiment}} \tag{4.4}$$

$$M_{non}(r) = \frac{M_\infty}{1 + e^{\alpha_M\left(\mu_{\mathrm{max}}(r)/\mu_{\mathrm{max}\,experiment} - M_0\right)}} \tag{4.5}$$

With this description, the range of variation of the plastic viral traits increases with the size of the host, thus allowing the plastic effect to be more observable for higher host sizes (see Fig.4.1).
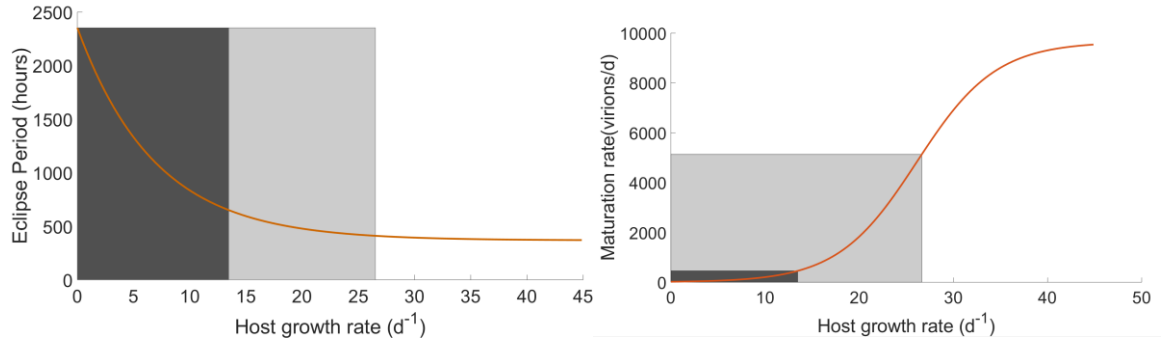
*Figure 4.1: Example of the range of variation for the eclipse period (left) and the maturation rate (right) for a host size of 0.5µm (dark grey rectangular) and 1 µm (clear grey rectangular).*

These expressions enable a plastic and nonplastic description of the burst size:

$$B = \begin{cases} M(\mu_n)\big(L - E(\mu_n)\big) & \text{in the plastic case} \\ M_{non}(r)(L - E_{non}(r)) & \text{in the nonplastic case} \end{cases} \qquad (4.6)$$

## 1.2   Analysis

To study how viral plasticity affects the coexistence of the host-phage system, we identifies four main parameters for which there is limited amount of information available and/or a large associated variability: the host radius, $r$; the viral latent period, $L$; the crowding strength, $\alpha$; and the dilution rate, $w$ (the latter represents environmental conditions). These four parameters define our parameter space. Table 1 shows their range of variation. The range for the host radius provides trait values (volume, $\mu_{max}$ and $K_n$, through Eqs.(2.7) and (2.6)) compatible with experimental observations (Füchslin, Schneider, and Egli 2012; Schulze and Lipe 1964; Loferer-Krößbacher, Klima, and Psenner 1998). We discretise this interval in 41 sections to obtain a computationally reasonable resolution. The range for the latent period covers 22 realistic values for T-phages. The dilution rate is incremented by $1d^{-1}$ until reaching the maximal growth rate possible limited by either the host size (i.e. $\mu_{max}(r)$) or the nutrient availability (i.e. $\mu(N_0)$). Above these values, bacterial growth cannot overcome dilution providing thus analytical limits of coexistence (i.e. Eq. (4.1) is constantly negative due to $\mu < w$) ultimately leading to extinction. Finally, the range for crowding strength is chosen in the order of magnitude

that provides a crowding term that shows values comparable to the rest of terms in Eq. (4.1).

*Table 4.1: Parameter values used in the model*

| Symbol | Description | Units | Value | References |
|--------|-------------|-------|-------|------------|
| N | Dissolved Inorganic Nutrient Concentration | mol l$^{-1}$ | Ecological variable | (Levin, Stewart, and Chao 1977) |
| C | Non-infected Host Concentration | cell l$^{-1}$ | Ecological variable | |
| I | Infected Host Concentration | cell l$^{-1}$ | Ecological variable | |
| V | Free Virus Concentration | cell l$^{-1}$ | Ecological variable | |
| $\mu$ | Non-infected Host population Growth Rate | d$^{-1}$ | Ecological variable | (Monod 1949) |
| **Host parameters** | | | | |
| r | Equivalent spherical radius | $\mu$m | 0.3 – 1.1 | (Loferer-Krößbacher, Klima, and Psenner 1998) |
| $\mu_{max}$ | Maximum Host Population Growth Rate | d$^{-1}$ | Allometry (Eq.2.7) | (Gallet, et al. 2017) |
| c, h | Parameters Eq.5 | – | f=0.33 p=3.8 | (Gallet, et al. 2017) |
| $K_{ref}$ | Half-Saturation constant for $\mu_{max}$ = 0 | mol l$^{-1}$ | 3.05 x 10$^{-8}$ | (Wirtz 2002) |
| $\mu_{ref}$ | Asymptotic $\mu_{max}$ for $K_n$ -> $\infty$ | d$^{-1}$ | 32.4 | (Wirtz 2002) |
| $K_n$ | Half-Saturation Constant for Growth | mol | Allometry (Eq.2.6) | (Wirtz 2002) |
| Y | Yield Parameter | cell mol$^{-1}$ | 9 x 10$^{13}$ | (Choua and Bonachela 2019) |
| $\mu_{max}$ experiment | Maximum Growth Rate in the experiment | d$^{-1}$ | 40.8 | (You, Suthers, and Yin 2002) |
| $\alpha$ | Parameter of crowding effect | l d$^{-1}$ cell$^{-1}$ | 0 - 12 x 10$^{-7}$ | Sensitivity analysis |
| **Viral parameters** | | | | |

| | | | | |
|---|---|---|---|---|
| D | Diffusion of Viral Particle | $m^2 s^{-1}$ | $4.3132 \times 10^{-12}$ | Calculated using Stokes-Einstein expression |
| k | Adsorption Rate | $l\ cell^{-1}\ d^{-1}$ | $4\pi\ D\ Conv_3\ r$ | (Delbrück 1940) |
| $E(\mu)$ | Eclipse Period | d | Eq. (4.2) | (Choua and Bonachela 2019) |
| $M(\mu)$ | Maturation Rate | $virions\ d^{-1}$ | Eq. (4.3) | (Choua and Bonachela 2019) |
| L | Latent Period | d | 0.01 - 1 | (You, Suthers, and Yin 2002; Golec, et al. 2014) |
| B | Burst Size | $virions\ cell^{-1}$ | $B = M\ (L-E)$ | (Wang 2006) |
| **Chemostat parameters** | | | | |
| w | Chemostat Dilution Rate | $d^{-1}$ | 1 - 30 | $\mu_{max}(r_{max})$, Eq.(2.7) |
| N0 | Dissolved Inorganic Nutrient Supply Concentration | $mol\ l^{-1}$ | $9 \times 10^{-5}$ | Sensitivity analysis |
| **Conversion constants** | | | | |
| $Conv_1$ | Constant to convert from (ml) to ($\mu m^3$) | $\mu m^3 ml^{-1}$ | $10^{-12}$ | — |
| $Conv_2$ | Constant to convert from ($hour^{-1}$) to ($d^{-1}$) | $hour\ d^{-1}$ | 24 | — |
| $Conv_3$ | Constant to convert from ($m^3\ s^{-1}$) to ($l\ d^{-1}$) | $l\ s\ d^{-1}\ m^{-3}$ | $86400 \times 10^3$ | — |

To analyse the stability of the ecological interactions (Eqs. (2.1), (4.1), (2.3) and (2.4)) in the parameter space ($r, L, w, \alpha$), we use Matlab computing environment to calculate the stationary states/cycles obtained with the model for each parameter combination. We then classify these outputs into one of these 3 categories: (i) "*no coexistence between bacteria and viruses*", *(ii) "coexistence with oscillations"*, and (iii) "*coexistence without oscillations*". There is no coexistence when the population of either the host or the virus falls below

the threshold of one individual per litre. This threshold avoids unrealistic recovery of effectively-extinct populations. To detect non-oscillatory coexistence, we check if the difference between the last value of the simulation and two other points that are separated in time by 1 and 2.3 days provides a similar value.

Finally, to compare the outcomes above with the predictions for a nonplastic virus, we repeat this analysis with $E = E_{non}$ and $M = M_{non}$. Although analytical expressions can be calculated for the nonplastic case, a closed expression cannot be obtained for the plastic case due to the dependence of $E$ and $M$ on $\mu(N)$. Therefore, for the sake of consistency, we used numerical simulations of the model for both plastic and nonplastic cases.

### *Dimensionality of the parameter space*

After classified the outcomes of all the combinations of the four parameters $(r, L, w, \alpha)$, we proceeded to reduce the dimensionality of the parameter space. To this end, we first select a fixed value for $\alpha$. Because density-dependence helps to stabilize oscillations, the expectation is that this term will contribute to widen the region of the parameter space where coexistence occurs. Thus, for each value of $\alpha$ we counted the number of cases that showed coexistence (with and without oscillations) in both the plastic and the nonplastic cases to focus on those $\alpha$ that provided the highest number of cases showing coexistence. This term, however, should not overwhelmingly regulate the dynamics. Therefore, to ensure that the system remains regulated by the host-virus interaction and not by intraspecific competition solely, we select the $\alpha$ that provides the highest number of cases where the ratio between viral mortality and intraspecific competition is above one (i.e. $k\, C_{st}\, V_{st}/(\alpha\, C_{st}^2) > 1$, where the subscript "$st$" refers to the stationary state obtained by averaging the 20 last days of the simulations that reached a stationary state).

Fixing $\alpha$ reduces the parameter space to 3 dimensions $(r, L, w)$. Simulations for all possible combinations of these three parameters allow us to analyse the

resulting manifold. Specifically, we focus on understanding (i) the boundary between the area of general coexistence and no-coexistence, (ii) the areas where plastic viruses show coexistence but nonplastic viruses do not, and (iii) vice-versa. To this end, we compare the results obtained for different $L$ (i.e. specific slices of the manifold). We also focus on particular host radii in order to explore the role of environmental conditions (represented by the dilution rate, $w$). To quantify whether plasticity makes coexistence more likely, we calculate the percentage of cases where the plastic virus is the only one showing coexistence with the host. Finally, to analyse the effect of plasticity on the emergence of oscillations and underlying mechanisms, we study the population dynamics observed in the "coexistence with oscillations" cases.

# 2. Results

## 2.1 Selection of the crowding strength parameter, α

For different values of $\alpha$, we count the number of cases for which coexistence is found (with and without oscillations) among all the combinations of ($r$, $L$, $w$). Within these cases of coexistence, we also count the number of cases in which the dynamics were dominated by viral mortality over crowding (i.e. $k\, C_{st}\, V_{st}/(\alpha\, C_{st}^2) > 1$).

Figure 4.2 shows the increase in the frequency of simultaneous coexistence (i.e. both host and virus surviving for plastic and nonplastic cases). This stability of the host-phage system increases with $\alpha$ until a certain value, then decreases. The frequency of coexistence when crowding is considered is up to 7 times higher than for $\alpha = 0$. The intraspecific competition parameter $\alpha = 60\, x\, 10^{-9}\, l\, cell^{-1} d^{-1}$ optimizes both the coexistence between bacteria and viruses, for plastic and nonplastic examples, and the cases regulated by viruses. Thus, we fixed the crowding strength to this value for the rest of the analysis.
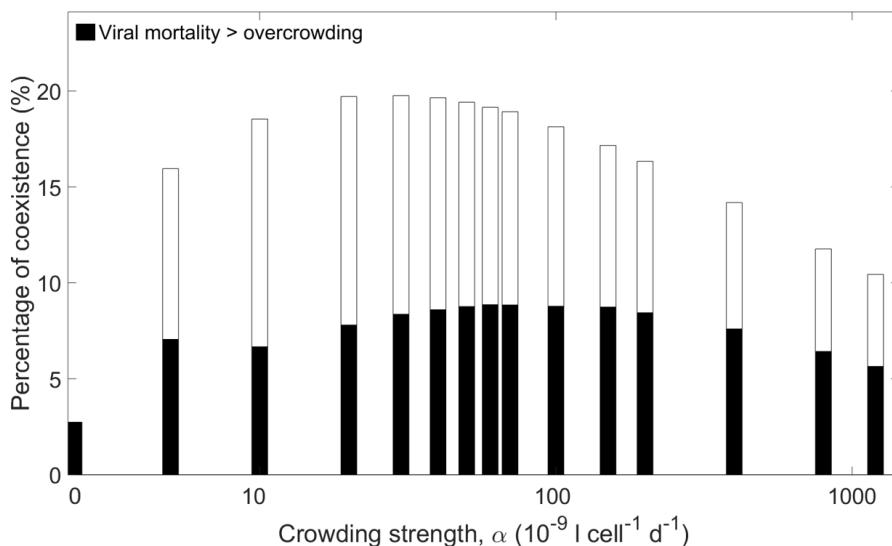
*Figure 4.2: Bar plot representing the number of cases that shows coexistence in both plastic and nonplastic cases (in white) overlapped by the number of cases where viral mortality overcomes the crowding (in plastic and nonplastic cases) within these cases of coexistence (in black).*

## 2.2   Exploration of the $(r, L, w)$ space

The outcome of comparing plastic and nonplastic models in the $(r, L, w)$ space formed a 3D manifold. For a better visulisation, we do not represent the cases where both plastic and nonplastic do not show coexistence (i.e. case 1 in following figures). The resulting manifold shows a consistent pattern that appears along the latent period axis (see Fig.4.3).
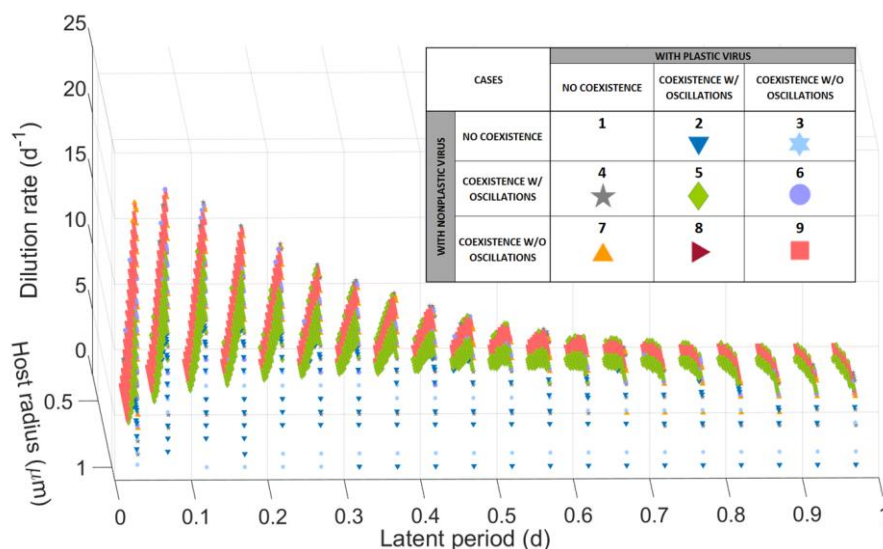


*Figure 4.3: Region of coexistence in the 3D space (latent period, host radius, dilution rate) where the legend of each symbol/colour is represented in the right corner of the figure.*

To further investigate this pattern, we explore slices of the manifold across the latent period axis (in Fig.4.4, $L = 0.07\,d$, $L = 0.47\,d$ and $L = 0.87\,d$). For a fixed latent period, the region of coexistence (with and without oscillations) starts at low-to-intermediate host radii and increases with $r$, becoming narrower at higher host sizes. As the latent period increases, the coexistence region is constrained to smaller dilution rates.
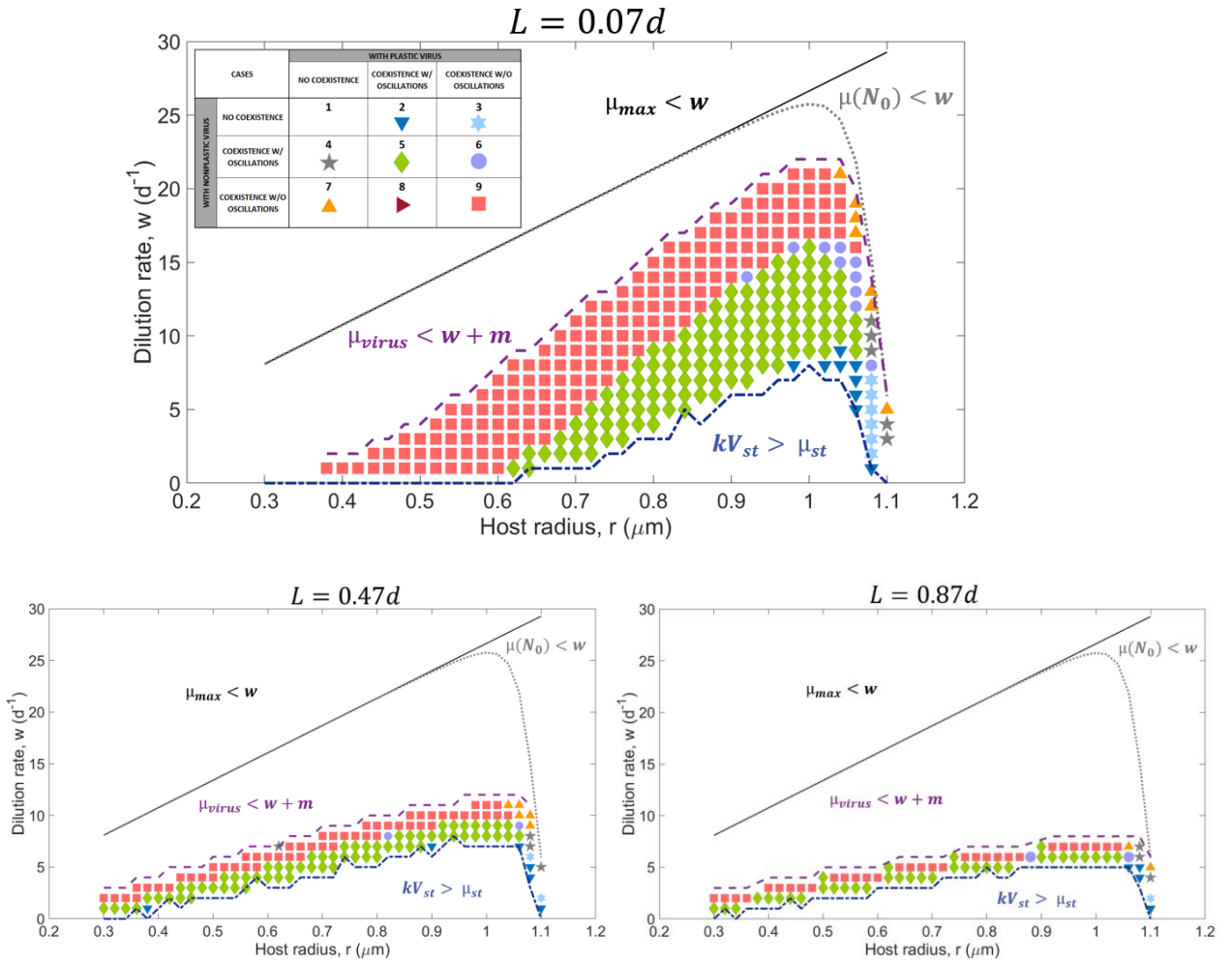


*Figure 4.4: Slices through the region of coexistence for L=0.07d (top), L=0.47d (bottom left) and L=0.87d (bottom right) for $\alpha = 60.\,10^{-9}d\;cell^{-1}$, where the borders between coexistence and non-coexistence explicitly appear. The legend of each symbol/colour is represented in the Table of the top figure.*

In Fig.4.4, we indicate the reasons for the lack coexistence, which allow us to differentiate four different areas of "no coexistence". In the bottom area (delineated by a blue dashed line) the host growth rate at the stationary state is smaller than the per-capita mortality rate induced by viruses, which drives the bacterial population to extinction (followed by the viral population). This

border, constrained to low *w*, reaches higher dilution rates for intermediate host radii. The sharp decrease for host radii bigger than 1 μm coincides with the area where only the plastic virus shows coexistence (blue downward triangles and hexagram) as well as with the size for which the growth is limited by the nutrient concentration in the chemostat (see Fig.4.5). Changes from Fig. 4.5 resulting from varying parameters in Eq. 2.6 affect the area where the effects of plasticity are observable, but do not alter qualitatively the results (see Appendix 1).
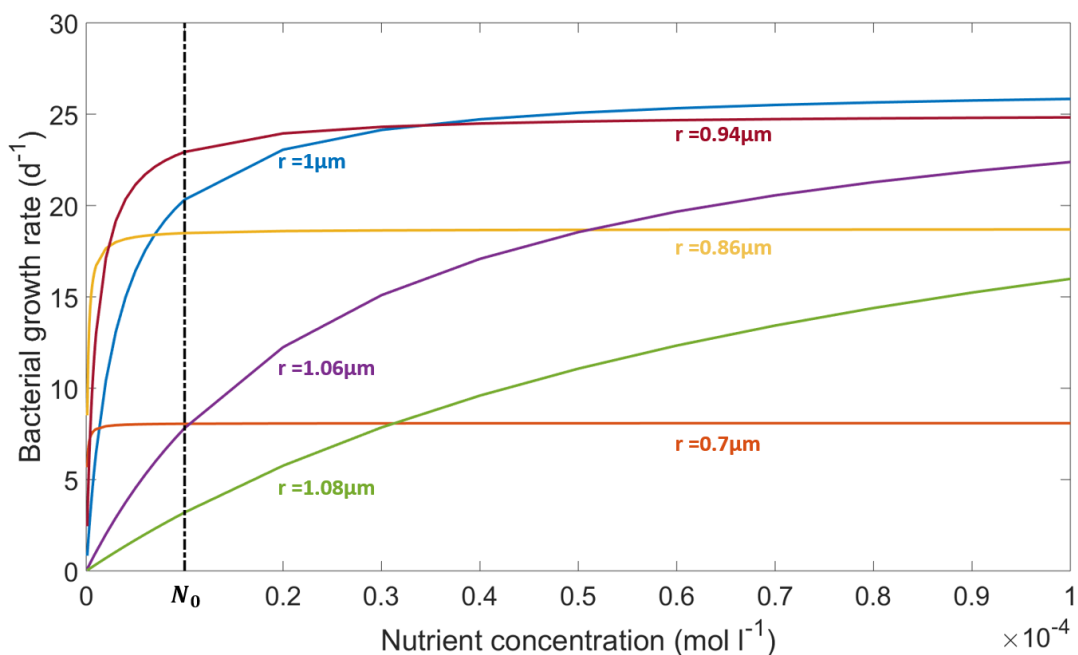


*Figure 4.5: Monod growth curves for different bacterial sizes, considering the trade-off in Eq.(2.6) and the allometry in Eq.(2.7). For sizes above 1 μm, the host growth rate decreases when the nutrient concentration equals the input of nutrient concentration $N_0$.*

In the area immediately above that of coexistence (i.e. above the purple dashed line in Fig.4.4), viral growth (i.e. per-capita change in the concentration of free virus, $\mu_{viral} = (Be^{-wL} - 1) k\, C_{st}$) cannot overcome dilution, which leads to viral extinction and the thriving of the bacterial population. Overall, this area of viral extinction increases as the latent period as well as the crowding strength increases (see Fig.4.6), and the bacteria population survives alone unless limited by the available nutrient (grey dotted line) or by its own physiological limits (black line). In these two cases, bacterial growth cannot overcome mortality due to dilution.
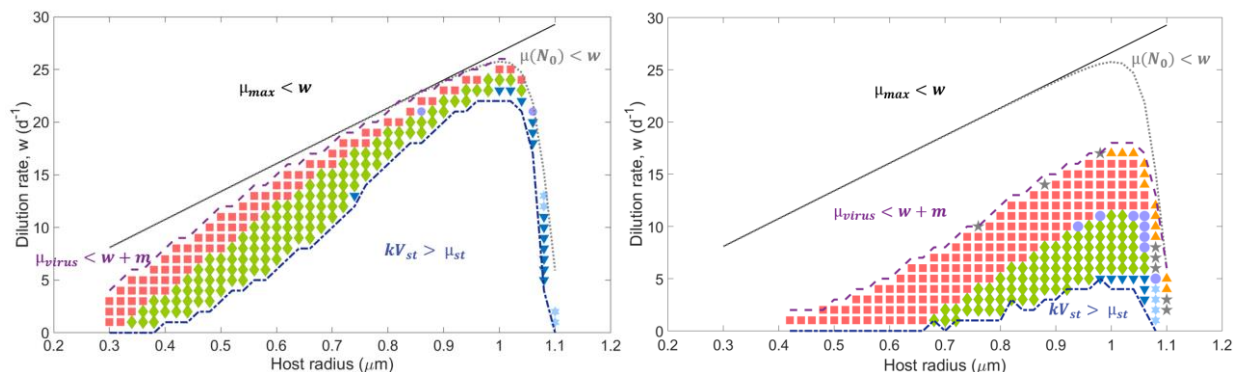
*Figure 4.6: Slice of the region of coexistence for L=0.07d for different crowding strength. Left: for $\alpha = 5.10^{-9}\, l\, cell^{-1}d^{-1}$. right: for $\alpha = 200.10^{-9}\, l\, cell^{-1}d^{-1}$. The legend of each symbol/colour is represented in the Table on the Fig 4.3.*

We also quantify the percentage of cases of exclusive coexistence between virus and host. The ratio between the area where only plasticity shows coexistence and the sum of all cases with exclusive coexistence (i.e. $(down\ triangle + hexagram)/(down\ triangle + hexagram + top\ triangle + pentagram)$ considering all latent periods) indicates that the plastic virus shows exclusive coexistence 66.92% cases, versus 33.08% for the nonplastic virus for the selected $\alpha$. Figure 4.7 summarises schematically the multiples transition between non-coexistence and coexistence, and between the various coexistence states observed in Fig. 4.4 as the dilution rate changes.
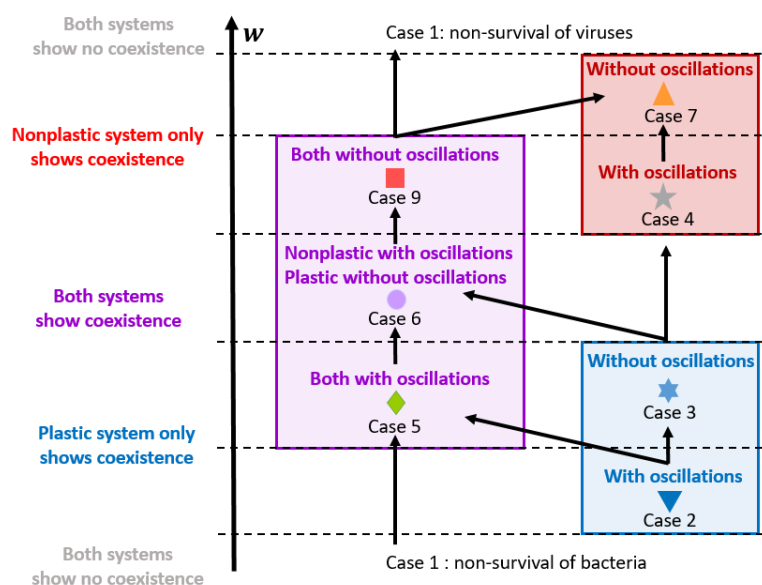


*Figure 4.7: Schematic diagram of the multiple paths of the system states observed within the different combinations of parameters $(r, L, \alpha)$ when the dilution rate (w) increases. Note that any cases can start by and/or end-up in case 1 without passing by other intermediary cases (e.g. case 5 can go directly to the upper case 1).*

Fig.4.7 shows that, for higher host size, only the plastic description of the model shows coexistence for low dilution (cases 2 and 3), while only the nonplastic virus coexists with its host for higher dilution rate (cases 4 and 7). The area where the host cannot coexist with the virus (case 1, bottom) is smaller when the virus is plastic than when it is nonplastic (i.e. smaller dilution rates required for cases 2 than for case 4), and the area where the bacteria thrive alone (i.e. case 1, top) is bigger in the plastic case. Oscillatory behaviour (i.e. limit cycle) occurs at low dilution rates, then becomes a stable equilibrium as $w$ increases. This shift happens for smaller $w$ in the plastic case, then in the non-plastic case (cases 5, 6 and 9). We never observed cases where the plastic system showed a limit cycle and the nonplastic system a stable equilibrium (case 8). When both plastic and nonplastic descriptions of the model show oscillations (case 6), the relative amplitude of the oscillation in the system with the plastic virus is always smaller than in the system with the nonplastic virus (see Fig.4.8).
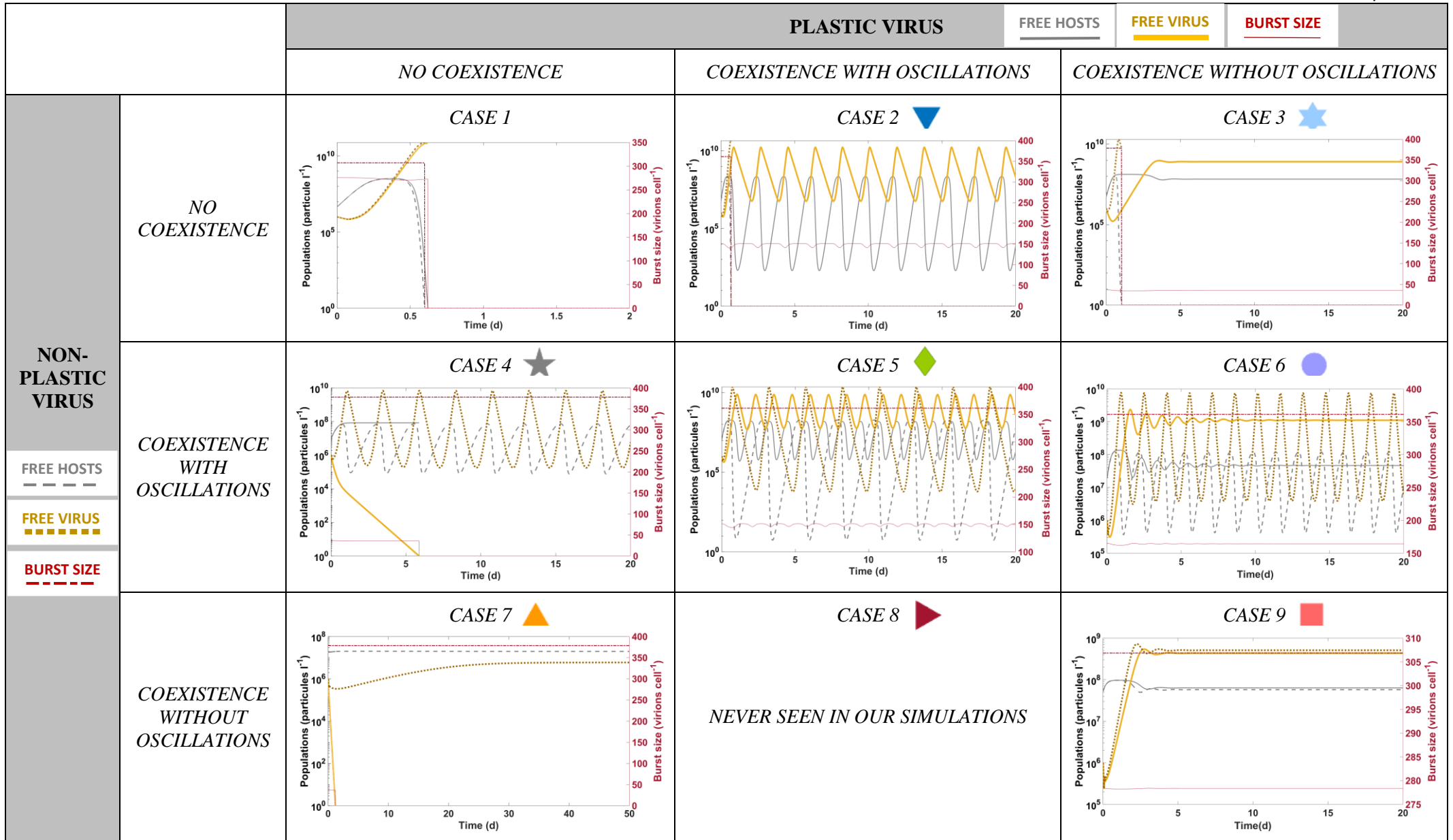
Figure 4.8: Examples of the dynamical profiles of the possible outcomes for plastic and nonplastic models.

# 3. Discussion

Viral reproduction depends intrinsically on the physiological state of the host. As shown experimentally, this dependence translates into changes of viral trait values (phenotypic plasticity) when the host growth rate changes. When included in models, this viral plasticity leads to important ecological and evolutionary differences with respect to classic models, which neglect viral plasticity (Choua and Bonachela 2019; Edwards and Steward 2018). Here, we focused on understanding how viral plasticity alters possible coexistence and dynamics between host and virus for a phage-bacteria system.

## 3.1 Influence of crowding and latent period on the stability of the system

The addition of a density dependent term generally contributes to dampen oscillations in models for antagonistic interactions (Gibert and Delong 2015), and this is indeed the case in our bacteria-phage systems. The selected value $\alpha = 60 \cdot 10^{-9} \, l \, cell^{-1} d^{-1}$, maximizes the coexistence area of the system regulated by viruses but does not affect the rest of our results qualitatively. Because $\alpha$ directly affects the bacteria, and the viruses only indirectly, the border delimiting the bacterial survival (i.e. bottom border in Fig.4.4) shifts to lower dilution rates faster than the border delimiting the viral survival (i.e. upper border) as $\alpha$ increases. This "lag" between the movement of the bottom and upper borders of the coexistence region widens the region in between (i.e. the area of coexistence), which facilitates the identification of the variety of dynamics shown in Fig.4.8. We also notice the increase of the region where the host survives alone (i.e. the area in between the black line and the purple dotted line In Fig. 4.4) as α increases, which raises the question of whether challenging environmental conditions that slow down bacterial growth or increase mortality may provide the counter-intuitive benefit of allowing the bacteria to avoid the virus.

Our results also reveal the effect of viral traits on the stability of the system. The latent period reflects the time that the virus spends inside the host producing virions, but also the loss of opportunities to establish parallel infections. These two factors are in turn influenced by the dilution rate: a high $w$ increases the infected-cell removal but also leads to higher host density due to the increased resources in the chemostat. Small $L$ entailed coexistence for areas with high $w$, while these same areas switch to no-coexistence status when $L$ increases. The reason is that the increase in host density linked to high dilution rates provides the viral offspring with more opportunities to establish subsequent infections and thus the virus can afford an earlier termination of infection (i.e. smaller $L$ values). These results are in line with previous studies (Abedon 1989; Choua and Bonachela 2019) that reported that both the host cell density and the infected-cell removal rate play a role in the selection of the latent period.

## 3.2   Comparison between plastic and nonplastic viruses

The mathematical form of lysis in our model differs between the nonplastic and plastic cases. In the former, the host losses are proportional to host abundance, which is commonly used in prey-predator models (e.g. Lotka-Volterra model (Lotka 1932)). In the plastic case, however, host losses depend also on the host growth rate, which renders the form of predation more appropriate to describe viral predation. On the other hand, viral infection is typically framed as "kill the winner" dynamics (Winter, et al. 2010) (i.e. the best performing host is subject to the highest viral pressure). Plasticity accentuates this effect as an increase in the host growth rate not only increases the host availability but also viral production, which maintains a highly performing host in lower abundance. This enhanced "kill the winner" effect may be the reason why the plastic model enables coexistence in some environments where classic models do not (and vice versa).

Figure 4.7 summarizes our results and, together with Figs.4.3 and 4.4, highlights the cases where viral plasticity enables coexistence while the classic model does not, as well as the cases where the nonplastic model show exclusive coexistence. Because the nonplastic virus, defined here as one with the best possible viral trait values (Eqs.(4.4) and (4.5)), can lead to a much-increased viral population, it can show coexistence in regions located close to the limit where plastic viruses cannot overcome dilution. For the plastic virus to survive in this area of the parameter space, the host must approach its maximal growth rate, which appears to be the case for smaller host sizes in our simulations while, for host with a size above 1μm, nutrient availability $N_0$ limits their growth (see Fig. 4.5). This limitation in nutrient forces these larger hosts to grow at a rate far from their maximum, which results in significant differences between the traits of the plastic and nonplastic virus. The plastic virus, responding to changes in the host growth rate, shows a decrease in performance for hosts that grow slowly, maintaining the survival of these hosts and thus the coexistence of the system where the nonplastic virus cannot. Because in nature maximal growth rates are the exception rather than the rule, the performance of the nonplastic virus is typically overstated in classical models that neglect plasticity; therefore, the most realistic plastic representation of the virus provides more reliable predictions.

For cases where both plastic and nonplastic viruses show coexistence, the amplitude of the limit cycle occurring with plastic viruses is always smaller than these of those occurring with nonplastic viruses. The difference in the behaviour observed for the bacterial population is mainly localized to the bottom of the oscillations, while the top varies less (see Fig.4.8). Because the nonplastic virus is always at its highest performance, the top-down pressure on the host is higher, which decreases the bacterial population to a level lower than the plastic virus (sometimes driving the host to extinction). When the host survives, fewer bacteria compete for nutrient in the lower part of the oscillation and we might expect the bacterial population to reach a higher

maximum than in the plastic case. However, this effect is damped when bacterial growth saturates (i.e. $\mu \approx \mu(N_0)$ or $\mu = \mu_{max}$).

Host availability is known to be an important factor regulating viral control. Previous studies have suggested that viruses limit the development of phytoplankton blooms (Brussaard 2004). However, it is still unclear how exactly viruses regulate the host population in nature, and when and how viruses can prevent blooms from happening (Brussaard 2004; Suttle 2007; He, Jin, and Zhang 2019). A previous study that considered host plasticity showed that the feedback between host and virus accentuates the decrease of viral control when the host availability is decimated by viral lysis (Thyrhaug, et al. 2003). However, to fully comprehend the impact of viral control on host populations it is essential to identify factors that affect viral infection and replication, which we know depend on the metabolism of the host (Brussaard 2004; He, Jin, and Zhang 2019). Viral plasticity may thus help to clarify this question. Our results combined with those from our previous chapter III reveal the thin barrier between coexistence and non-coexistence of the host-phage system and the importance of the interplay between host, virus and environment. Indeed, when compared with a nonplastic description (in which viral control is entirely regulated by host availability), the plastic virus can drive the bacterial population to either lower or higher abundances than the nonplastic case depending on the balance between host availability and host physiological state, which may captures the variable viral control observed in nature.

# 4. Conclusion

The flexibility of the viral traits conferred by plasticity can (i) increase the probability of coexistence between host and phage, and (ii) either reduce amplitude of oscillation or reinforce the feedbacks between the system and the environment. Plasticity enables coexistence in regions of the parameter space where the classic version of the model predicts a collapse of the system. The

cases where the nonplatic case shows exclusive coexistence, on the other hand, should be considered with caution, as the high performance of the virus imposed in nonplastic models keeps the viral population artificially alive. Moreover, the plastic virus can drive the bacterial population to either lower or higher abundances than the nonplastic case (in which viral control is entirely regulated by host availability) depending on the balance between host availability and host physiological state, which captures some of the multiple facets of viral control observed in nature. Additional experimental information regarding how different environment factors regulate viral dynamics and host-virus interactions are required to generalize our theory. Incorporating explicitly some of these aspects (e.g. viral dynamics and plasticity) into global biogeochemical models should significantly improve their accuracy, but still remains a big challenge (He, Jin, and Zhang 2019).

# CHAPTER V

# The effect of viral plasticity on the coevolution with the host

In the previous two chapters, we explored how viral plasticity affected (i) the evolution of the virus in presence of single host phenotype and (ii) the stability of a host-phage system for different combinations of fixed host and viral phenotypes. Here, we delve deeper to understand the effect of viral plasticity in a system where both virus and host evolve, affecting not only viral latent period but also host size.

Body size is a strong predictor of the structure and function of ecosystems, as it influences trophic exchanges between consumers and their resources, resulting in a food web structured primarily by size. Yet, the specific factors selecting for certain body sizes are still not well understood (Gibert and Delong 2015). For virus-bacteria interactions, the size of the host is a key trait because it affects the host physiological state (Litchman, et al. 2007), which in turn influences the lytic viral infection and thus the dynamics of both populations (Choua and Bonachela 2019). Therefore, it is justified to hypothesize that viral pressure, shaped by viral plasticity, might be one of the factors that select for specific host body sizes. In this chapter, we shed light on how the presence of inherently plastic viruses and coevolution with their bacterial hosts affect the size of the host.

Bacteria-phage coevolution has previously been studied, mainly on an arms race context. For example, systems where the host evolves resistance by changing its viral receptors at a fitness cost, and the phage responds to this resistance by adapting its tail fiber (Weitz, Hartman, and Levin 2005; Menge and Weitz 2009). These studies showed that, e.g. coevolution maintains

phenotypic and genetic diversity within microbial communities (Koskella and Brockhurst 2014). However, none of these studies focused explicitly on the effect of viral plasticity on the body size of the bacterial host, nor vice versa.

Higher bacterial sizes lead to higher maximal growth rates (see Eq. 2.7, (Gallet, et al. 2017)), but decreased substrate affinity (see Eq. 2.6, (Wirtz 2002)) and render the host more susceptible to adsorb viruses (see Eq.2.8, chapter II section 1.2). On the other hand, increasing the latent period allows the virus to release more virions, but entails missing opportunities of new infections by this offspring. Including the effect of viral plasticity in this picture adds a layer of complexity, as a host with a higher growth rate will not only replicate faster but will also increase the performance of the virus (i.e. the virus will release more virions in a shorter time). We thus aim to understand what strategies host and virus will use in different environments in order to understand better the effect they have on each other, including how viral plasticity alters their coevolution.

To this end, we use the standard host-phage model from chapter II modified to include viral plasticity and crowding effect as in chapter IV. For its analysis, we use our unconstrained eco-evolutionary framework (described in chapter II section 3), now including both host and virus mutants. We compare the ESS emerging for plastic and nonplastic descriptions of such host-virus interactions under different environmental conditions. We then contrast the strategy emerging from coevolution with the strategy obtained when only the virus evolves, or when the host evolves in the absence of the virus. We finally discuss on how selection acts on both host and virus in these scenarios.

# 1. Methodology

Here, we use the same environmental set-up as in chapter IV (i.e. a one stage chemostat). In addition, in this chapter, we represent host and phage coevolution by letting the host size and viral latent period evolve using the genetic algorithm in our unconstrained eco-evolutionary framework. In this framework, both ecological interactions and mutations occur simultaneously (see chap II section 3): new mutations are introduced as new phenotype populations, which leads to the addition of a new set of equations every time a host mutant $i$ and/or a virus mutant $j$ join the system. Host mutants differ from their parents in their size (only evolving trait for the host). Viral mutants differ from their parents in their latent period (only evolving trait for the virus). Taking all these details into consideration, the equations for our model needs to be rewritten as follows:

$$\frac{dN}{dt} = w(N_0 - N) - \frac{1}{Y}\sum_i \mu_i(N)\, C_i \tag{5.1}$$

$$\frac{dC_i(t)}{dt} = \mu_i\, C_i - k_i\, C_i \sum_j V_j - w\, C_i - \alpha\, C_i \sum_i C_i \tag{5.2}$$

$$\frac{dI_j(t)}{dt} = \sum_i k_i\, C_i\, V_j - \sum_i k_i C_{i_{t-L_j}} V_{j_{t-L_j}} e^{-wL_j} - w\, I_j \tag{5.3}$$

$$\frac{dV_j(t)}{dt} = \left( B_{j\mu_i} \sum_i k_i C_{i_{t-L_j}} V_{j_{t-L_j}} \right) e^{-wL_j} - \sum_i k_i\, C_i\, V_j - (m + w)\, V_j \tag{5.4}$$

We explicitly write $i$ the j subscripts for hosts and viruses, respectively, in order to emphasize the very diverse phenotype space, and to help to differentiate the bacterial to the viral influence. Note that we did not do that in chapter III for simplicity, as there only the virus was evolving. Here, the first equation represents the dynamics of the nutrient concentration within the chemostat, with an inflow and outflow of nutrient (first term) and the nutrient uptake by all the different host phenotypes present in the chemostat at that time (second term). Note that the yield factor Y is the same for all host

phenotypes/sizes ($r_i$), and the growth rate $\mu_i(N)$ follows the Monod model (Monod 1949):

$$\mu_i(N) = \mu_{max}(r_i)\frac{N}{K_n(\mu_{max}) + N} \tag{5.5}$$

where $\mu_{max}(r_i)$ is the maximal growth rate represented by the allometric expression in Eq. (2.7), and $K_n(\mu_{max})$ is the half-saturation constant set by the trade-off in Eq. (2.6).

Equation (5.2) describes the growth of each host phenotype population, $C_i$, as a result of reproduction (first term), the negative effect of infection coming from all the different viral phenotypes present in the chemostat at that time (second term), bacterial loss by dilution (third term) and population growth slowdown due to crowding (fourth term). Note that adsorption depends on the size of the host (Eq. (2.8)). Equation (5.3) keeps track of the cells infected by viral phenotype $j$. The first term represents the new infected individuals resulting from the adsorption of that specific $j$ viral phenotype to the diverse hosts present in the chemostat. Infected cells disappear during dilution (last term) or due to the lysis of all the cells that became infected exactly one latent period ($L_j$) in the past (second term, where $e^{-wL_j}$ is the probability for infected cells to survive the dilution during the latent period). The lysis of these infected cells releases new free phages for phenotype $j$ (first term in Eq. (5.4)) where the production of virions, $B_{j\mu_i}$, depends on the infection time $L_j$ but also on the growth rate that the host showed at the moment of adsorption, through the maturate rate and eclipse period:

$$B_{j\mu_i} = M(\mu_i)(L_j - E(\mu_i)) \tag{5.6}$$

where $M$ and $E$ are the functional forms we used in previous chapter (see Eqs. (4.2) – (4.3)). The extracellular density for each viral phenotype population then declines by adsorption (second term in Eq. (5.4)), and natural mortality and dilution (last two terms).

The virus is thus ultimately influenced by host size, as adsorption rate depends on host radius (see Eq.(2.8)) but also the eclipse period and maturation rate depend on host growth rate for the plastic description (Eq. (5.6)), and therefore on $\mu_{max}(r)$ and $K_n(\mu_{max})$ through Eq.(5.5). In the nonplastic case, on the other hand, $E$ and $M$ depend on the maximal host growth rate (see justification in chapter IV, and Eqs. (4.4) and (4.5)) which leads to:

$$B_{j\mu_i} = M_{non}(\mu_{max_i})(L_j - E_{non}(\mu_{max_i})) \tag{5.7}$$

We integrate these equations under different environmental conditions (i.e. different values of $w$ and $N_0$), and for different crowding strengths ($\alpha$ from 0 to $10^{-7}$ l cell$^{-1}$d$^{-1}$), for up to $10^4$ simulated days. During these days, multiple hosts compete for the common nutrient in while experiencing the mortality exerted by the viral populations, which compete for the available hosts. We assume that any virus can infect any host (i.e. generalist virus). In our system, host size can evolve between 0.3 to 1.1 µm, range that provides trait values (volume, $\mu_{max}$, and $K_n$) compatible with experimental observations (Füchslin, Schneider, and Egli 2012; Schulze and Lipe 1964; Loferer-Krößbacher, Klima, and Psenner 1998). On the other hand, the viral latent period can evolve between a minimal value fixed by the eclipse period until to realistic maximal value of 2 days. Such minimal value is calculated based on the host phenotype that shows the highest growth rate (i.e. the smallest $E$) among all the host mutants (i.e. generalist virus), this border ensures a minimal latent period bigger than any eclipse period.

With this model and constraints, mutation and selection enable the stochastic exploration of the phenotypic space where eventually, a combination of ESS for the host and viral traits ($L_{ESS}, r_{ESS}$) emerges. In order to find the ESS for each combination of $w$ and $\alpha$, we run up to 500 replicates for each example. We also consider that both host and virus mutate at similar times (or, to test this simplification, that the virus can mutate up to 5 times faster than the host).

To compare this ESS with the predictions for nonplastic viruses, we repeat this analysis with a nonplastic version of the model (Eq. 5.7).

Out of the many replicates, we select the cases that show coexistence at the end of the simulation, and reject those that lead to host and/or viral extinction. Among the cases that show coexistence, we retain the replicates for which a true dominant phenotype can be discerned, specifically, we label as dominant the phenotype such that its fraction represents more than 75% of the total mutant community (i.e. both $[C]_{ESS_{st}}/\sum_i [C_i]_{st}$ and $[V]_{ESS_{st}}/\sum_j [V_j]_{st}$ above 0.75 where the subscript "st" refers to the stationary state obtained by averaging the 20 last days of the simulation).

We then analyse how these $(L_{ESS}, r_{ESS})$ combinations vary as $w$, $N_0$ and $\alpha$ change. For each case, we compare the $(L_{ESS}, r_{ESS})$ for the plastic case to those obtained for the nonplastic description of the system. Finally, we compare (i) the $L_{ESS}$ emerging from coevolution to the analytical expression we obtained for a system where only virus evolves (i.e. Eq. 3.14); and (ii) the $r_{ESS}$ emerging from coevolution to the ESS obtained in a system where bacteria evolve in the absence of viruses. We did not study the case where host only evolves in the presence of a single (i.e. non-evolving) virus phenotype as there is no ecologically meaningful setup where this scenario is plausible: this case would require a set-up where e.g. a large amount of fresh viruses are added into the chemostat to reduce evolutionary pressures on the virus and therefore its evolution, but such addition would with certainty drive the host to extinction.

## 2. Results

For any parametrization, we take the convention to filter the cases that either did not show coexistence, or the candidate to host (virus) ESS did not represent a fraction 0.75 of the host (virus) population. In consequence, the number of useable combinations $(L_{ESS}, r_{ESS})$ is lower than our original number of replicates. Increasing the viral mutation rate to up to 5 times that of the host

did not change the probability of coexistence nor the number of functional combination (results not shown), and therefore we set the less-computationally expensive limit of equal timing for both host and viral mutation.

Also for any parametrization, there are extreme cases for which coexistence between phage and bacteria is not biologically possible. At low dilution rates, virus and host cannot coexist as the associated low growth rate eventually leads to the extinction of the host (followed by the extinction of virus); at high dilution rates, viral mortality is very high and the viral population goes to extinction, which allows the host to thrive alone.

## 2.1   Emergent host size and latent period $(L_{ESS}, r_{ESS})$

As Fig. 5.1 shows, the $(L_{ESS}, r_{ESS})$ emerging from a same dilution rate are clustered around a clear mean value, indicating that only one true combination of host size and latent period results from each environment. For all crowding strengths $\alpha$, there exists a negative correlation between the emergent host size and viral latent period. The difference between the plastic and nonplastic cases is noticeable at low crowding strength but decreases as $\alpha$ increases; for high-enough $\alpha$, both cases produce overlapping $r_{ESS}$ vs $L_{ESS}$ combinations. When the difference is noticeable, the same parametrization typically produces smaller $L_{ESS}$ and $r_{ESS}$ for the plastic case. Increasing $\alpha$ reduces the range for $r_{ESS}$.

Figure 5.1: Evolutionary stable strategy (ESS) for the host and virus obtained at $N_0 = 10^{-5}\ mol\ l^{-1}$ for different dilution rates and crowding effect. Top: $\alpha = 0$. Bottom left: $\alpha = 10x10^{-9}\ l\ cell^{-1}$. Bottom right: $\alpha = 100x10^{-9}\ l\ cell^{-1}d^{-1}$

The latter is also observed when we increase the input nutrient concentration $N_0$ (see Fig. 5.2). Both $L_{ESS}$ and $r_{ESS}$ increase as the input nutrient concentration increases, $r_{ESS}$ saturates as the dilution rates increases.
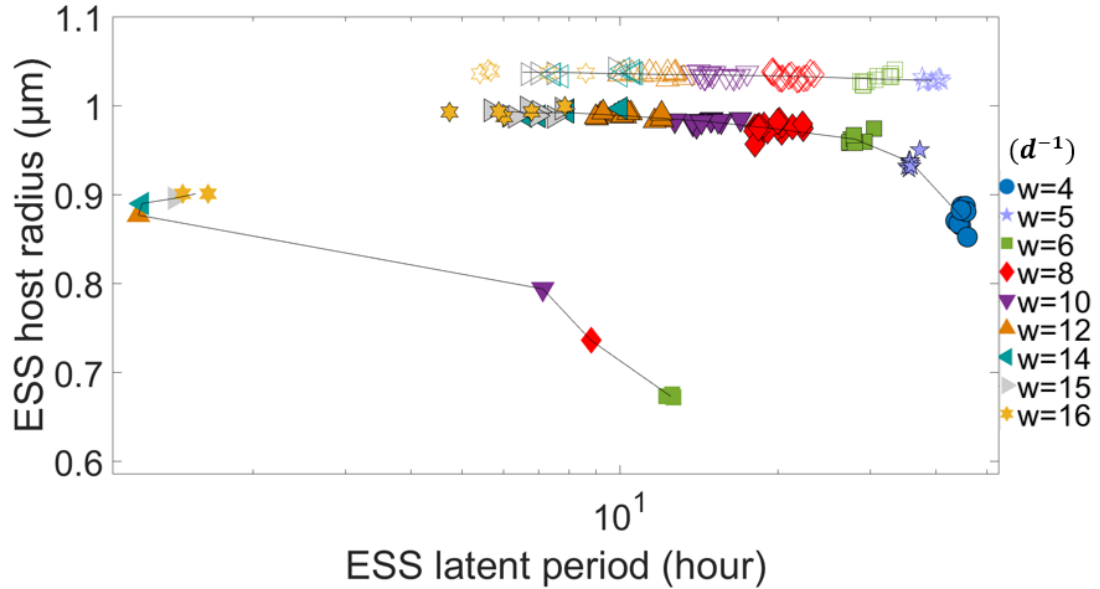
*Figure 5.2: Evolutionary stable strategy (ESS) for the host and virus obtained for different dilution rates and different input nutrient concentrations for the plastic case at $\alpha = 10^{-8} \, l \, cell^{-1} d^{-1}$. The fully coloured symbols with no contour represent the $N_0 = 10^{-5} \, mol \, l^{-1}$ case; symbols with black contour, $N_0 = 9x10^{-5} \, mol \, l^{-1}$; and empty symbols, $N_0 = 5x10^{-4} \, mol \, l^{-1}$. Symbols as in Fig. 5.1.*

Each $N_0$ case saturates close to the host size that provides the highest growth for that given $N_0$ (i.e. the value for $r$ that provides the highest growth rate if $N \to N_0$, see Table 5.1 for values). Indeed, sizes higher than those in Table 5.1 shows a smaller growth rate at $N = N_0$ due to the trade-off in Eq. (2.6) (see also Fig. (4.4) for more details).

*Table 5.1: Values of the host radius that shows the highest growth rate when the nutrient concentration in the chemostat is at its highest possible concentration (i.e. $N = N_0$).*

| $N_0 \ [mol \ l^{-1}]$ | $10^{-5}$ | $9 \ 10^{-5}$ | $5 \ 10^{-4}$ |
|---|---|---|---|
| $\mu(\tilde{r}) \ [d^{-1}]$ | 14.8 | 15.9 | 16.6 |
| $\tilde{r} \ [\mu m]$ | 0.93 (0.01) | 1.00 (0.01) | 1.04 (0.01) |

### a)     *Comparison with the case in which only the virus evolves*

In order to understand the role of host coevolution in the selection of the viral evolving trait (latent period), we compare these emerging $L_{ESS}$ with our

analytical solution from chapter III section 1.3, where only one single host phenotype/genotype was present (see Eq. (3.14) and Figs. 3.4 and 3.6).
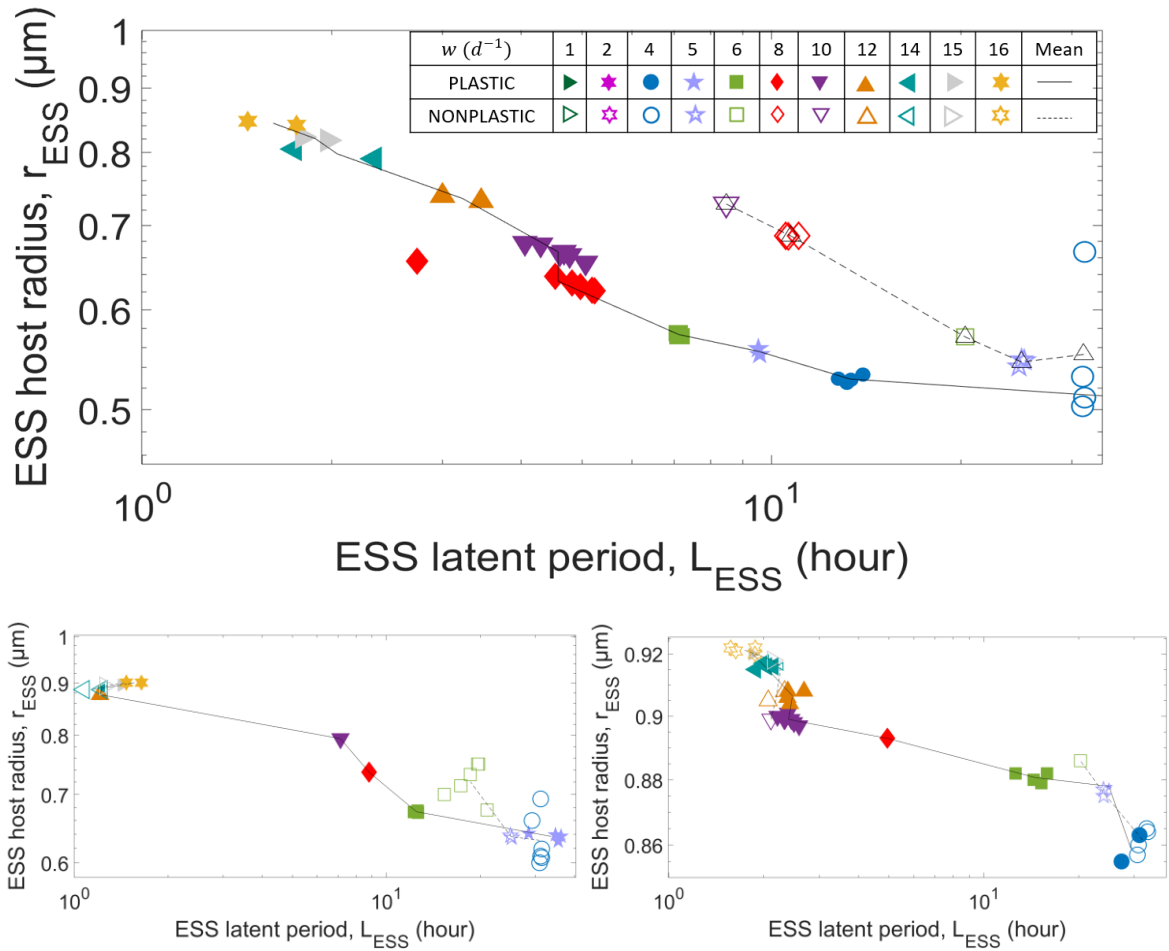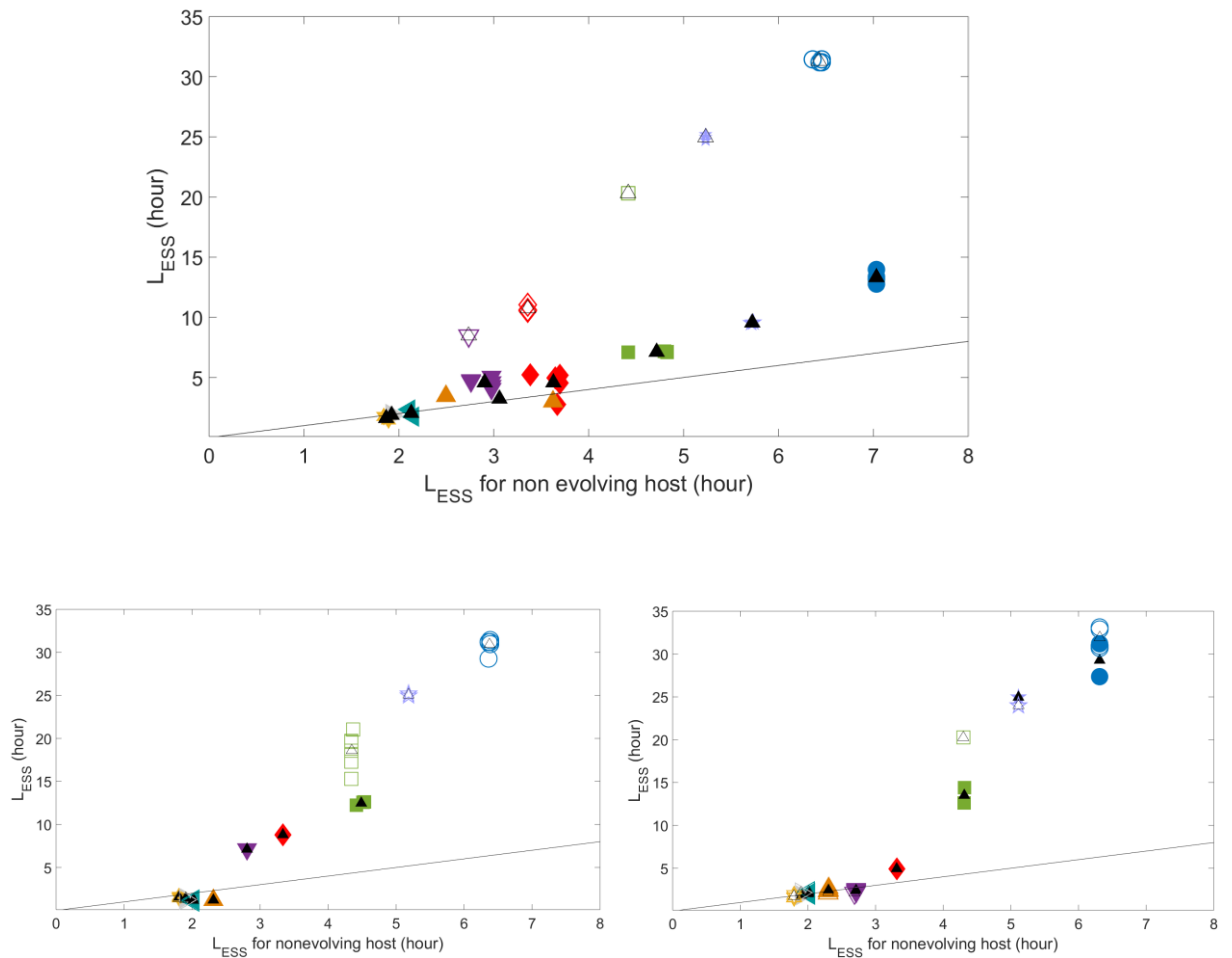


*Figure 5.3: Evolutionary stable strategy (ESS) for the virus obtained when host evolves at $N_0 = 10^{-5}$ mol $l^{-1}$ for different dilution rates compared with the ESS of the virus when host does not evolve. The black line represents the line in which the y axis equals the x axis. Top: $\alpha = 0$. Middle : $\alpha = 10x10^{-9}$ $l$ $cell^{-1}d^{-1}$. Bottom: $\alpha = 100x10^{-9}$ $l$ $cell^{-1}d^{-1}$. Symbols as in Fig. 5.1 except the mean, which is here represented by black triangles (fully coloured in the plastic case, black contour in the nonplastic case).*

As Fig. 5.3 shows, coevolution leads to larger $L_{ESS}$ than in the case of viral evolution alone for high dilution rates. This difference is more noticeable for the nonplastic case. Increasing the dilution rate or crowding effect reduces the difference between the with- and without-host-coevolution latent period for both plastic and nonplastic cases.

## b)    Comparison with case in which host evolves in the absence of virus

➤ **No crowding effect, $\alpha = 0$**

In a simple system where the virus and crowding effect are neglected (i.e. $V = \alpha = 0$), the bacterial dynamics are described by :

$$\frac{dC_i(t)}{dt} = (\mu_i - w)C_i \tag{5.8}$$

$$\frac{dN}{dt} = w(N_0 - N) - \frac{1}{Y}\sum_i \mu_i(N)\, C_i \tag{5.9}$$

Such simplified system enables reaching analytical stationary states for both the ecological and evolutionary dynamics. For the ecological stationary state, we first focus on one single phenotype and calculate the solution to the equations $dN/dt = dC/dt = 0$ given by:

$$C_{st} = Y(N_0 - N_{st}) \tag{5.10}$$

$$N_{st} = \frac{w\, Kn}{\mu_{max} - w} \tag{5.11}$$

For the evolutionary stationary state, we conduct the invasion analyses by studying the stability of this resident bacteria-nutrient system that, after reaching equilibrium, is perturbed by an invading bacterial phenotype (or, equivalently, i.e. bacterial strain with a different size and associated metabolic rates) that challenges the resident. Because the mutant is initially rare, both $N$ and $C_R$ stay at their stationary values (i.e. $C = C_{R_{st}} = C_{st}$ and $N = N_{R_{st}} = N_{st}$) and the system dynamics is reduced to the following equation:

$$\frac{dC_M(t)}{dt} = (\mu_M - w)\, C_M \tag{5.12}$$

The stability of the system is thus given by the sign of the eigenvalues $\lambda$ obtained by solving the characteristic equation given by $\mu_M - w - \lambda = 0$, where $\lambda$ is the associated eigenvalue. The system is stable (i.e. the perturbation

fades away) if $\lambda < 0$, i.e. if $\mu_M < w$, which leads to:

$$\mu_M = \mu_{max_M} \frac{N_{st}}{K_{n_M} + N_{st}} < w \Leftrightarrow \mu_{max_M} N_{st} < K_{n_M} w + N_{st} w$$

$$N_{st}(\mu_{max_M} - w) < K_{n_M} w \Leftrightarrow N_{st} < \frac{K_{n_M} w}{(\mu_{max_M} - w)}$$

$$\xLeftrightarrow[using \ Eq \ 5.10]{} N_{st_R} < N_{st_M}$$

Therefore, the bacterial resident that resists any invasion shows a size such that minimizes nutrient requirement, in agreement with classic competition theory (Tilman 1982). Thus, we look for the value of $r$ such that:

$$\frac{dN_{st}}{dr} = \frac{dN_{st}}{d\mu_{max}} \cdot \frac{d\mu_{max}}{dr} = 0 \tag{5.13}$$

Because $\frac{d\mu_{max}}{dr}$ equals zero only when $r = 0$, we thus focus on $\frac{dN_{st}}{d\mu_{max}} = 0$. Using Eq. (5.11), we obtain 2 extrema, and the minimum ($d^2N_{st}/dr^2 > 0$) is given by:

$$\mu_{max} = \frac{3 \mu_{ref} - \sqrt{5 \mu_{ref}^2 - 4 \mu_{ref} w}}{2} \tag{5.14}$$

Using the equation that links $\mu_{max}$ and $r$ (i.e. Eq. 2.7), we extract $r_{ESS}$:

$$r_{ESS_{V=0,\alpha=0}} = \sqrt[3]{\frac{3}{4\pi \ Conv_1} \cdot 10^{\frac{log_{10}(\mu_{max \ ESS}/Conv2)-p}{f}}} \tag{5.15}$$

Consequently, $r_{ESS}$ depends only on $w$ in the absence of the virus and the crowding effect. Note that Eq. (5.14) is feasible only for $w < \frac{5}{4}\mu_{ref} = 40.5 \ d^{-1}$, which is always the case here. Indeed, for dilution rate above values equal to $\mu(\tilde{r})$ appearing in Table 5.1, any bacterial phenotype goes to extinction (i.e. Eq.(5.8) negative due to $\mu < w$).

We compare this $r_{ESS_{V=0,\alpha=0}}$ to the $r_{ESS_{V\neq0,\alpha=0}}$ obtained from coevolution with the plastic and nonplastic virus for different dilution rates. Fig.5.4 shows

that the resulting $r_{ESS}$ departs from that obtained in the virus-free case for mid-to-high dilution rates: the resulting host is larger in the presence of the plastic virus, and even larger for nonplastic version of the model.
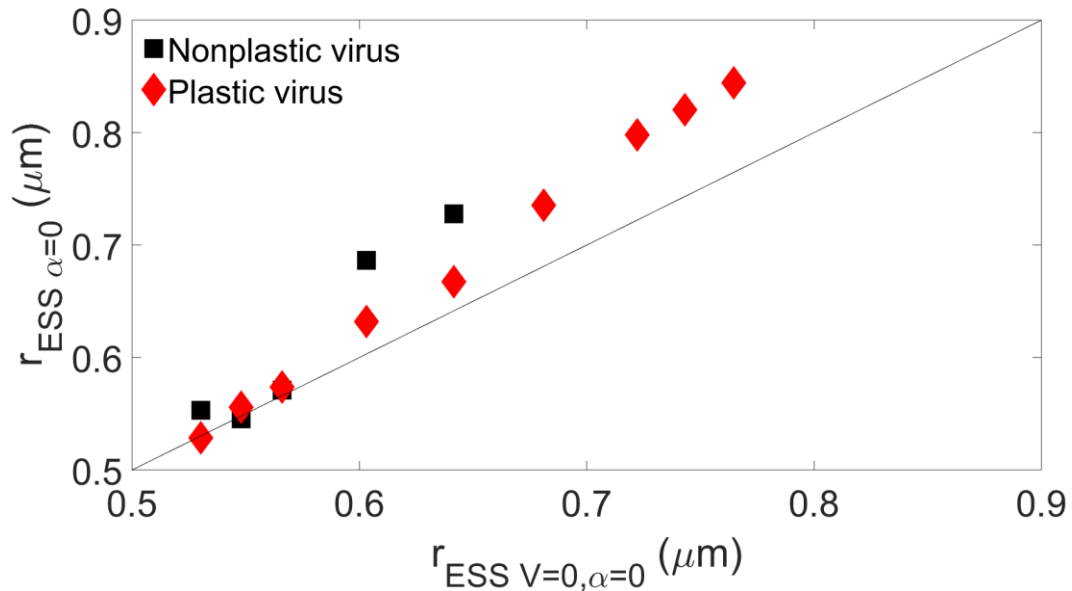


*Figure 5.4: Evolutionary stable strategy (ESS) for the host obtained when it coevolves with the virus at $N_0 = 10^{-5}$ mol $l^{-1}$ and $\alpha = 0$ for different dilution rates compared with the ESS of the host in absence of virus. The black line represents the line in which the y axis equals the x axis.*

➢ **With crowding effect, $\alpha \neq 0$**

In cases where the crowding effect is considered (i.e. $\alpha \neq 0$), the evolutionary stationary state of the host in the absence of the virus is calculated numerically using the genetic algorithm described previously. The resulting $r_{ESS_{V=0,\alpha \neq 0}}$ is then collected for different $w$, and compared to (i) $r_{ESS_{V=0,\alpha=0}}$ in order to see the effect of crowding effect on the host size evolution, and (ii) the $r_{ESS}$ obtained during coevolution with the plastic and nonplastic virus (see Fig.

5.5).
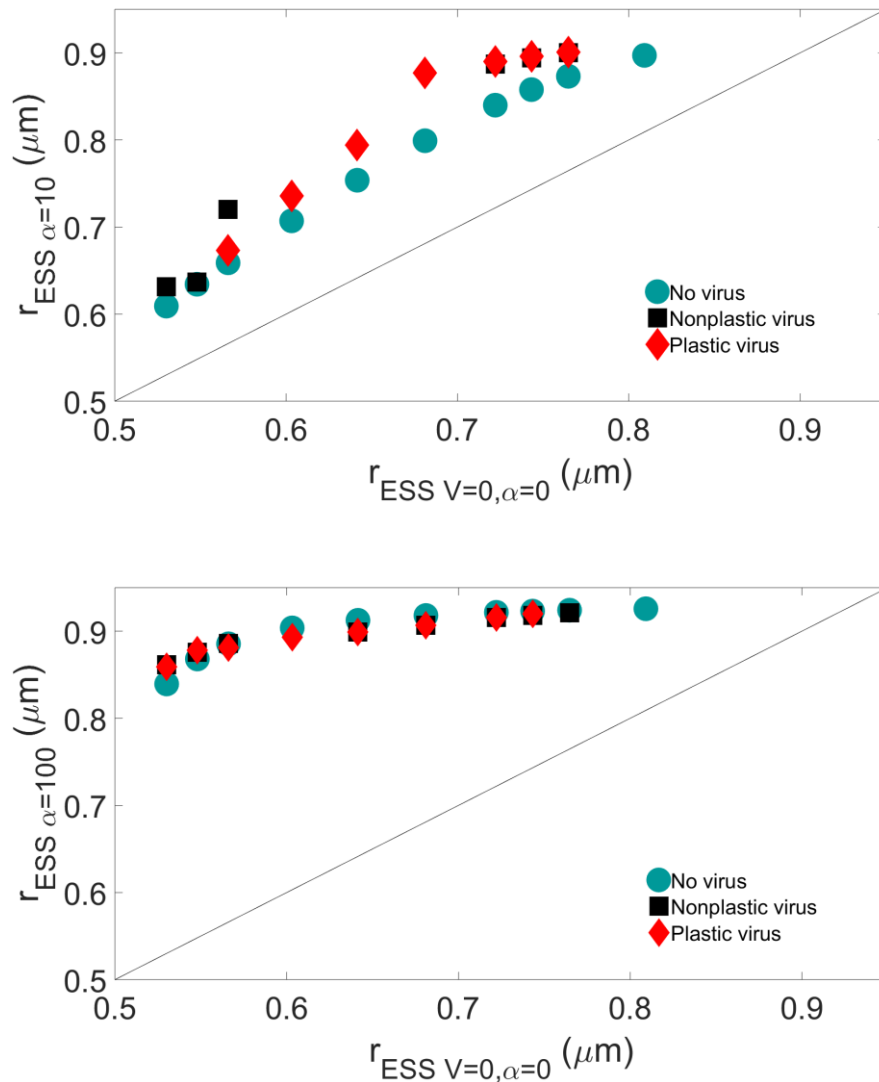


*Figure 5.5: : Evolutionary stable strategy (ESS) for the host obtained when it coevolves with the virus at $N_0 = 10^{-5} \ mol \ l^{-1}$ for different dilution rates compared with the ESS of the host in absence of virus and $\alpha = 0$. The black line represents the line in which the y axis equals the x axis. Top: $\alpha = 10x10^{-9} \ l \ cell^{-1}$. Bottom: $\alpha = 100x10^{-9} \ l \ cell^{-1}d^{-1}$.*

The emerging $r_{ESS}$ increases with the dilution rate and crowding strength, and eventually converges to $\tilde{r}$ (see Table 5.1). Convergence to this value is faster in the presence of viruses, and as the crowding effect increases. At high α values, the presence of the virus does not make a significant difference for the evolutionary strategy of the host, and the effect of plasticity is not easily discernible with this parametrization.

# 3. Discussion

Understanding the strategies that organisms use to survive under different ecological scenarios is key to understand their role within its ecosystem. Here, we study the coevolution of a bacterial host and a phage. Viruses can impose significant mortality rates on their hosts, constraining them to evolve to defend themselves against phage infection as repeatedly reported in the literature (Morgan and Koskella 2011). Our study can help understand which strategies are predominant for bacteria and viruses under different scenarios, and the effect of the viral dependence on its host (i.e. viral plasticity) on these strategies. In our case, the defence strategy of the host would be to decrease its size and thus its adsorption rate, which comes however with the evolutionary cost of growing more slowly. The virus in turn can respond by adapting its infection time (i.e. latent period) which comes with the trade-off of either releasing fewer virions (shorter time) or losing opportunities of new infections (longer time).

Although coevolutionary branching is a possibility that has been observed in laboratory and natural populations (Koskella and Brockhurst 2014), our study reveals that our system shows well-defined ESS emerging for each simulated environment. This is evidenced by the clustered points obtained from the different replicates, as each cluster could be represented by a single, well-defined mean value. Diversification can occur, for example, when a mutant virus adsorbs to only a limited subset of the total bacteria, i.e. specialist (Weitz, Hartman, and Levin 2005). In our case, however, viral phenotypes are all generalists, as each viral mutant can infect any of the host phenotypes, which may explain why we do not observe coevolutionary branching.

The emerging host strategy ($r_{ESS}$) shows smaller sizes in environments with low nutrient concentration (which result from low dilution rates). This evolutionary strategy resonates with the fact that smaller phytoplankton are better competitors for the available nutrient in oligotrophic waters (Mena, et

al. 2019). In our oligotrophic environments, the presence of the virus does not affect this strategy (see Fig. 5.1 Top). Selection seems thus to mainly result from bottom-up regulation in low-nutrient limit of our system.

Although, in poor nutrient environments, the host shows a similar size for plastic and nonplastic cases, the virus does show a different $L_{ESS}$ (see Fig. 5.1 top). Specifically, the virus adapts to the host showing a shorter infection time in the plastic case. This result is surprising as it is opposite to what was observed previously when only the virus evolved in the presence of a constant host phenotype. In that case, the nonplastic virus, defined as one with the best possible viral trait values, always showed a smaller eclipse period and thus a smaller $L_{ESS}$ with respect to the plastic virus (see Fig. 3.3). Therefore, we conclude that coevolution slows down viral infection (as seen in Fig 5.3), the more so for a nonplastic virus. This delay is amplified in poor nutrient environments (i.e. for small dilution rates).

Mathematically, the evolution of the host must thus introduce an extra positive term in our previous expression of the latent period (Eq. (3.14)). This additional delay is negligible compared to the others term at high dilution rates but becomes dominant at low $w$ (similarly what occurs to Eq. (3.3) at high $w$). Without further empirical information, we cannot go further in the explanation about the mechanisms underlying these strategies.

*Role of virus in coevolution*

The presence of the virus has a stronger effect on the emergent host size as nutrient availability increases, with the host showing a larger size. For a same environment (i.e. for a fixed $w$), the phage pressure maintains the bacterial population to a lower level than in the absence of virus (as observed in chapter III or (Choua and Bonachela 2019)). Consequently, fewer bacteria compete for the nutrient, allowing the host to increase their growth rate and evolve larger sizes. We could have expected the host to show a smaller size in the presence of the virus to avoid viral infection, but instead its increase in size and

consequently metabolic rate, compensates being a larger target for viral adsorption. The increase in host size due the presence of virus correlates with the increase in host maximal growth rate, in turn positively correlated with microbial fitness (Wiser and Lenski 2015). This strategy also benefits the virus as it increases adsorption and host physiological state.

Host size plays two distinct roles in our model, as it affects the host growth rate and the adsorption rate. In order to uncouple these two distinct roles, we also tested a version of the model in which the adsorption rate is constant. Specifically, we set $k = 3\ 10^{-9}\ l\ cell^{-1}d^{-1}$, which in the previous version would correspond to a host size $r = 0.64\ \mu m$. The results show that for a fixed $k$, the larger the $k$, the smaller the $r_{ESS}$ becomes because the host aims to reduce viral pressure. However, the $r_{ESS}$ still remains larger that the $r_{ESS}$ obtained in absence of virus, showing that the role of host size in the host growth rate predominates over its role in the adsorption rate although this latter is still significant. The virus, in return, shows a $L_{ESS}$ that matches the combination ($r_{ESS}$, $L_{ESS}$) previously observed now emerging for different environmental conditions (i.e. different w). Consequently, the change affects $r_{ESS}$ which in turn drive the value of $L_{ESS}$.

The crowding effect is an additional factor that regulates the bacterial population decreasing the population. This allows the host to reach the highest size that maximizes its metabolic rate for lower dilution rates due to the lower competition for nutrient (as explained above). For sufficiently high alpha, the bacterial population is entirely regulated by the crowding effect, which explains the similar emergent size in the presence or absence of the virus (i.e. the viral pressure is negligible).

# 4. Conclusion

Although most of studies define pathogens as having detrimental effects on their hosts, in some cases, parasitic organisms may evolve to benefit the host

by increasing the host fitness, thus shifting the interaction to a mutualistic one (Morgan and Koskella 2011). This seems to be the case in this study, where coevolution results in the presence of virus helping the host to increase its fitness, which is also in the interest of the virus as it accelerates host proliferation. However, we notice that viral presence has a negligible effect on the host evolution in poor nutrient environments where nutrient availability is the main driver of the evolution of the bacterial cell size, in agreement with existing observations (Chien, Hill, and Levin 2012). In such environment, the host cell size reflecting the host physiological state has a strong influence on the evolution of the viral traits, which in turn affect quantitatively the host population. The latter highlights the importance of considering viral plasticity in future models for the estimation of primary production, especially in oligotrophic parts of the ocean.

# Conclusion

Marine viruses contribute to regulating the phytoplankton/bacterioplankton community, playing a key role in the most important biogeochemical cycles on earth. Therefore, an accurate representation of the viral regulation is crucial to predict these community dynamics, and its effects on the rest of the marine food web and biogeochemical cycles, still a big challenge (He, Jin, and Zhang 2019).

The parasitic life style of viruses leads to an intrinsic dependence of viral reproduction on the physiological state of the host. Experiments show this dependence leads in turn to changes of viral traits ($E$, $M$, $L$ and $B$) when the host growth rate changes ($\mu$). Although no information is available to determine whether these changes in viral traits are a passive consequence or an active response of the virus to host changes, they are referred to as viral plasticity (Abedon, Herschler, and Stopar 2001; Choua and Bonachela 2019).

In this thesis, we compiled available data on how T-phage traits change with the growth rate of its host, *Escherichia.Coli*. Based on these data, we deduced functional forms for the eclipse period ($E(\mu)$) and maturation rate ($M(\mu)$) that are biologically meaningful and compatible with multiple viral strains: the increase in the transcription and translation machinery that occurs as $\mu$ increases leads to a decline in the time needed to synthesize the viral component (i.e.decreasing $E(\mu)$) and an increase in the virion assembly rate (i.e. increasing $M(\mu)$). Both curves reach a plateau at high $\mu$ that relates to physiological limits of the host (e.g. limitation of ribosomes efficiency, etc.). This biological interpretation of the proposed functions stays coherent across examples using different phage strains and temperatures.

We included these functional forms in a standard ecological host-phage model, then studied analytically and computationally the ecology, evolution

and eco-evolutionary interactions of the host-virus system. We first analysed the impact of viral plasticity on the evolution of the latent period ($L$), as the mechanisms determining this key viral trait(duration of infection) are still not well understood (Wang, Smith, and Young 2000; White, et al. 2011). Our analysis revealed how plasticity affects $L$, and in consequence viral offspring (i.e. $B$), providing expressions for their optimal values. The optimal infection time results from the interaction between extracellular factors and the use of the host's (intracellular) resources, specifically between the timing for infected cell removal from the system and the synthesis time encoded in $E(\mu)$. For the burst size, our results show that the effect of plasticity is more pronounced. Plasticity in L and B, in turn, affects the host-virus ecological dynamics, inverting the predictions for the host population when the system is represented using classic models that neglect such plasticity. For example, in the nonplastic case, the expected decrease of host availability during the starvation period is damped by the decrease of viral infection keeping the density of available host constant. In the plastic case, however, the viral infection not only decreases due to the decrease in host availability but also due to the host physiological state leading to a decreases phage-induced mortality rate that increases the host density. This variation in timing and strength due to changes in the host physiological state can reinforce or damp the dynamic feedback between host, virus and their environment.

Viral plasticity also affects the persistence of the host-phage system. Including viral plasticity in models under different environmental conditions led us to conclude that plasticity enables coexistence in some environment where classic models predict the collapse of the system, and whereas the opposite occurs in conditions typically not reachable in reality. Overall, the flexibility of viral traits conferred by plasticity increases the probability of coexistence between host and phage.

Finally, our study of the coevolution of host size and viral latent period revealed that nutrient availability is the strongest factor driving host size.

Importantly, the presence of virus, regulating the host population, decreases host competition for nutrient and therefore is ultimately beneficial for the host, which showed bigger size and increased fitness. On the other hand, the viral infection time increases compared to that obtained when evolving with only one fixed host phenotype, showing an adaptation of the infection time to the availability and the physiological state of the host.

By providing simple mathematical expressions linking the host metabolism to the viral-mediated processes that regulates the host population, and studying the consequences of such regulation, this thesis sheds light on the complex host-phage interaction, which is still far from being completely understood (Brussaard 2004; He, Jin, and Zhang 2019) and not well represented in models (Mateus 2017). Still, incorporating viral dynamics and plasticity into global biogeochemical models, which could significantly improve our prediction for e.g. primary productivity and $CO_2$ level under a variety of climate change scenarios, remains a big theoretical and technical challenge (He, Jin, and Zhang 2019).

# Appendix

## 1. Consequences of the trade-off in the substrate affinity

We tested two variations for the relationship between the maximum growth rate and half-saturation constant: (i) a parametrisation of $K_{ref}$ in Eq.(6) eight times bigger than its initial value, and (ii) the use of a new relationship for $K_n(r) = 10^{-6}10^{-0.94+0.33\,log_{10}(\frac{4\pi r^3}{3})}$ borrowed from marine phytoplankton (with nitrogen as focal nutrient, see (Edwards, et al. 2012)). The former shows that hosts with size smaller than the previous limit of 1µm cannot reach maximal growth for $N \leq N_0$. The latter prevents saturation in $\mu_{max}(K_n)$, oppositely to Eq.(2.6), and thus any host size can reach its $\mu_{max}$ for $N \leq N_0$ (see Fig.A1.1 left column). As a consequence, the coexistence area shifts towards lower values of the host size for the high $K_n$ case, and some of the reported behaviours in Fig. 4.7 are lost for the new $K_n(r)$ case (see Fig.A1.1 right column). Indeed, the wider range of host sizes that reach maximal growth rates leads to negligible differences between plastic and nonplastic cases. None of these changes, however, altered qualitatively the sequence of behaviours observed as the dilution rate increases.
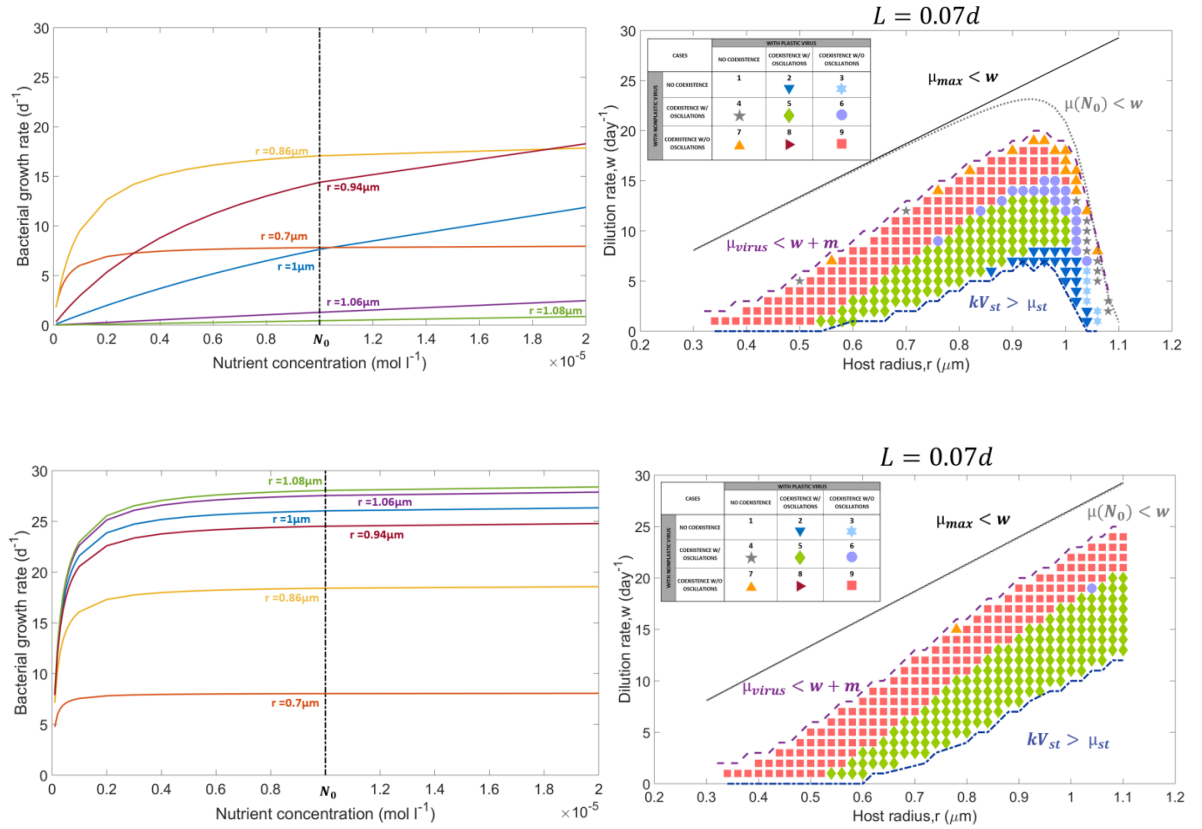
*Figure A1.1: Growth curves (left) and coexistence areas (right) observed when: (top) increasing $K_{ref}$ by a factor 8 and (bottom) Eq.(2.6) is replaced by the marine-phytoplankton-based allometry $K_n(r) = 10^{-6}10^{-0.84+0.33log_{10}(4\pi r^3/3)}$ (Edwards et al 2012).*

# References

Abedon, S. T. 1989. "Selection for Bacteriophage Latent Period Length by Bacterial Density: A Theoretical Examination." *Microbial Ecology* 18, no. 2: 79-88.

Abedon, S.T., T. D. Herschler, and D. Stopar. 2001. "Bacteriophage Latent-Period Evolution as a Response to Resource Availability." *Applied and Environmental Microbiology* 67, no. 9: 4233-4241. http://dx.doi.org/10.1128/AEM.67.9.4233-4241.2001.

Abedon, Stephen T, Paul Hyman, and Cameron Thomas. 2003. "Experimental Examination of Bacteriophage Latent-Period Evolution as a Response to Bacterial Availability." *Applied and environmental microbiology* 69, no. 12: 7499-7506.

Abedon, Stephen T., et al. 2011. "Phage Treatment of Human Infections." *Bacteriophage* 1, no. 2: 66-85. http://dx.doi.org/10.4161/bact.1.2.15845.

Aksyuk, Anastasia A., and Michael G. Rossmann. 2011. "Bacteriophage Assembly." *Viruses* 3, no. 3: 172-203. http://dx.doi.org/10.3390/v3030172.

Anderson, Thomas F. 1949. "The Reactions of Bacterial Viruses with Their Host Cells." *Botanical Review* 15, no. 7: 464-505.

Ashelford, Kevin E., et al. 2000. "Seasonal Population Dynamics and Interactions of Competing Bacteriophages and Their Host in the Rhizosphere." *Applied and Environmental Microbiology* 66, no. 10: 4193-4199.

Beretta, E. 2001. "Modeling and Analysis of a Marine Bacteriophage Infection with Latency Period." *Nonlinear Analysis, RWA* 2 (2001): 35-74. http://dx.doi.org/10.1016/S0362-546X(99)00285-0.

Beretta, E., and Y. Kuang. 1998. "Modeling and Analysis of a Marine Bacteriophage Infection." *Math Biosci* 149, no. 1 (Apr): 57-76.

Berg, H. C., and E. M. Purcell. 1977. "Physics of Chemoreception." *Biophysical Journal* 20, no. 2 (1977/11/01/): 193-219. http://dx.doi.org/https://doi.org/10.1016/S0006-3495(77)85544-6.

Bertozzi Silva, J., Z. Storms, and D. Sauvageau. 2016. "Host Receptors for Bacteriophage Adsorption." *FEMS Microbiol Lett* 363, no. 4 (Feb). http://dx.doi.org/10.1093/femsle/fnw002.

Birch, Elsa W, Nicholas A Ruggero, and Markus W Covert. 2012. "Determining Host Metabolic Limitations on Viral Replication Via Integrated Modeling and Experimental Perturbation." *PLoS Comput Biol* 8, no. 10: e1002746.

Bonachela, J. A., and S. A. Levin. 2014. "Evolutionary Comparison between Viral Lysis Rate and Latent Period." *J Theor Biol* 345 (Mar 21): 32-42. http://dx.doi.org/10.1016/j.jtbi.2013.12.006.

Bonachela, Juan A., Michael Raghib, and Simon A. Levin. 2011. "Dynamic Model of Flexible Phytoplankton Nutrient Uptake." *Proceedings of the National Academy of Sciences* 108, no. 51: 20633-20638. http://dx.doi.org/10.1073/pnas.1118012108.

Bratbak, Gunnar, Jorun K Egge, and Mikal Heldal. 1993. "Viral Mortality of the Marine Alga Emiliania Huxleyi (Haptophyceae) and Termination of Algal Blooms." *Marine Ecology Progress Series*.

Bremer, H., and P. P. Dennis. 2008. "Modulation of Chemical Composition and Other Parameters of the Cell at Different Exponential Growth Rates. Lid - 10.1128/Ecosal.5.2.3 [Doi]." no. 2324-6200 (Electronic) (20151007 DCOM-20151008).

Brussaard, Corina P. D. 2004. "Viral Control of Phytoplankton Populations—a Review1." *Journal of Eukaryotic Microbiology* 51, no. 2: 125-138. http://dx.doi.org/10.1111/j.1550-7408.2004.tb00537.x.

Buchan, Alison, et al. 2014. "Master Recyclers: Features and Functions of Bacteria Associated with Phytoplankton Blooms." *Nature Reviews Microbiology* 12 (08/19/online): 686. http://dx.doi.org/10.1038/nrmicro3326.

Bull, J. J., et al. 2006. "Evolutionary Feedback Mediated through Population Density, Illustrated with Viruses in Chemostats." *Am Nat* 167, no. 2 (Feb): E39-51. http://dx.doi.org/10.1086/499374.

Calendar, R.L., and S.T. Abedon. 2005. *The Bacteriophages*: Oxford University Press.

Calendar, Richard. 2006. *The Bacteriophages*: Oxford University Press on Demand.

Chien, An-Chun, Norbert S. Hill, and Petra Anne Levin. 2012. "Cell Size Control in Bacteria." *Current Biology* 22, no. 9 (05/07): R340-R349. http://dx.doi.org/10.1016/j.cub.2012.02.032.

Choua, M., and J.A. Bonachela. 2019. "Ecological and Evolutionary Consequences of Viral Plasticity." *The American Naturalist* 193, no. 3: 346-358. http://dx.doi.org/https://doi.org/10.1086/701668.

Choua, M., et al. 2020. "The Effect of Viral Plasticity on the Persistence of Host-Virus Systems." *Journal of Theoretical Biology*, no. (coming soon).

Delbrück, M. 1940. "Adsoprtion of Bacteriophage under Various Physiological Conditions of the Host." *The Journal of General Physiology* 23, no. 5 (01/29/received): 631-642.

---. 1945. "The Burst Size Distribution in the Growth of Bacterial Viruses (Bacteriophages)." *Journal of Bacteriology* 50, no. 2: 131-135.

Dercole, Fabio, and Sergio Rinaldi. 2008. *Analysis of Evolutionary Processes: The Adaptive Dynamics Approach and Its Applications*: Princeton University Press.

Edwards, K.F., and G. F. Steward. 2018. "Host Traits Drive Viral Life Histories across Phytoplankton Viruses." *American Naturalist* 191: 566-581.

Edwards, Kyle F., et al. 2012. "Allometric Scaling and Taxonomic Variation in Nutrient Utilization Traits and Maximum Growth Rate of Phytoplankton." *Limnology and Oceanography* 57, no. 2: 554-566. http://dx.doi.org/10.4319/lo.2012.57.2.0554.

Ellis, Emory L., and Max Delbrück. 1939. "The Growth of Bacteriophage." *The Journal of General Physiology* 22, no. 3 (09/07/accepted): 365-384.

Endy, D., J. Kong D Fau - Yin, and J. Yin. "Intracellular Kinetics of a Growing Virus: A Genetically Structured Simulation for Bacteriophage T7." no. 0006-3592 (Print).

Erez, Zohar, et al. 2017. "Communication between Viruses Guides Lysis-Lysogeny Decisions." *Nature* 541, no. 7638: 488-493. http://dx.doi.org/10.1038/nature21049.

Farewell, A., and F. C. Neidhardt. 1998. "Effect of Temperature on in Vivo Protein Synthetic Capacity in Escherichia Coli." *Journal of bacteriology* 180, no. 17: 4704-4710.

Forsman, A. 2015. "Rethinking Phenotypic Plasticity and Its Consequences for Individuals, Populations and Species." *Heredity* 115, no. 4: 276-284. http://dx.doi.org/10.1038/hdy.2014.92.

Fuhrman, Ja Fau, and G. B. McManus. 1984. "Do Bacteria-Sized Marine Eukaryotes Consume Significant Bacterial Production?", no. 0036-8075 (Print).

Fuhrman, Jed. 1992. "Bacterioplankton Roles in Cycling of Organic Matter: The Microbial Food Web." In *Primary Productivity and Biogeochemical Cycles in the Sea*, edited by Paul G. Falkowski, Avril D. Woodhead, and Katherine Vivirito, 361-383. Boston, MA: Springer US.

Füchslin, H. P., C. Schneider, and T. Egli. 2012. "In Glucose-Limited Continuous Culture the Minimum Substrate Concentration for Growth, S(Min), Is Crucial in the Competition between the Enterobacterium Escherichia Coli and Chelatobacter Heintzii, an Environmentally Abundant Bacterium." *The ISME Journal* 6, no. 4: 777-789. http://dx.doi.org/https://doi.org/10.1038/ismej.2011.143.

Gaedke, Ursula, Silke Hochstädter, and Dietmar Straile. 2002. "Interplay between Energy Limitation and Nutritional Deficiency: Empirical Data and Food Web Models." *Ecological Monographs* 72, no. 2: 251-270. http://dx.doi.org/doi:10.1890/0012-9615(2002)072[0251:IBELAN]2.0.CO;2.

Gallet, R., et al. 2017. "The Evolution of Bacterial Cell Size: The Internal Diffusion-Constraint Hypothesis." *ISME J* 11, no. 7 (07//print): 1559-1568. http://dx.doi.org/https://doi.org/10.1038/ismej.2017.35.

García, L. R., and I. J. Molineux. 1996. "Transcription-Independent Dna Translocation of Bacteriophage T7 Dna into Escherichia Coli." *Journal of Bacteriology* 178, no. 23: 6921-6929.

Gelderblom, Hans R. 1996. *Structure and Classification of Viruses*. 4th ed.: University of Texas Medical Branch at Galveston, Galveston (TX).

Gibert, Jean, and John Delong. 2015. *Individual Variation Decreases Interference Competition but Increases Species Persistence*. Vol. 52.

Golec, Piotr, et al. 2014. "Bacteriophage T4 Can Produce Progeny Virions in Extremely Slowly Growing *Escherichia Coli* Host: Comparison of a Mathematical Model with the Experimental Data." *FEMS Microbiology Letters* 351, no. 2: 156-161. http://dx.doi.org/10.1111/1574-6968.12372.

Guerrero-Ferreira, Ricardo C., et al. 2011. "Alternative Mechanism for Bacteriophage Adsorption to the Motile Bacterium <Em>Caulobacter Crescentus</Em>." *Proceedings of the National Academy of Sciences* 108, no. 24: 9963.

Gutiérrez, Diana, et al. 2017. "Applicability of Commercial Phage-Based Products against Listeria Monocytogenes for Improvement of Food Safety in Spanish Dry-Cured Ham and Food Contact Surfaces." *Food Control* 73 (2017/03/01/): 1474-1482. http://dx.doi.org/https://doi.org/10.1016/j.foodcont.2016.11.007.

Hadas, Hilla, et al. 1997. "Bacteriophage T4 Development Depends on the Physiology of Its Host Escherichia Coli." *Microbiology* 143, no. 1: 179-185. http://dx.doi.org/doi:10.1099/00221287-143-1-179.

Hantke, Klaus, and Volkmar Braun. 1975. "Membrane Receptor Dependent Iron Transport in Escherichia Coli." *FEBS Letters* 49, no. 3 (1975/01/01): 301-305. http://dx.doi.org/http://dx.doi.org/10.1016/0014-5793(75)80771-X.

He, Tianliang, Min Jin, and Xiaobo Zhang. 2019. "Marine Viruses." In *Virus Infection and Tumorigenesis: Hints from Marine Hosts' Stress Responses*, edited by Xiaobo Zhang, 25-62. Singapore: Springer Singapore.

Herendeen, S. L., R. A. VanBogelen, and F. C. Neidhardt. 1979. "Levels of Major Proteins of Escherichia Coli During Growth at Different Temperatures." no. 0021-9193 (Print).

Hobbs, Zack, and Stephen T. Abedon. 2016. "Diversity of Phage Infection Types and Associated Terminology: The Problem with 'Lytic or Lysogenic'." *FEMS Microbiology Letters* 363, no. 7: fnw047-fnw047. http://dx.doi.org/10.1093/femsle/fnw047.

Hoverman, J. T. 2010. "Predator-Induced Plasticity." *eLS* 67: 309-318. Accessed 2018/09/18. http://dx.doi.org/https://doi.org/10.1002/9780470015902.a0003305.pub2.

Hu, B., et al. 2013. "The Bacteriophage T7 Virion Undergoes Extensive Structural Remodeling During Infection." no. 1095-9203 (Electronic).

Husimi Y Fau - Nishigaki, K., et al. 1982. "Cellstat-a Continuous Culture System of a Bacteriophage for the Study of the Mutation Rate and the Selection Process of the Dna Level." no. 0034-6748 (Print).

Hutchinson, G. E. 1961. "The Paradox of the Plankton." *The American Naturalist* 95, no. 882: 137-145.

Koskella, Britt, and Michael A. Brockhurst. 2014. "Bacteria-Phage Coevolution as a Driver of Ecological and Evolutionary Processes in Microbial Communities." *FEMS microbiology reviews* 38, no. 5: 916-931. http://dx.doi.org/10.1111/1574-6976.12072.

Levin, Bruce R., Frank M. Stewart, and Lin Chao. 1977. "Resource-Limited Growth, Competition, and Predation: A Model and Experimental Studies with Bacteria and Bacteriophage." *The American Naturalist* 111, no. 977 (1977/01/01): 3-24. Accessed 2016/11/02. http://dx.doi.org/10.1086/283134.

Litchman, E., et al. 2007. "The Role of Functional Traits and Trade-Offs in Structuring Phytoplankton Communities: Scaling from Cellular to Ecosystem Level." *Ecol Lett* 10, no. 12 (Dec): 1170-81. http://dx.doi.org/10.1111/j.1461-0248.2007.01117.x.

Loferer-Krößbacher, M., J. Klima, and R. Psenner. 1998. "Determination of Bacterial Cell Dry Mass by Transmission Electron Microscopy and Densitometric Image Analysis." *Applied and Environmental Microbiology* 64, no. 2: 688-694.

Lomas, M. W., et al. 2014. "Impact of Ocean Phytoplankton Diversity on Phosphate Uptake." *Proc Natl Acad Sci U S A* 111, no. 49 (Dec 09): 17540-5. http://dx.doi.org/10.1073/pnas.1420760111.

Lotka, Alfred J. 1932. "The Growth of Mixed Populations: Two Species Competing for a Common Food Supply." *Journal of the Washington Academy of Sciences* 22, no. 16/17: 461-469. Accessed 2020/02/20/.

Lwoff, A. F., and P. Tournier. 1966. "The Classification of Viruses." no. 0066-4227 (Print).

Lwoff, André. 1953. "Lysogeny." *Bacteriological Reviews* 17, no. 4: 269-337.

Maat, D. S., et al. 2016. "Virus Production in Phosphorus-Limited Micromonas Pusilla Stimulated by a Supply of Naturally Low Concentrations of Different Phosphorus Sources, Far into the Lytic Cycle. Lid - 10.1093/Femsec/Fiw136 [Doi] Lid - Fiw136 [Pii]." no. 1574-6941 (Electronic).

Mann, N. H. 2003. "Phages of the Marine Cyanobacterial Picophytoplankton." no. 0168-6445 (Print) (20030416 DCOM- 20030728).

Mateus, Marcos D. 2017. "Bridging the Gap between Knowing and Modeling Viruses in Marine Systems—an Upcoming Frontier." *Frontiers in Marine Science* 3, no. 284 (2017-January-06). http://dx.doi.org/10.3389/fmars.2016.00284.

Maynard-Smith, J.M. 1982. *Evolution and the Theory of Games*: Cambridge University Press.

McAllister, William T., et al. 1981. "Utilization of Bacteriophage T7 Late Promoters in Recombinant Plasmids During Infection." *Journal of Molecular Biology* 153, no. 3 (1981/12/15/): 527-544. http://dx.doi.org/https://doi.org/10.1016/0022-2836(81)90406-X.

Mena, Catalina, et al. 2019. "Phytoplankton Community Structure Is Driven by Stratification in the Oligotrophic Mediterranean Sea." *Frontiers in Microbiology* 10, no. 1698 (2019-July-24). http://dx.doi.org/10.3389/fmicb.2019.01698.

Menge, D. N., and J. S. Weitz. 2009. "Dangerous Nutrients: Evolution of Phytoplankton Resource Uptake Subject to Virus Attack." *J Theor Biol* 257, no. 1 (Mar 7): 104-15. http://dx.doi.org/10.1016/j.jtbi.2008.10.032.

Middelboe, M. 2000. "Bacterial Growth Rate and Marine Virus-Host Dynamics." *Microb Ecol* 40, no. 2 (Aug): 114-124.

Miller, M. R., A. F. White, and M. Boots. 2005. "The Evolution of Host Resistance: Tolerance and Control as Distinct Strategies." no. 0022-5193 (Print).

Monod, Jacques. 1949. "The Growth of Bacterial Cultures." *Annual Review of Microbiology* 3, no. 1 (1949/10/01): 371-394. Accessed 2019/05/27. http://dx.doi.org/https://doi.org/10.1146/annurev.mi.03.100149.002103.

Morgan, Andrew D., and Britt Koskella. 2011. "6 - Coevolution of Host and Pathogen." In *Genetics and Evolution of Infectious Disease*, edited by Michel Tibayrenc, 147-171. London: Elsevier.

Mougi, A., and O. Kishida. 2009. "Reciprocal Phenotypic Plasticity Can Lead to Stable Predator-Prey Interaction." *Journal of Animal Ecology* 78, no. 6.

Nikaido, H., and M. Vaara. 1985. "Molecular Basis of Bacterial Outer Membrane Permeability." *Microbiol Rev* 49, no. 1 (Mar): 1-32.

Noinaj, Nicholas, et al. 2010. "Tonb-Dependent Transporters: Regulation, Structure, and Function." *Annual review of microbiology* 64: 43-60. http://dx.doi.org/10.1146/annurev.micro.112408.134247.

O'Malley, Maureen A. 2016. "The Ecological Virus." *Studies in History and Philosophy of Science Part C: Studies in History and Philosophy of Biological and Biomedical Sciences* 59 (2016/10/01/): 71-79. http://dx.doi.org/https://doi.org/10.1016/j.shpsc.2016.02.012.

Puck Tt Fau - Garen, A., J. Garen A Fau - Cline, and J. Cline. "The Mechanism of Virus Attachment to Host Cells. I. The Role of Ions in the Primary Reaction." no. 0022-1007 (Print). http://dx.doi.org/D - CLML: 5120:34836:440:485 OTO - NLM.

Rabinovitch, A., et al. 2002. "Bacteriophage T4 Development in Escherichia Coli Is Growth Rate Dependent." *J Theor Biol* 216, no. 1 (May 7): 1-4. http://dx.doi.org/10.1006/jtbi.2002.2543.

---. 1999. "Model for Bacteriophage T4 Development in Escherichia Coli." *J Bacteriol* 181, no. 5 (Mar): 1677-83.

Rakhuba, D. V., et al. 2010. "Bacteriophage Receptors, Mechanisms of Phage Adsorption and Penetration into Host Cell." no. 1733-1331 (Print).

Ramanculov, E., and R. Young. 2001. "Genetic Analysis of the T4 Holin: Timing and Topology." no. 0378-1119 (Print).

Ramos-Jiliberto, Rodrigo, Hector Duarte, and Ernesto Frodden. 2008. "Dynamic Effects of Inducible Defenses in a One-Prey Two-Predators System." *Ecological Modelling* 214, no. 2 (2008/06/24/): 242-250. http://dx.doi.org/https://doi.org/10.1016/j.ecolmodel.2008.02.004.

Rothenberg, E., et al. 2011. "Single-Virus Tracking Reveals a Spatial Receptor-Dependent Search Mechanism." no. 1542-0086 (Electronic).

Roux, Simon, et al. 2016. "Ecogenomics and Potential Biogeochemical Impacts of Globally Abundant Ocean Viruses." *Nature* 537, no. 7622 (09/29/print): 689-693. http://dx.doi.org/http://dx.doi.org/10.1038/nature19366.

Schaechter, M., O. MaalØe, and N. O. Kjeldgaard. 1958. "Dependency on Medium and Temperature of Cell Size and Chemical Composition During Balanced Growth of Salmonella Typhimurium." *Microbiology* 19, no. 3: 592-606. http://dx.doi.org/doi:10.1099/00221287-19-3-592.

Schulze, Karl L., and Robert S. Lipe. 1964. "Relationship between Substrate Concentration, Growth Rate, and Respiration Rate of Escherichia Coli in Continuous Culture." *Archiv für Mikrobiologie* 48, no. 1: 1-20. http://dx.doi.org/10.1007/bf00406595.

Schwartz, M. 1976. "The Adsorption of Coliphage Lambda to Its Host: Effect of Variations in the Surface Density of Receptor and in Phage-Receptor Affinity." no. 0022-2836 (Print) (19760925 DCOM- 19760925).

Schwartz, Maxime. 1983. "[10] Phage Λ Receptor (Lamb Protein) in Escherichia Coli." *Methods in Enzymology* 97 (1983/01/01): 100-112. http://dx.doi.org/http://dx.doi.org/10.1016/0076-6879(83)97123-9.

Servais, Pierre, Gilles Billen, and Jose Vives Rego. 1985. "Rate of Bacterial Mortality in Aquatic Environments." *Applied and Environmental Microbiology* 49, no. 6: 1448-1454.

Sherr, E. B., and Carlos Pedrós-Alió. 1989. *Simultaneous Measurement of Bacterioplankton Production and Protozoan Bactivory in Estuarine Water*. Vol. 54.

Shestopaloff, Yuri K. 2016. "Interspecific Allometric Scaling of Unicellular Organisms as an Evolutionary Process of Food Chain Creation." *arXiv preprint arXiv:1611.09824*.

Stoddard, Lauren I., Jennifer B. H. Martiny, and Marcia F. Marston. 2007. "Selection and Characterization of Cyanophage Resistance in Marine Synechococcus Strains." *Applied and Environmental Microbiology* 73, no. 17: 5516-5522. http://dx.doi.org/10.1128/AEM.00356-07.

Storms, Zachary J., and Dominic Sauvageau. 2015. "Modeling Tailed Bacteriophage Adsorption: Insight into Mechanisms." *Virology* 485 (2015/11/01/): 355-362. http://dx.doi.org/https://doi.org/10.1016/j.virol.2015.08.007.

Sullivan, Matthew B., et al. 2005. "Three Prochlorococcus Cyanophage Genomes: Signature Features and Ecological Interpretations." *PLoS Biology* 3, no. 5: e144. http://dx.doi.org/10.1371/journal.pbio.0030144.

---. 2010. "Genomic Analysis of Oceanic Cyanobacterial Myoviruses Compared with T4-Like Myoviruses from Diverse Hosts and Environments." *Environmental Microbiology* 12, no. 11: 3035-3056. http://dx.doi.org/10.1111/j.1462-2920.2010.02280.x.

Suttle, Curtis A. 2007. "Marine Viruses — Major Players in the Global Ecosystem." *Nature Reviews Microbiology* 5 (10/01/online): 801. http://dx.doi.org/10.1038/nrmicro1750.

Thyrhaug, R., et al. 2003. "Stable Coexistence in Marine Algal Host-Virus Systems." *Marine Ecology Progress Series* 254: 27-35. Accessed 2018/09/20. http://dx.doi.org/10.3354/meps254027.

Tilman, D. 1982. "Resource Competition and Community Structure." *Monographs in population biology* 17 (1982): 1-296.

Wang, Ing-Nang. 2006. "Lysis Timing and Bacteriophage Fitness." *Genetics* 172, no. 1: 17-26. http://dx.doi.org/10.1534/genetics.105.045922.

Wang, Ing-Nang, DanielE Dykhuizen, and LawrenceB Slobodkin. 1996. "The Evolution of Phage Lysis Timing." *Evolutionary Ecology* 10, no. 5 (1996/09/01): 545-558. http://dx.doi.org/10.1007/BF01237884.

Wang, Ing-Nang, David L. Smith, and Ry Young. 2000. "Holins: The Protein Clocks of Bacteriophage Infections." *Annual Review of Microbiology* 54, no. 1 (2000/10/01): 799-825. Accessed 2018/06/22. http://dx.doi.org/10.1146/annurev.micro.54.1.799.

Ward, Ben A., et al. 2017. "The Size Dependence of Phytoplankton Growth Rates: A Trade-Off between Nutrient Uptake and Metabolism." *The American Naturalist* 189, no. 2 (2017/02/01): 170-177. Accessed 2020/01/29. http://dx.doi.org/10.1086/689992.

Webb, Vera, Eugene Leduc, and George B. Spiegelman. 1982. "Burst Size of Bacteriophage Sp82 as a Function of Growth Rate of Its Host Bacillus Subtilis." *Canadian Journal of Microbiology* 28, no. 11 (1982/11/01): 1277-1280. Accessed 2018/06/14. http://dx.doi.org/10.1139/m82-190.

Weitz, J. S., H. Hartman, and S. A. Levin. 2005. "Coevolutionary Arms Races between Bacteria and Bacteriophage." *Proceedings of the National Academy of Sciences of*

*the United States of America* 102, no. 27: 9535-9540.
http://dx.doi.org/10.1073/pnas.0504062102.

Weitz, Joshua S., and Jonathan Dushoff. 2008. "Alternative Stable States in Host–Phage Dynamics." *Theoretical Ecology* 1, no. 1 (2008/03/01): 13-19. http://dx.doi.org/10.1007/s12080-007-0001-1.

White, Rebecca, et al. 2011. "Holin Triggering in Real Time." *Proceedings of the National Academy of Sciences* 108, no. 2: 798.

Wilson, W. H., and N. H. Mann. 1997. "Lysogenic and Lytic Viral Production in Marine Microbial Communities." *Aquatic Microbial Ecology* 13, no. 1: 95-100.

Winter, C., et al. 2010. "Trade-Offs between Competition and Defense Specialists among Unicellular Planktonic Organisms: The "Killing the Winner" Hypothesis Revisited." *Microbiol Mol Biol Rev* 74, no. 1 (Mar): 42-57. http://dx.doi.org/10.1128/mmbr.00034-09.

Wirtz, Kai W. 2002. "A Generic Model for Changes in Microbial Kinetic Coefficients." *Journal of Biotechnology* 97, no. 2: 147-162.

Wiser, Michael J., and Richard E. Lenski. 2015. "A Comparison of Methods to Measure Fitness in Escherichia Coli." *PloS one* 10, no. 5: e0126210-e0126210. http://dx.doi.org/10.1371/journal.pone.0126210.

Woznica, W. M., J. Bigos, and M. B. Lobocka. 2015. "Lysis of Bacterial Cells in the Process of Bacteriophage Release:Canonical and Newly Discovered Mechanisms." no. 1732-2693 (Electronic).

Xu, X., I. Khudyakov, and C. P. Wolk. 1997. "Lipopolysaccharide Dependence of Cyanophage Sensitivity and Aerobic Nitrogen Fixation in Anabaena Sp. Strain Pcc 7120." *Journal of Bacteriology* 179, no. 9: 2884-2891.

Yamamichi, Masato, Takehito Yoshida, and Akira Sasaki. 2011. "Comparing the Effects of Rapid Evolution and Phenotypic Plasticity on Predator-Prey Dynamics." *The American Naturalist* 178: 287-304. http://dx.doi.org/10.1086/661241.

You, L., P. Suthers, and J. Yin. 2002. "Effects of Escherichia Coli Physiology on Growth of Phage T7 in Vivo and in Silico." *Journal of Bacteriology* 184, no. 7: 1888-1894.

Young, R. 1992. "Bacteriophage Lysis: Mechanism and Regulation." *Microbiol Rev* 56, no. 3 (Sep): 430-81.

Young, Ry, and Udo Bläsi. 1995. "Holins: Form and Function in Bacteriophage Lysis." *FEMS Microbiology Reviews* 17, no. 1 (1995/08/01/): 191-205. http://dx.doi.org/https://doi.org/10.1016/0168-6445(94)00079-4.

Yu, F., and S. Mizushima. 1982. "Roles of Lipopolysaccharide and Outer Membrane Protein Ompc of Escherichia Coli K-12 in the Receptor Function for Bacteriophage T4." *Journal of Bacteriology* 151, no. 2: 718-722.

Zarybnicky, V., M. Reich, and G. Wolf. 1980. "A Mathematical Model for the Reversible Two-Step Interaction between the T5 Phage and Its Receptor in Vitro." *FEMS Microbiology Letters* 7, no. 1: 29-33. http://dx.doi.org/10.1111/j.1574-6941.1980.tb01570.x.

Zimmer, Carl. 2012. *A Planet of Viruses*. Chicago: University of Chicago Press.